Title

Meiotic chromosome dynamics and organization in C. elegans

Author

Kim, Hyung Jun

Publication Date

2024

Peer reviewed|Thesis/dissertation

Meiotic Chromosome Dynamics and Organization in *C. elegans*

By

Hyung Jun Kim

A dissertation submitted in partial satisfaction of the

requirements for the degree of

Doctor of Philosophy

in

Molecular and Cell Biology

in the

Graduate Division

of the

University of California, Berkeley

Committee in charge:

Professor Abby F. Dernburg, Chair
Professor David Bilder
Professor Rebecca W. Heald
Professor Elçin Ünal

Spring 2024

Abstract

Meiotic Chromosome Dynamics and Organization in *C. elegans*

by

Hyung Jun Kim

Doctor of Philosophy in Molecular and Cell Biology

University of California, Berkeley

Professor Abby F. Dernburg, Chair

Sexual reproduction relies on meiosis, a specialized cell division process that produces haploid gametes. Successful segregation of homologous chromosomes during meiosis requires the pairing of homologs, synapsis, and crossover recombination during meiotic prophase.

Upon initiation of meiosis, in many organisms, chromosome ends establish connections with the nuclear envelope (NE) and interact with motor proteins that drive processive movements along the NE, facilitating homolog chromosome pairing and synapsis. In *C. elegans*, specialized chromosome regions known as "pairing centers" (PCs) serve this role. To understand the roles of PCs in *C. elegans* meiosis, I exploited a genetic screen and identified a novel protein required for homolog pairing and synapsis. Chapter 1 focuses on this newly discovered NE protein, MJL-1, which is essential for homolog pairing and the regulation of synapsis at the PCs.

Chapter 2 describes my efforts to develop methodology for genome-wide profiling of chromosome-interacting proteins in the *C. elegans* germline, leading to new insights into chromosome organization during meiosis. Through this work, I have discovered correlations between the genome-wide distribution of chromosome axis proteins, active chromatin marks, and a protein required for meiotic double-strand breaks (DSBs), DSB-2, during meiosis in *C. elegans*.

Acknowledgements

I am grateful to Abby Dernburg for her mentorship throughout my graduate years; to Chenshu Liu, Liangyu Zhang, and Renzo Adilardi for their contributions to Chapter 1; to Rui Jiang, Fan Wu, Gina Caldas, and Peter Meister for their contributions to Chapter 2; to all past and present members of the Dernburg lab, including Fan Wu, Zhouliang Yu, Fenmiao Zhong, Noor Abuzahriyeh, Xinyi Liu, Hoang Pham, Weston Stauffer, Regina Bohn, and Taniya Kaur, for their support and guidance over the past six years; and to my family, friends, and teachers who provided support and helped me to grow.

Introduction

This chapter includes text modified from published work (H. J. Kim et al., 2022) and is included here with the permission of the copyright holder.

Segregation of homologous chromosomes during meiosis is essential for sexual reproduction. Accurate segregation of homologs relies on their prior pairing, synapsis, and crossover (CO) recombination during meiotic prophase.

Homolog pairing and synapsis during meiosis

In most eukaryotes, the process of homolog pairing is coupled with assembly of the synaptonemal complex (SC), although some organisms have lost the ability to form this structure. SC assembly initiates at discrete points between each chromosome pair and extends processively from these sites, thereby "zippering" homologs into side-by-side alignment along their lengths (reviewed in Cahoon & Hawley, 2016; Zickler & Kleckner, 2015). SCs play a crucial role in the repair of programmed DSBs via CO recombination, which creates chiasmata – physical linkages between homologs – that persist until segregation.

In some species, including budding yeast and mammals, nucleation of synapsis depends on and occurs at sites where a double-strand break (DSB) has been made and initial steps in homologous recombination, including inter-homolog strand invasion, have occurred (Agarwal & Roeder, 2000). Proximity to a chromosome-NE attachment site likely facilitates the homology search required for strand invasion; this may account for the tendency of synapsis to initiate in subtelomeric regions in many species (Blokhina et al., 2019; Calderón et al., 2014; Corredor et al., 2007; D.-Q. Ding et al., 2004). DSBs may also be enriched in these regions, perhaps as a mechanism to promote efficient pairing and synapsis (Blokhina et al., 2019).

In a few organisms, homologous synapsis occurs even in the absence of DSB induction. These include the fruit fly *Drosophila melanogaster* and nematode *Caenorhabditis elegans*, which have independently derived recombination-independent pathways for pairing and synapsis (reviewed in Rog & Dernburg, 2013; Zickler & Kleckner, 2015). In *Drosophila* females, centromeric regions first cluster near the nuclear envelope and then pair in premeiotic cells (Christophorou et al., 2013; Joyce et al., 2013). Homologs probably separate during the intervening mitotic divisions, so it is unclear how this premeiotic pairing contributes to homologous synapsis during meiotic prophase; it may simply be that mechanisms that promote pairing during meiotic prophase are initiated prior to meiotic entry.

Chromosome-Nuclear Envelope (NE) attachments and dynamic chromosome movements during meiosis

The processes of pairing and synapsis are facilitated by active movements of chromosomes within the nucleus. These are mediated by connections between specific chromosome loci and cytoskeletal motors outside of the nucleus, which are usually established upon meiotic entry and require transmembrane proteins that span the intact nuclear envelope (NE). In some cases, the nucleus also rotates, oscillates, or translocates within the cell volume (Christophorou et al., 2015; D. Q. Ding et al., 1998; C.-Y. Lee et al., 2015; PARVINEN & SÖDERSTRÖM, 1976). They can lead to the clustering of chromosome regions in a region of the nuclear envelope near the spindle polar body (SPB) or centrosome, resulting in a

chromosome configuration called the "meiotic bouquet" (reviewed in Hiraoka, 1998; Link & Jantsch, 2019; Scherthan, 2001; Zickler & Kleckner, 1998, 2015). These movements typically abate once chromosomes are fully paired and synapsed.

Telomeres, the physical ends of linear eukaryotic chromosomes, are typically the loci that mediate attachment to the NE, but analogous roles are played by centromeric regions in Drosophila and specialized meiotic "Pairing Centers" in the nematode *Caenorhabditis elegans* (Christophorou et al., 2015; A. Penkner et al., 2007; A. M. Penkner et al., 2009; Sato et al., 2009). In the ciliate Tetrahymena thermophila, centromeres and telomeres are both tethered and form clusters at opposite ends of the nucleus (Loidl et al., 2012). While the chromosome loci that mediate attachment vary, in most or all organisms, these connections depend on LINC (linker of nucleoskeleton and cytoskeleton) complexes, comprised of pairs of SUN (Sad1 and UNC-84 homology) and KASH (Klarsicht, ANC-1, and Syne-1 homology) domain proteins that span the inner and outer nuclear membranes, respectively, and interact within the perinuclear lumen—the space between the nuclear membranes (reviewed in Link & Jantsch, 2019; Rubin et al., 2020). These proteins are more broadly conserved than lamins and have diversified within some clades to form large families (Hiraoka & Dernburg, 2009; Razafsky & Hodzic, 2009). The amino termini of SUN domain proteins are typically intrinsically disordered and extend into the nucleus to interact with proteins bound to telomeres or other chromosome regions, while carboxy termini containing the SUN domain reside in the lumen, where they interact with the KASH domains. The amino termini of KASH domain proteins protrude into the cytosol and typically interact with cytoskeletal filaments or motors (Hiraoka & Dernburg, 2009; Link & Jantsch, 2019).

In some cases, two or more SUN domain proteins contribute to meiotic chromosome movements, and loss of one results in only partial defects (Schmitt et al., 2007; Varas et al., 2015; F. Zhang et al., 2020). LINC proteins that contribute to meiotic chromosome movement typically play other essential roles, e.g., as components of the spindle pole body in fungi, as well as the links between the centrosomes, nucleus, and mediators of nuclear positioning and movement in metazoans (Y. L. Lee & Burke, 2018; Mejat & Misteli, 2010; Razafsky & Hodzic, 2009). Thus, they are typically broadly expressed, but some may be restricted to meiosis—e.g., budding yeast Csm4 is a meiosis-specific paralog of Msp2 (Conrad et al., 2008).

Meiotic chromosome attachments and movements often depend on additional inner nuclear membrane proteins, expressed specifically during meiosis. These include Bqt3 and Bqt4 in fission yeast and MAJIN (membrane-anchored junction protein) in most metazoans (Chikashige et al., 2009; Cruz et al., 2020; Shibuya et al., 2015). How these transmembrane proteins contribute to meiotic attachment and movement remains unclear; they may serve as adaptors to connect SUN proteins to chromatin-binding proteins and/or promote other activities of the LINC complexes, such as clustering or force transduction.

SUN domains form homo- or heterotrimers (Wang et al., 2012); these trimers may dimerize to form symmetrical hexamers, which have been proposed to lead to extended branched networks (Figure 1) (Gurusaran & Davies, 2021); however, it is unclear whether such interactions occur *in vivo*. If so, extended networks may contribute to the clustering of LINC proteins during meiosis, as well as to their ability to sustain and/or respond to forces acting tangential to the plane of the NE. However, deletion of much of the trimeric coiled-coil region of *C. elegans* SUN-1 does not impair meiosis, suggesting that if such networks indeed promote clustering of LINC complexes in meiosis, they do not depend on this coiled-coil region (Daryabeigi et al., 2016). Alternatively, meiosis-specific transmembrane proteins, such as MAJIN and Bqt3/4, may promote associations between LINC proteins that lead to clustering.

Chromosome attachment to LINC complexes typically also requires expression of meiosis-specific proteins that bind to chromosomes. These include Ndj1 (*S. cerevisiae*), Bqt1/2 (*S. pombe*), TERB1/2 (most metazoans), and the pairing center proteins HIM-8 and ZIM-1, -2, - and -3 (*C. elegans*) (Chikashige et al., 2006; Chua & Roeder, 1997; Conrad et al., 1997; Cruz et al., 2020; Phillips et al., 2005; Phillips & Dernburg, 2006; Shibuya et al., 2014, 2015). Some of these have DNA-interacting domains, while others interact with constitutively expressed DNA-binding proteins, such as Rap1 (yeast) or TRF1 (vertebrates). In budding yeast, the incorporation of the histone variant H2A.Z at telomeres during meiosis is also important for their interaction with the SUN domain protein Mps3 (González-Arranz et al., 2018, 2020).

In addition to the structural components of the chromosome–NE linkage complexes, regulatory kinases are often concentrated at these sites. In *C. elegans*, two meiotic kinases, CHK-2 and PLK-2, are recruited by the HIM-8 and ZIM proteins, which contain zinc finger domains that recognize the DNA sequence motifs enriched in the pairing center regions (Harper et al., 2011; Y. Kim et al., 2015; Labella et al., 2011). In mice, SUN1 interacts with CDK2 during meiosis, likely by binding directly to a cyclin-like protein, Speedy A, that partners with CDK2 at these sites (Chen et al., 2021; Mikolcevic et al., 2016; Tu et al., 2017). In fission yeast, telomeres recruit Cdk1 and promote the accumulation of the kinase with the spindle pole body, which eventually leads to the exit from the bouquet stage and nuclear division (MacKenzie & Lacefield, 2020; Moiseeva et al., 2017).

In some cases, these kinases are thought to directly promote chromosome attachment or movement, e.g., by modifying the LINC proteins and/or lamina (Labella et al., 2011; Link et al., 2013; A. M. Penkner et al., 2009; Tu et al., 2017; Viera et al., 2015). Kinase activity may also contribute to regulating synapsis initiation and/or may be components of checkpoints that monitor synapsis (Harper et al., 2011; Y. Kim et al., 2015; Labella et al., 2011; Mikolcevic et al., 2016). Intriguingly, some kinases associated with attachment sites also play roles in crossover formation (Palmer et al., 2020; L. Zhang et al., 2023). Thus, chromosome–LINC complex attachments not only promote pairing and synapsis, but often act as regulatory hubs that control meiotic progression.

Although NE attachment and movement of chromosomes during meiosis are widely conserved across eukaryotes, the key functions of these chromosome dynamics are still under debate (reviewed in Hiraoka & Dernburg, 2009). A longstanding hypothesis is that associations between chromosomes and the NE may promote homology search by reducing its dimensionality from the 3D nuclear volume to the 2D nuclear surface. Some evidence directly supports the role of attachment and/or movement in accelerating homolog pairing (D.-Q. Ding et al., 2004; X. Ding et al., 2007; C.-Y. Lee et al., 2012; Marshall & Fung, 2016). Subtelomeric sequences play key roles in recombination partner choice in some organisms, consistent with the idea that telomere-led movements promote homology search within adjacent regions (Blokhina et al., 2019; Calderón et al., 2014; Corredor et al., 2007). However, homolog pairing is observed even prior to chromosome association with LINC complexes in some organisms, and active chromosome movements often persist until, or even after, synapsis is completed, suggesting that these interactions may also play other roles (Zickler, 2006; Zickler & Kleckner, 2015). In *C. elegans*, the disruption of these attachments leads to nonhomologous synapsis, indicating that they inhibit inappropriate pairing and/or SC formation, in addition to promoting proper pairing (Hiraoka & Dernburg, 2009; A. Penkner et al., 2007; Sato et al., 2009). Both computational simulations and experimental evidence have indicated that chromosome attachments to LINC complexes and the resulting chromosome movements help to eliminate nonhomologous

interactions and/or resolve chromosome entanglements (Chacón et al., 2016; Davis & Smith, 2006; Marshall & Fung, 2016). They can also promote spreading of the SC along paired chromosomes from sites of nucleation (Kosaka et al., 2008; Rog & Dernburg, 2013).

Programmed double strand break (DSB) and crossover (CO) recombination

For faithful segregation of homologs during meiosis I, each pair of homologous chromosomes must undergo at least one programmed double strand break (DSB) that is eventually repaired to form a crossover (CO) recombination product. Feedback mechanisms are thought to ensure the formation of adequate DSBs and CO intermediates.

Programmed DSBs during meiosis are catalyzed by a conserved meiosis-specific enzyme, Spo11 (Keeney, 2008; Keeney et al., 1997, p. 1). Spo11 is a homolog of Topoisomerase VI from archaea. It acts as a dimer to introduce nicks into each strand of the DNA helix, resulting in a DSB. The activity of Spo11 depends on several other proteins. In budding yeast, these include the RMM (Rec114/Mei4/Mer2) and MRX (Mre11/Rad50/Xrs2) complexes (Lam & Keeney, 2015). Many, but not all, of these factors are widely conserved (reviewed in Yadav & Claeys Bouuaert, 2021). Homologs of Rec114 and Mei4 have been identified in diverse organisms, including *C. elegans*. In *C. elegans*, there are two Rec114 homologs, known as DSB-1 and DSB-2, while DSB-3 is a Mei4 homolog (Hinman et al., 2021; Rosu et al., 2013; Stamper et al., 2013).

Cohesins and meiotic HORMA domain proteins, which form the chromosome axis during meiosis, are also crucial for DSBs. Disruption of either cohesins or HORMA domain proteins leads to reduced meiotic DSBs in many organisms. For example, in budding yeast, loss of either of the axis proteins, Hop1 or Red1, significantly reduces meiotic DSBs (Yadav & Claeys Bouuaert, 2021). Similarly, in mice, HORMAD1 is required for the recruitment of accessory proteins necessary for DSB induction, and its disruption leads to reduced DSBs (Stanzione et al., 2016). The loss of cohesin also results in reduced DSB formation in mice (Bhattacharyya et al., 2019). In *C. elegans*, the loss of HORMA domain protein HTP-3 or meiotic cohesin complexes leads to a complete absence of meiotic DSBs (Goodyer et al., 2008; Severson & Meyer, 2014).

Meiotic DSBs preferentially occur in regions of the genome known as “hotspots”. In some organisms, hotspots are "very hot," often several-fold more likely to undergo breaks than the genome-wide average, while in others, they are merely "warmer" than surrounding regions. Hotspots are correlated with nucleosome-free regions and/or active histone modifications in some organisms such as yeast. In yeast, hotspots also tend to be located within chromosome loops (Gerton et al., 2000; Tock & Henderson, 2018). In mammals, histone H3K4 methyltransferase PRDM9, which contains zinc-finger arrays that can bind to DNA in a sequence-specific manner, is required for hotspot designation (Baudat et al., 2010). In *C. elegans*, the chromosome arms exhibit higher recombination rates than the central regions, suggesting that hotspots might be enriched in the chromosome arms (Gerstein et al., 2010; Liu et al., 2011).

Following cleavage by Spo11, DSBs undergo end resection by endo- and exonucleases, resulting in a 3’ overhang, which are coated by RecA homologs Dmc1 and/or Rad51. In *C. elegans*, these stretches of ssDNA initially recruit the ssDNA-binding protein RPA-1, which is then displaced by the RecA homolog Rad51. This leads to homology search and strand invasion into a homologous sequence. These “single-end invasion” (SEI) intermediates are then further processed to produce both non-crossover and crossover (CO) products (reviewed in Yu et al.,

2016; Zickler & Kleckner, 2015). CO designation happens along the chromosome with nonrandom, wide spacing between CO designated sites. Designated CO sites are marked by the recruitment of the cyclin homolog COSA-1 (Yokoo et al., 2012).

Pairing Centers (PCs) mediate pairing and synapsis during meiosis in *C. elegans*

Meiotic mechanisms in *C. elegans* have been studied extensively. Mutations that affect meiosis have been isolated in numerous screens (Hodgkin et al., 1979; Kelly et al., 2000). Characterization of the effects of these mutations is facilitated by the physical organization of the germline, which contains a gradient of all stages of meiotic nuclei. During meiosis in *C. elegans*, the pairing of chromosomes is coordinated by the PCs. PCs play a pivotal role in achieving chromosome pairing, mediating recognition of homologous chromosomes regardless of homology in other regions (McKim et al., 1988; Rosenbluth & Baillie, 1981; Villeneuve, 1994). Furthermore, evidence indicates that SC assembly is initiated from PCs, underscoring their significance in regulating SC assembly (Hayashi et al., 2010; MacQueen et al., 2005; Rog & Dernburg, 2015). PCs are characterized by a high density of dispersed repeat motifs that recruit zinc finger proteins, including HIM-8 (High Incidence of Males) and ZIM-1, -2, and -3 (Zinc finger In Meiosis) (Phillips et al., 2005; Phillips & Dernburg, 2006). HIM-8 specifically binds to X chromosomes, while ZIM-1, -2, and -3 each bind to one or two autosomes (Phillips et al., 2009). The loss of PC proteins results in severe pairing and synapsis defects, similar to the consequences of PCs being deleted. PCs also interact with a pair of SUN/KASH proteins, SUN-1/ZYG-12, inducing aggregation and rapid movement along the NE to promote chromosome pairing (A. Penkner et al., 2007; Sato et al., 2009; Wynne et al., 2012).

Upon entry into meiosis, at least two meiotic kinases, CHK-2 and PLK-2, localize to the PCs through direct interaction with PC proteins (Harper et al., 2011; Y. Kim et al., 2015; Labella et al., 2011). CHK-2 is a meiosis-specific ortholog of mammalian Chk2 that functions as a "master kinase" during early meiosis. Absence of CHK-2 results in the bypass of crucial early meiotic events, including chromosome pairing, movement, and synapsis (MacQueen & Villeneuve, 2001). Moreover, CHK-2-dependent phosphorylation of PC proteins is essential for the localization of PLK-2 (Harper et al., 2011; Labella et al., 2011). PLK-2, a meiotic Polo-like kinase closely related to mammalian Plk1, is another key kinase in the process. Depletion of PLK-2, like CHK-2, results in abrogated pairing, PC-NE attachment, and synapsis. While PLK-1, a kinase in the PLK family, primarily functions in mitosis, it can partially substitute for its paralog PLK-2 during meiosis (Harper et al., 2011; Labella et al., 2011).

Concluding remark

I conducted a genetic screen to identify novel factors involved in homolog pairing and synapsis. Chapter 1 focuses on the newly discovered meiotic NE protein MJL-1, identified through the screen. MJL-1 tethers PCs to the NE and is required for homolog pairing and regulation of synapsis during meiosis in *C. elegans*.

In Chapter 2, I describe an efficient method for genome-wide profiling of chromosome-interacting proteins and histone modifications in the *C. elegans* germline. As preliminary results, I demonstrate a correlation between meiotic chromosome axis proteins, active chromatin, and one of the factors responsible for inducing programmed DSBs, DSB-2, as revealed by my method.

References

Agarwal, S., & Roeder, G. S. (2000). Zip3 provides a link between recombination enzymes and synaptonemal complex proteins. *Cell*, *102*(2), Article 2. https://doi.org/10.1016/s0092-8674(00)00029-5

Baudat, F., Buard, J., Grey, C., Fledel-Alon, A., Ober, C., Przeworski, M., Coop, G., & de Massy, B. (2010). PRDM9 Is a Major Determinant of Meiotic Recombination Hotspots in Humans and Mice. *Science*, *327*(5967), 836–840. https://doi.org/10.1126/science.1183439

Bhattacharyya, T., Walker, M., Powers, N. R., Brunton, C., Fine, A. D., Petkov, P. M., & Handel, M. A. (2019). Prdm9 and Meiotic Cohesin Proteins Cooperatively Promote DNA Double-Strand Break Formation in Mammalian Spermatocytes. *Current Biology*, *29*(6), 1002-1018.e7. https://doi.org/10.1016/j.cub.2019.02.007

Blokhina, Y. P., Nguyen, A. D., Draper, B. W., & Burgess, S. M. (2019). The telomere bouquet is a hub where meiotic double-strand breaks, synapsis, and stable homolog juxtaposition are coordinated in the zebrafish, Danio rerio. *PLoS Genetics*, *15*(1), Article 1. https://doi.org/10.1371/journal.pgen.1007730

Cahoon, C. K., & Hawley, R. S. (2016). Regulating the construction and demolition of the synaptonemal complex. *Nature Structural & Molecular Biology*, *23*(5), Article 5. https://doi.org/10.1038/nsmb.3208

Calderón, M. del C., Rey, M.-D., Cabrera, A., & Prieto, P. (2014). The subtelomeric region is important for chromosome recognition and pairing during meiosis. *Scientific Reports*, *4*(1), Article 1. https://doi.org/10.1038/srep06488

Chacón, M. R., Delivani, P., & Tolić, I. M. (2016). Meiotic Nuclear Oscillations Are Necessary to Avoid Excessive Chromosome Associations. *Cell Reports*, *17*(6), Article 6. https://doi.org/10.1016/j.celrep.2016.10.014

Chen, Y., Wang, Y., Chen, J., Zuo, W., Fan, Y., Huang, S., Liu, Y., Chen, G., Li, Q., Li, J., Wu, J., Bian, Q., Huang, C., & Lei, M. (2021). The SUN1-SPDYA interaction plays an essential role in meiosis prophase I. *Nature Communications*, *12*(1), Article 1. https://doi.org/10.1038/s41467-021-23550-w

Chikashige, Y., Tsutsumi, C., Yamane, M., Okamasa, K., Haraguchi, T., & Hiraoka, Y. (2006). Meiotic proteins bqt1 and bqt2 tether telomeres to form the bouquet arrangement of chromosomes. *Cell*, *125*(1), Article 1. https://doi.org/10.1016/j.cell.2006.01.048

Chikashige, Y., Yamane, M., Okamasa, K., Tsutsumi, C., Kojidani, T., Sato, M., Haraguchi, T., & Hiraoka, Y. (2009). Membrane proteins Bqt3 and -4 anchor telomeres to the nuclear envelope to ensure chromosomal bouquet formation. *The Journal of Cell Biology*, *187*(3), Article 3. https://doi.org/10.1083/jcb.200902122

Christophorou, N., Rubin, T., Bonnet, I., Piolot, T., Arnaud, M., & Huynh, J.-R. (2015). Microtubule-driven nuclear rotations promote meiotic chromosome dynamics. *Nature Cell Biology*, *17*(11), Article 11. https://doi.org/10.1038/ncb3249

Christophorou, N., Rubin, T., & Huynh, J.-R. (2013). Synaptonemal complex components promote centromere pairing in pre-meiotic germ cells. *PLoS Genetics*, *9*(12), Article 12. https://doi.org/10.1371/journal.pgen.1004012

Chua, P. R., & Roeder, G. S. (1997). Tam1, a telomere-associated meiotic protein, functions in chromosome synapsis and crossover interference. *Genes & Development*, *11*(14), Article 14. https://doi.org/10.1101/gad.11.14.1786

Conrad, M. N., Dominguez, A. M., & Dresser, M. E. (1997). Ndj1p, a Meiotic Telomere Protein Required for Normal Chromosome Synapsis and Segregation in Yeast. *Science*. https://doi.org/10.1126/science.276.5316.1252

Conrad, M. N., Lee, C.-Y., Chao, G., Shinohara, M., Kosaka, H., Shinohara, A., Conchello, J.-A., & Dresser, M. E. (2008). Rapid Telomere Movement in Meiotic Prophase Is Promoted By NDJ1, MPS3, and CSM4 and Is Modulated by Recombination. *Cell*, *133*(7), Article 7. https://doi.org/10.1016/j.cell.2008.04.047

Corredor, E., Lukaszewski, A. J., Pachón, P., Allen, D. C., & Naranjo, T. (2007). Terminal Regions of Wheat Chromosomes Select Their Pairing Partners in Meiosis. *Genetics*, *177*(2), Article 2. https://doi.org/10.1534/genetics.107.078121

Cruz, I. da, Brochier-Armanet, C., & Benavente, R. (2020). The TERB1-TERB2-MAJIN complex of mouse meiotic telomeres dates back to the common ancestor of metazoans. *BMC Evolutionary Biology*, *20*(1), Article 1. https://doi.org/10.1186/s12862-020-01612-9

Daryabeigi, A., Woglar, A., Baudrimont, A., Silva, N., Paouneskou, D., Vesely, C., Rauter, M., Penkner, A., Jantsch, M., & Jantsch, V. (2016). Nuclear Envelope Retention of LINC Complexes Is Promoted by SUN-1 Oligomerization in the Caenorhabditis elegans Germ Line. *Genetics*, *203*(2), 733–748. https://doi.org/10.1534/genetics.116.188094

Davis, L., & Smith, G. R. (2006). The meiotic bouquet promotes homolog interactions and restricts ectopic recombination in Schizosaccharomyces pombe. *Genetics*, *174*(1), Article 1. https://doi.org/10.1534/genetics.106.059733

Ding, D. Q., Chikashige, Y., Haraguchi, T., & Hiraoka, Y. (1998). Oscillatory nuclear movement in fission yeast meiotic prophase is driven by astral microtubules, as revealed by continuous observation of chromosomes and microtubules in living cells. *Journal of Cell Science*, *111*(6), Article 6. https://doi.org/10.1242/jcs.111.6.701

Ding, D.-Q., Yamamoto, A., Haraguchi, T., & Hiraoka, Y. (2004). Dynamics of Homologous Chromosome Pairing during Meiotic Prophase in Fission Yeast. *Developmental Cell*, *6*(3), Article 3. https://doi.org/10.1016/S1534-5807(04)00059-0

Ding, X., Xu, R., Yu, J., Xu, T., Zhuang, Y., & Han, M. (2007). SUN1 is required for telomere attachment to nuclear envelope and gametogenesis in mice. *Developmental Cell*, *12*(6), Article 6. https://doi.org/10.1016/j.devcel.2007.03.018

Gerstein, M. B., Lu, Z. J., Van Nostrand, E. L., Cheng, C., Arshinoff, B. I., Liu, T., Yip, K. Y., Robilotto, R., Rechtsteiner, A., Ikegami, K., Alves, P., Chateigner, A., Perry, M., Morris, M., Auerbach, R. K., Feng, X., Leng, J., Vielle, A., Niu, W., … Waterston, R. H. (2010). Integrative Analysis of the *Caenorhabditis elegans* Genome by the modENCODE Project. *Science*, *330*(6012), 1775–1787. https://doi.org/10.1126/science.1196914

Gerton, J. L., DeRisi, J., Shroff, R., Lichten, M., Brown, P. O., & Petes, T. D. (2000). Global mapping of meiotic recombination hotspots and coldspots in the yeast *Saccharomyces cerevisiae*. *Proceedings of the National Academy of Sciences*, *97*(21), 11383–11390. https://doi.org/10.1073/pnas.97.21.11383

González-Arranz, S., Cavero, S., Morillo-Huesca, M., Andújar, E., Pérez-Alegre, M., Prado, F., & San-Segundo, P. (2018). Functional Impact of the H2A.Z Histone Variant During Meiosis in Saccharomyces cerevisiae. *Genetics*, *209*(4), Article 4. https://doi.org/10.1534/genetics.118.301110

González-Arranz, S., Gardner, J. M., Yu, Z., Patel, N. J., Heldrich, J., Santos, B., Carballo, J. A., Jaspersen, S. L., Hochwagen, A., & San-Segundo, P. A. (2020). SWR1-Independent Association of H2A.Z to the LINC Complex Promotes Meiotic Chromosome Motion.

Frontiers in Cell and Developmental Biology, *8*, 594092. https://doi.org/10.3389/fcell.2020.594092

Goodyer, W., Kaitna, S., Couteau, F., Ward, J. D., Boulton, S. J., & Zetka, M. (2008). HTP-3 Links DSB Formation with Homolog Pairing and Crossing Over during C. elegans Meiosis. *Developmental Cell*, *14*(2), 263–274. https://doi.org/10.1016/j.devcel.2007.11.016

Gurusaran, M., & Davies, O. R. (2021). A molecular mechanism for LINC complex branching by structurally diverse SUN-KASH 6:6 assemblies. *ELife*, *10*. https://doi.org/10.7554/eLife.60175

Harper, N. C., Rillo, R., Jover-Gil, S., Assaf, Z. J., Bhalla, N., & Dernburg, A. F. (2011). Pairing centers recruit a Polo-like kinase to orchestrate meiotic chromosome dynamics in C. elegans. *Developmental Cell*, *21*(5), Article 5. https://doi.org/10.1016/j.devcel.2011.09.001

Hayashi, M., Mlynarczyk-Evans, S., & Villeneuve, A. M. (2010). The Synaptonemal Complex Shapes the Crossover Landscape Through Cooperative Assembly, Crossover Promotion and Crossover Inhibition During *Caenorhabditis elegans* Meiosis. *Genetics*, *186*(1), 45–58. https://doi.org/10.1534/genetics.110.115501

Hinman, A. W., Yeh, H.-Y., Roelens, B., Yamaya, K., Woglar, A., Bourbon, H.-M. G., Chi, P., & Villeneuve, A. M. (2021). *Caenorhabditis elegans* DSB-3 reveals conservation and divergence among protein complexes promoting meiotic double-strand breaks. *Proceedings of the National Academy of Sciences*, *118*(33), e2109306118. https://doi.org/10.1073/pnas.2109306118

Hiraoka, Y. (1998). Meiotic telomeres: A matchmaker for homologous chromosomes. *Genes to Cells: Devoted to Molecular & Cellular Mechanisms*, *3*(7), Article 7. https://doi.org/10.1046/j.1365-2443.1998.00205.x

Hiraoka, Y., & Dernburg, A. F. (2009). The SUN rises on meiotic chromosome dynamics. *Developmental Cell*, *17*(5), Article 5. https://doi.org/10.1016/j.devcel.2009.10.014

Hodgkin, J., Horvitz, H. R., & Brenner, S. (1979). Nondisjunction Mutants of the Nematode CAENORHABDITIS ELEGANS. *Genetics*, *91*(1), 67–94. https://doi.org/10.1093/genetics/91.1.67

Joyce, E. F., Apostolopoulos, N., Beliveau, B. J., & Wu, C. -ting. (2013). Germline progenitors escape the widespread phenomenon of homolog pairing during Drosophila development. *PLoS Genetics*, *9*(12), Article 12. https://doi.org/10.1371/journal.pgen.1004013

Keeney, S. (2008). Spo11 and the Formation of DNA Double-Strand Breaks in Meiosis. In R. Egel & D.-H. Lankenau (Eds.), *Recombination and Meiosis* (Vol. 2, pp. 81–123). Springer Berlin Heidelberg. https://doi.org/10.1007/7050_2007_026

Keeney, S., Giroux, C. N., & Kleckner, N. (1997). Meiosis-Specific DNA Double-Strand Breaks Are Catalyzed by Spo11, a Member of a Widely Conserved Protein Family. *Cell*, *88*(3), 375–384. https://doi.org/10.1016/S0092-8674(00)81876-0

Kelly, K. O., Dernburg, A. F., Stanfield, G. M., & Villeneuve, A. M. (2000). Caenorhabditis elegans msh-5 is required for both normal and radiation-induced meiotic crossing over but not for completion of meiosis. *Genetics*, *156*(2), 617–630. https://doi.org/10.1093/genetics/156.2.617

Kim, H. J., Liu, C., & Dernburg, A. F. (2022). How and Why Chromosomes Interact with the Cytoskeleton during Meiosis. *Genes*, *13*(5), 901. https://doi.org/10.3390/genes13050901

Kim, Y., Kostow, N., & Dernburg, A. F. (2015). The Chromosome Axis Mediates Feedback Control of CHK-2 to Ensure Crossover Formation in C. elegans. *Developmental Cell*, *35*(2), Article 2. https://doi.org/10.1016/j.devcel.2015.09.021

Kim, Y., Rosenberg, S. C., Kugel, C. L., Kostow, N., Rog, O., Davydov, V., Su, T. Y., Dernburg, A. F., & Corbett, K. D. (2014). The Chromosome Axis Controls Meiotic Events through a Hierarchical Assembly of HORMA Domain Proteins. *Developmental Cell*, *31*(4), 487–502. https://doi.org/10.1016/j.devcel.2014.09.013

Kosaka, H., Shinohara, M., & Shinohara, A. (2008). Csm4-dependent telomere movement on nuclear envelope promotes meiotic recombination. *PLoS Genetics*, *4*(9), Article 9. https://doi.org/10.1371/journal.pgen.1000196

Labella, S., Woglar, A., Jantsch, V., & Zetka, M. (2011). Polo kinases establish links between meiotic chromosomes and cytoskeletal forces essential for homolog pairing. *Developmental Cell*, *21*(5), Article 5. https://doi.org/10.1016/j.devcel.2011.07.011

Lam, I., & Keeney, S. (2015). Nonparadoxical evolutionary stability of the recombination initiation landscape in yeast. *Science*, *350*(6263), 932–937. https://doi.org/10.1126/science.aad0814

Lee, C.-Y., Conrad, M. N., & Dresser, M. E. (2012). Meiotic chromosome pairing is promoted by telomere-led chromosome movements independent of bouquet formation. *PLoS Genetics*, *8*(5), Article 5. https://doi.org/10.1371/journal.pgen.1002730

Lee, C.-Y., Horn, H. F., Stewart, C. L., Burke, B., Bolcun-Filas, E., Schimenti, J. C., Dresser, M. E., & Pezza, R. J. (2015). Mechanism and regulation of rapid telomere prophase movements in mouse meiotic chromosomes. *Cell Reports*, *11*(4), Article 4. https://doi.org/10.1016/j.celrep.2015.03.045

Lee, Y. L., & Burke, B. (2018). LINC complexes and nuclear positioning. *Seminars in Cell & Developmental Biology*, *82*, 67–76. https://doi.org/10.1016/j.semcdb.2017.11.008

Link, J., Jahn, D., Schmitt, J., Göb, E., Baar, J., Ortega, S., Benavente, R., & Alsheimer, M. (2013). The meiotic nuclear lamina regulates chromosome dynamics and promotes efficient homologous recombination in the mouse. *PLoS Genetics*, *9*(1), Article 1. https://doi.org/10.1371/journal.pgen.1003261

Link, J., & Jantsch, V. (2019). Meiotic chromosomes in motion: A perspective from Mus musculus and Caenorhabditis elegans. *Chromosoma*, *128*(3), Article 3. https://doi.org/10.1007/s00412-019-00698-5

Liu, T., Rechtsteiner, A., Egelhofer, T. A., Vielle, A., Latorre, I., Cheung, M.-S., Ercan, S., Ikegami, K., Jensen, M., Kolasinska-Zwierz, P., Rosenbaum, H., Shin, H., Taing, S., Takasaki, T., Iniguez, A. L., Desai, A., Dernburg, A. F., Kimura, H., Lieb, J. D., … Liu, X. S. (2011). Broad chromosomal domains of histone modification patterns in *C. elegans*. *Genome Research*, *21*(2), 227–236. https://doi.org/10.1101/gr.115519.110

Loidl, J., Lukaszewicz, A., Howard-Till, R. A., & Koestler, T. (2012). The Tetrahymena meiotic chromosome bouquet is organized by centromeres and promotes interhomolog recombination. *Journal of Cell Science*, *125*(Pt 23), Article Pt 23. https://doi.org/10.1242/jcs.112664

MacKenzie, A. M., & Lacefield, S. (2020). CDK Regulation of Meiosis: Lessons from S. cerevisiae and S. pombe. *Genes*, *11*(7), Article 7. https://doi.org/10.3390/genes11070723

MacQueen, A. J., Phillips, C. M., Bhalla, N., Weiser, P., Villeneuve, A. M., & Dernburg, A. F. (2005). Chromosome sites play dual roles to establish homologous synapsis during meiosis in C. elegans. *Cell*, *123*(6), Article 6. https://doi.org/10.1016/j.cell.2005.09.034

MacQueen, A. J., & Villeneuve, A. M. (2001). Nuclear reorganization and homologous chromosome pairing during meiotic prophase require C. elegans chk-2. *Genes & Development*, *15*(13), Article 13. https://doi.org/10.1101/gad.902601

Marshall, W. F., & Fung, J. C. (2016). Modeling meiotic chromosome pairing: Nuclear envelope attachment, telomere-led active random motion, and anomalous diffusion. *Physical Biology*, *13*(2), Article 2. https://doi.org/10.1088/1478-3975/13/2/026003

McKim, K. S., Howell, A. M., & Rose, A. M. (1988). The effects of translocations on recombination frequency in Caenorhabditis elegans. *Genetics*, *120*(4), 987–1001. https://doi.org/10.1093/genetics/120.4.987

Mejat, A., & Misteli, T. (2010). LINC complexes in health and disease. *Nucleus*, *1*(1), Article 1.

Mikolcevic, P., Isoda, M., Shibuya, H., Barrantes, I. del B., Igea, A., Suja, J. A., Shackleton, S., Watanabe, Y., & Nebreda, A. R. (2016). Essential role of the Cdk2 activator RingoA in meiotic telomere tethering to the nuclear envelope. *Nature Communications*, *7*(1), Article 1. https://doi.org/10.1038/ncomms11084

Moiseeva, V., Amelina, H., Collopy, L. C., Armstrong, C. A., Pearson, S. R., & Tomita, K. (2017). The telomere bouquet facilitates meiotic prophase progression and exit in fission yeast. *Cell Discovery*, *3*(1), Article 1. https://doi.org/10.1038/celldisc.2017.41

Palmer, N., Talib, S. Z. A., Singh, P., Goh, C. M. F., Liu, K., Schimenti, J. C., & Kaldis, P. (2020). A novel function for CDK2 activity at meiotic crossover sites. *PLoS Biology*, *18*(10), Article 10. https://doi.org/10.1371/journal.pbio.3000903

PARVINEN, M., & SÖDERSTRÖM, K.-O. (1976). Chromosome rotation and formation of synapsis. *Nature (London)*, *260*(5551), Article 5551. https://doi.org/10.1038/260534a0

Penkner, A. M., Fridkin, A., Gloggnitzer, J., Baudrimont, A., Machacek, T., Woglar, A., Csaszar, E., Pasierbek, P., Ammerer, G., Gruenbaum, Y., & Jantsch, V. (2009). Meiotic Chromosome Homology Search Involves Modifications of the Nuclear Envelope Protein Matefin/SUN-1. *Cell*, *139*(5), Article 5. https://doi.org/10.1016/j.cell.2009.10.045

Penkner, A., Tang, L., Novatchkova, M., Ladurner, M., Fridkin, A., Gruenbaum, Y., Schweizer, D., Loidl, J., & Jantsch, V. (2007). The Nuclear Envelope Protein Matefin/SUN-1 Is Required for Homologous Pairing in C. elegans Meiosis. *Developmental Cell*, *12*(6), Article 6. https://doi.org/10.1016/j.devcel.2007.05.004

Phillips, C. M., & Dernburg, A. F. (2006). A family of zinc-finger proteins is required for chromosome-specific pairing and synapsis during meiosis in C. elegans. *Developmental Cell*, *11*(6), Article 6. https://doi.org/10.1016/j.devcel.2006.09.020

Phillips, C. M., Meng, X., Zhang, L., Chretien, J. H., Urnov, F. D., & Dernburg, A. F. (2009). Identification of chromosome sequence motifs that mediate meiotic pairing and synapsis in C. elegans. *Nature Cell Biology*, *11*(8), Article 8. https://doi.org/10.1038/ncb1904

Phillips, C. M., Wong, C., Bhalla, N., Carlton, P. M., Weiser, P., Meneely, P. M., & Dernburg, A. F. (2005). HIM-8 Binds to the X Chromosome Pairing Center and Mediates Chromosome-Specific Meiotic Synapsis. *Cell*, *123*(6), Article 6. https://doi.org/10.1016/j.cell.2005.09.035

Razafsky, D., & Hodzic, D. (2009). Bringing KASH under the SUN: the many faces of nucleo-cytoskeletal connections. *The Journal of Cell Biology*, *186*(4), Article 4. https://doi.org/10.1083/jcb.200906068

Rog, O., & Dernburg, A. F. (2013). Chromosome pairing and synapsis during Caenorhabditis elegans meiosis. *Current Opinion in Cell Biology*, *25*(3), Article 3. https://doi.org/10.1016/j.ceb.2013.03.003

Rog, O., & Dernburg, A. F. (2015). Direct Visualization Reveals Kinetics of Meiotic Chromosome Synapsis. *Cell Reports*, *10*(10), Article 10. https://doi.org/10.1016/j.celrep.2015.02.032

Rosenbluth, R. E., & Baillie, D. L. (1981). The genetic analysis of a reciprocal translocation, eT1(III; V), in Caenorhabditis elegans. *Genetics*, *99*(3–4), 415–428. https://doi.org/10.1093/genetics/99.3-4.415

Rosu, S., Zawadzki, K. A., Stamper, E. L., Libuda, D. E., Reese, A. L., Dernburg, A. F., & Villeneuve, A. M. (2013). The C. elegans DSB-2 Protein Reveals a Regulatory Network that Controls Competence for Meiotic DSB Formation and Promotes Crossover Assurance. *PLoS Genetics*, *9*(8), e1003674. https://doi.org/10.1371/journal.pgen.1003674

Rubin, T., Macaisne, N., & Huynh, J.-R. (2020). Mixing and Matching Chromosomes during Female Meiosis. *Cells*, *9*(3), Article 3. https://doi.org/10.3390/cells9030696

Sato, A., Isaac, B., Phillips, C. M., Rillo, R., Carlton, P. M., Wynne, D. J., Kasad, R. A., & Dernburg, A. F. (2009). Cytoskeletal forces span the nuclear envelope to coordinate meiotic chromosome pairing and synapsis. *Cell*, *139*(5), Article 5. https://doi.org/10.1016/j.cell.2009.10.039

Scherthan, H. (2001). A bouquet makes ends meet. *Nature Reviews. Molecular Cell Biology*, *2*(8), Article 8. https://doi.org/10.1038/35085086

Schmitt, J., Benavente, R., Hodzic, D., Höög, C., Stewart, C. L., & Alsheimer, M. (2007). Transmembrane protein Sun2 is involved in tethering mammalian meiotic telomeres to the nuclear envelope. *Proceedings of the National Academy of Sciences of the United States of America*, *104*(18), Article 18. https://doi.org/10.1073/pnas.0609198104

Severson, A. F., & Meyer, B. J. (2014). Divergent kleisin subunits of cohesin specify mechanisms to tether and release meiotic chromosomes. *ELife*, *3*, e03467. https://doi.org/10.7554/eLife.03467

Shibuya, H., Hernández-Hernández, A., Morimoto, A., Negishi, L., Höög, C., & Watanabe, Y. (2015). MAJIN Links Telomeric DNA to the Nuclear Membrane by Exchanging Telomere Cap. *Cell*, *163*(5), Article 5. https://doi.org/10.1016/j.cell.2015.10.030

Shibuya, H., Ishiguro, K., & Watanabe, Y. (2014). The TRF1-binding protein TERB1 promotes chromosome movement and telomere rigidity in meiosis. *Nature Cell Biology*, *16*(2), Article 2. https://doi.org/10.1038/ncb2896

Stamper, E. L., Rodenbusch, S. E., Rosu, S., Ahringer, J., Villeneuve, A. M., & Dernburg, A. F. (2013). Identification of DSB-1, a Protein Required for Initiation of Meiotic Recombination in Caenorhabditis elegans, Illuminates a Crossover Assurance Checkpoint. *PLoS Genetics*, *9*(8), e1003679. https://doi.org/10.1371/journal.pgen.1003679

Stanzione, M., Baumann, M., Papanikos, F., Dereli, I., Lange, J., Ramlal, A., Tränkner, D., Shibuya, H., de Massy, B., Watanabe, Y., Jasin, M., Keeney, S., & Tóth, A. (2016). Meiotic DNA break formation requires the unsynapsed chromosome axis-binding protein IHO1 (CCDC36) in mice. *Nature Cell Biology*, *18*(11), 1208–1220. https://doi.org/10.1038/ncb3417

Tock, A. J., & Henderson, I. R. (2018). Hotspots for Initiation of Meiotic Recombination. *Frontiers in Genetics*, *9*, 521. https://doi.org/10.3389/fgene.2018.00521

Tu, Z., Bayazit, M. B., Liu, H., Zhang, J., Busayavalasa, K., Risal, S., Shao, J., Satyanarayana, A., Coppola, V., Tessarollo, L., Singh, M., Zheng, C., Han, C., Chen, Z., Kaldis, P., Gustafsson, J.-Å., & Liu, K. (2017). Speedy A-Cdk2 binding mediates initial telomere-

nuclear envelope attachment during meiotic prophase I independent of Cdk2 activation. *Proceedings of the National Academy of Sciences of the United States of America*, *114*(3), Article 3. https://doi.org/10.1073/pnas.1618465114

Varas, J., Graumann, K., Osman, K., Pradillo, M., Evans, D. E., Santos, J. L., & Armstrong, S. J. (2015). Absence of SUN1 and SUN2 proteins in Arabidopsis thaliana leads to a delay in meiotic progression and defects in synapsis and recombination. *The Plant Journal: For Cell and Molecular Biology*, *81*(2), Article 2. https://doi.org/10.1111/tpj.12730

Viera, A., Alsheimer, M., Gómez, R., Berenguer, I., Ortega, S., Symonds, C. E., Santamaría, D., Benavente, R., & Suja, J. A. (2015). CDK2 regulates nuclear envelope protein dynamics and telomere attachment in mouse meiotic prophase. *Journal of Cell Science*, *128*(1), Article 1. https://doi.org/10.1242/jcs.154922

Villeneuve, A. M. (1994). A cis-acting locus that promotes crossing over between X chromosomes in Caenorhabditis elegans. *Genetics*, *136*(3), 887–902. https://doi.org/10.1093/genetics/136.3.887

Wang, W., Shi, Z., Jiao, S., Chen, C., Wang, H., Liu, G., Wang, Q., Zhao, Y., Greene, M. I., & Zhou, Z. (2012). Structural insights into SUN-KASH complexes across the nuclear envelope. *Cell Research*, *22*(10), Article 10. https://doi.org/10.1038/cr.2012.126

Wynne, D. J., Rog, O., Carlton, P. M., & Dernburg, A. F. (2012). Dynein-dependent processive chromosome motions promote homologous pairing in C. elegans meiosis. *The Journal of Cell Biology*, *196*(1), Article 1. https://doi.org/10.1083/jcb.201106022

Yadav, V. K., & Claeys Bouuaert, C. (2021). Mechanism and Control of Meiotic DNA Double-Strand Break Formation in S. cerevisiae. *Frontiers in Cell and Developmental Biology*, *9*, 642737. https://doi.org/10.3389/fcell.2021.642737

Yokoo, R., Zawadzki, K. A., Nabeshima, K., Drake, M., Arur, S., & Villeneuve, A. M. (2012). COSA-1 Reveals Robust Homeostasis and Separable Licensing and Reinforcement Steps Governing Meiotic Crossovers. *Cell*, *149*(1), 75–87. https://doi.org/10.1016/j.cell.2012.01.052

Yu, Z., Kim, Y., & Dernburg, A. F. (2016). Meiotic recombination and the crossover assurance checkpoint in Caenorhabditis elegans. *Seminars in Cell & Developmental Biology*, *54*, 106–116. https://doi.org/10.1016/j.semcdb.2016.03.014

Zhang, F., Ma, L., Zhang, C., Du, G., Shen, Y., Tang, D., Li, Y., Yu, H., Ma, B., & Cheng, Z. (2020). The SUN Domain Proteins OsSUN1 and OsSUN2 Play Critical but Partially Redundant Roles in Meiosis. *Plant Physiology*, *183*(4), Article 4. https://doi.org/10.1104/pp.20.00140

Zhang, L., Stauffer, W. T., Wang, J. S., Wu, F., Yu, Z., Liu, C., Kim, H. J., & Dernburg, A. F. (2023). Recruitment of Polo-like kinase couples synapsis to meiotic progression via inactivation of CHK-2. *ELife*, *12*, e84492. https://doi.org/10.7554/eLife.84492

Zickler, D. (2006). From early homologue recognition to synaptonemal complex formation. *Chromosoma*, *115*(3), Article 3. https://doi.org/10.1007/s00412-006-0048-6

Zickler, D., & Kleckner, N. (1998). The leptotene-zygotene transition of meiosis. *Annual Review of Genetics*, *32*, 619–697. https://doi.org/10.1146/annurev.genet.32.1.619

Zickler, D., & Kleckner, N. (2015). Recombination, Pairing, and Synapsis of Homologs during Meiosis. *Cold Spring Harbor Perspectives in Biology*, *7*(6), Article 6. https://doi.org/10.1101/cshperspect.a016626

Figure

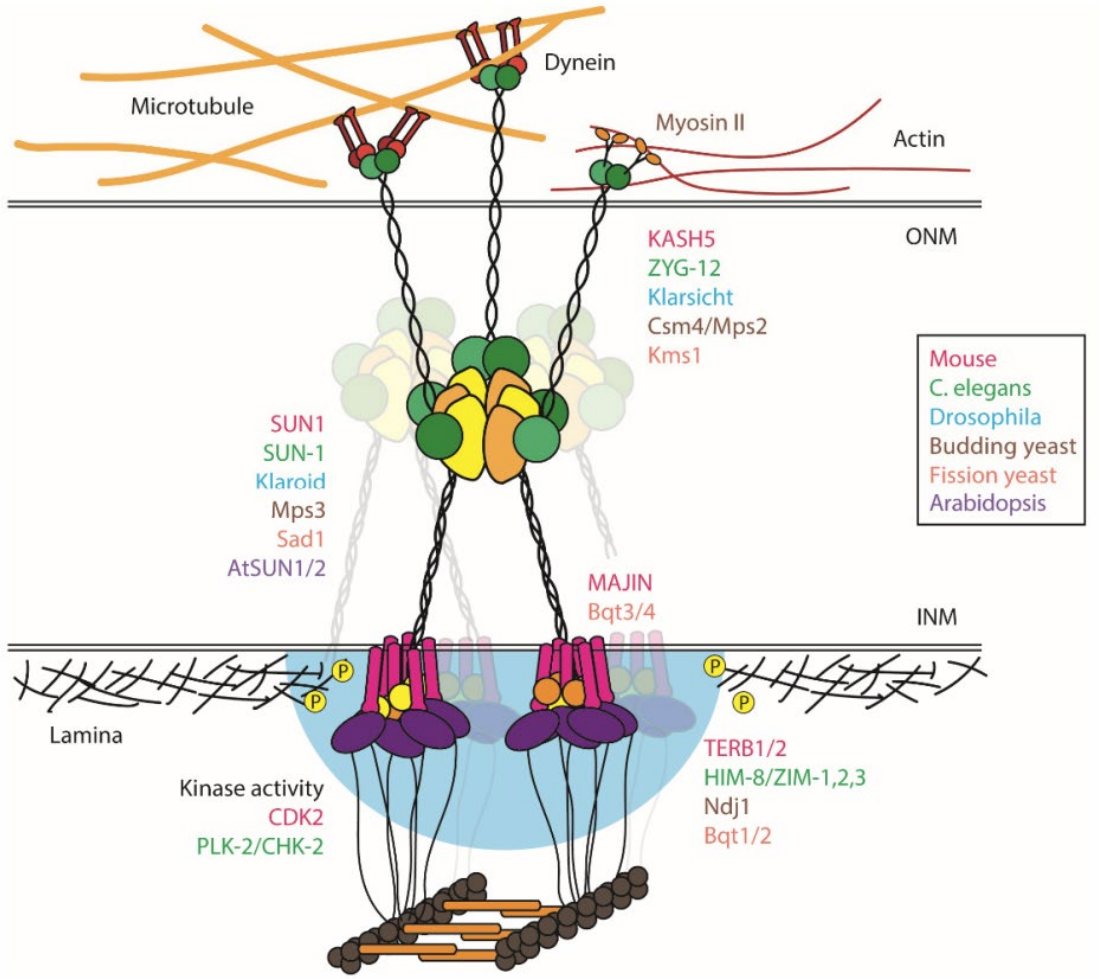

Figure 1. Schematic representation of meiotic chromosome–NE–cytoskeletal complexes in diverse species. The SUN domain forms a trimer, and an adjacent extended α-helical domain forms trimeric coiled-coils, while KASH domain proteins dimerize. SUN domain trimers can dimerize and are proposed to interact with KASH domains from different dimers to create branched complexes, which may contribute to the clustering of chromosome attachment sites during meiosis. The nucleoplasmic domain of SUN proteins interact with chromosomal proteins, which often depends on the expression of meiosis-specific adapter proteins. Small proteins that span the inner nuclear membrane, including MAJIN in most metazoans and Bqt3/4 in fission yeast, are also essential for the coupling of chromosomes to the LINC complex and/or clustering of LINC complexes (translucent structures in the background). Cytosolic domains of KASH domain proteins often interact with dynein or microtubules; however, in budding yeast, they link telomeres to Myosin II on actin filaments. CDK2 and PLK-2/CHK-2 kinases are recruited to chromosome–LINC complex attachment sites in mice and *C. elegans*, respectively, and their activities (blue cloud) are required for the connection of telomeres/Pairing Centers to LINC complexes. In *C. elegans*, phosphorylation of the nuclear lamina by PLK-2 liquefies or disrupts

the nuclear lamina to promote chromosome movements. In mice, CDK2 activity also limits promiscuous synapsis between nonhomologous chromosomes.

Chapter 1: MJL-1 is a nuclear envelope protein required for homologous chromosome pairing and regulation of synapsis during meiosis in *C. elegans*

This chapter is a slightly modified version of published work (H. J. Kim et al., 2023) and reproduced here with the permission of the copyright holder.

Summary

Interactions between chromosomes and LINC (linker of nucleoskeleton and cytoskeleton) complexes in the nuclear envelope (NE) promote homolog pairing and synapsis during meiosis. By tethering chromosomes to cytoskeletal motors, these connections lead to processive chromosome movements along the NE. This activity is usually mediated by telomeres, but in the nematode *Caenorhabditis elegans*, special chromosome regions called "pairing centers" (PCs) have acquired this meiotic function. Here, I identify a previously uncharacterized meiosis-specific NE protein, MJL-1 (MAJIN-Like-1), that is essential for interactions between PCs and LINC complexes in C. elegans. Mutations in *mjl-1* eliminate active chromosome movements during meiosis, resulting in nonhomologous synapsis and impaired homolog pairing. Fission yeast and mice also require NE proteins to connect chromosomes to LINC complexes. Extensive similarities in the molecular architecture of meiotic chromosome-NE attachments across eukaryotes suggest a common origin and/or functions of this architecture during meiosis.

Introduction

Sexual reproduction relies on meiosis, the specialized cell division program that produces haploid gametes. During meiosis, homologous chromosomes must pair, synapse, and undergo crossover recombination to segregate accurately. Upon meiotic entry, each replicated chromosome is assembled into an array of loops anchored to a linear structure known as the chromosome axis (Blat et al., 2002; Zickler & Kleckner, 1999). Pairing of homologs is gradually stabilized by assembly of a protein matrix, the synaptonemal complex (SC), between axes (Cahoon & Hawley, 2016; Page & Hawley, 2004; Zickler & Kleckner, 1999). SCs promote and regulate crossover recombination, which results in chiasmata, physical linkages between homologous chromosomes that persist until segregation and mediate bipolar alignment on the spindle (Kleckner, 2006; Page & Hawley, 2004; Zickler & Kleckner, 2015).

Chromosome pairing, synapsis, and recombination are promoted by nuclear envelope (NE)-associated chromosome dynamics during meiosis (Chua & Roeder, 1997; Conrad et al., 1997, 2008; Cooper et al., 1998; D.-Q. Ding et al., 2004; X. Ding et al., 2007). At meiotic entry, chromosomes become tethered to LINC (Linker of Nucleoskeleton and Cytoskeleton) complexes comprised of SUN and KASH domain proteins that span the two membranes of the NE (Hiraoka & Dernburg, 2009; Link & Jantsch, 2019). Cytoskeletal motors interact with LINC complexes on the cytoplasmic face of the NE, resulting in dramatic chromosome movements during early meiotic prophase (Chikashige et al., 1994; Hiraoka, 1998; Scherthan et al., 1996). This often leads to clustering of chromosome ends near cytoplasmic microtubule organizing centers (MTOCs) to form a chromosome configuration known as the "meiotic bouquet" (Hiraoka, 1998; Scherthan, 2001; Zickler & Kleckner, 1998). However, in meiocytes that lack focal MTOCs, such as those in *C. elegans*, clustering of the NE attachment sites is absent or less prominent (Rog & Dernburg, 2013; Wynne et al., 2012).

In the nematode *Caenorhabditis elegans*, specialized regions on each chromosome known as "Pairing Centers" (PCs) promote homolog pairing and initiate synapsis (MacQueen et al., 2005; McKim et al., 1988; Rog & Dernburg, 2013; Rosenbluth & Baillie, 1981; Villeneuve, 1994). Each PC recruits one of four meiosis-specific zinc finger proteins, ZIM-1, ZIM-2, ZIM-3, or HIM-8, through DNA binding sites present in clusters throughout the PC regions (Phillips et al., 2005, 2009; Phillips & Dernburg, 2006). During early meiotic prophase, PCs associate with LINC complexes comprised of SUN-1 and ZYG-12 (A. Penkner et al., 2007; Sato et al., 2009). ZYG-12 interacts with cytoplasmic dynein and perhaps other microtubule motors to drive processive movement of chromosomes that promote pairing and synapsis (Baudrimont et al., 2010; A. M. Penkner et al., 2009; Sato et al., 2009; Wynne et al., 2012).

In fission yeast, inner NE proteins Bqt3 and Bqt4 are required for tethering of telomeres to LINC complexes (Chikashige et al., 2006, 2009). In mouse spermatocytes, the small NE protein MAJIN (Membrane-Anchored Junction Protein) connects the meiosis-specific shelterin-binding proteins TERB1 and TERB2 to LINC complexes (Shibuya et al., 2014, 2015). Bqt4 and MAJIN share a similar structure, with a single transmembrane domain near their C termini (Hu et al., 2019; Shibuya et al., 2015). Homologs of the mouse protein MAJIN have been identified in many metazoans, but not in nematodes (Cruz et al., 2020).

Here I report the identification and characterization of a previously-uncharacterized meiosis-specific NE protein that is essential for interactions between PCs and LINC complexes in *C. elegans*. Based on the functions I have characterized, I named it MJL-1 (MAJIN-Like-1).

Results

MJL-1 is a previously-uncharacterized meiosis-specific NE protein

In *C. elegans*, defects in meiosis result in a High incidence of males (Him) phenotype due to nondisjunction of the *X* chromosome (Hodgkin et al., 1979); most meiotic mutants also produce many inviable embryos due to autosomal aneuploidy. I used an established "Green eggs and Him" screen based on a *xol-1p::gfp* reporter expressed in *XO* (male) embryos to identify hermaphrodites with elevated meiotic nondisjunction (Kelly et al., 2000, p. 2). Molecular lesions in the mutants were identified by outcrossing to the CB4856 Hawaiian strain, reisolating homozygous mutants, whole-genome sequencing of their progeny, and computational analysis to identify likely causal mutations (Doitsidou et al., 2010; Swan et al., 2002; Wicks et al., 2001). Most of the mutations I identified (50/52) were in genes previously shown to be important for meiosis, indicating that such Him screens are nearing saturation. Two mutations were found in previously-uncharacterized genes. One of these resulted in a premature stop codon in C17E4.4, which encodes a small protein with a single predicted transmembrane domain. Based on previous transcriptome data, this gene is specifically expressed in germline and arcade cells (Grün et al., 2014; Han et al., 2017; Spencer et al., 2011).

Using Cas9/CRISPR-based editing, I inserted an HA epitope tag at the N-terminus of the C17E4.4 protein. Hermaphrodites homozygous for this insertion produced a normal number of embryos and a slightly elevated frequency of male self-progeny (~1%, compared to 0.2% in wild-type broods). Immunofluorescence of the HA-tagged protein showed NE-specific localization throughout the meiotic region of the germline. The protein was undetectable in proliferating germline stem cells (GSCs) but was clearly observed at the NE upon meiotic entry and concentrated to form NE "patches" in transition zone (leptotene-zygotene) nuclei. Following synapsis, the protein redistributed throughout the NE and persisted until late pachytene (Figure 1A, 1B).

During pairing and synapsis, the zinc finger proteins HIM-8, ZIM-1, -2, and -3 (PC proteins) bind to PCs and interact with the LINC complex proteins SUN-1 and ZYG-12, which concentrate within the NE to form multiple patches. Immunofluorescence revealed that HA-tagged C17E4.4 colocalized with SUN-1 and all four PC proteins during this transient stage (Figure 1C).

Based on structural and functional similarities between C17E4.4 and mouse MAJIN (Shibuya et al., 2015), I named the gene *mjl-1 (majin-like-1)*. Although MJL-1 shares no discernible sequence homology with MAJIN, both are small, single-pass transmembrane proteins with similar meiosis-specific functions (below) (Figure 2A). MJL-1 is only weakly conserved within the genus *Caenorhabditis*, and its homologs have not yet been identified in other nematode genera, including those that express homologs of the PC proteins (Figure 3) (Rillo-Bohn et al., 2021).

MJL-1 is required for association of PCs with LINC complexes

The mutation identified in my screen, *mjl-1(ie142)*, is likely a null allele since it contains a stop codon before its transmembrane domain. I also obtained a deletion allele, *mjl-1(tm1651)*, from the Japanese National BioResource Project (NBRP) (Figure 2A). Hermaphrodites homozygous for either mutant allele produced very few viable self-progeny (< 1%), and among these, many were males (29% and 33%, statistically indistinguishable), indicative of extensive meiotic nondisjunction. At diakinesis, most oocytes in *mjl-1(ie142)* and *mjl-1(tm1651)*

hermaphrodites displayed 10-12 DAPI-staining bodies (Figure 2B), indicating that chromosomes failed to undergo crossing-over.

I tested whether MJL-1 is required for interaction between PCs and LINC complexes. Immunofluorescence revealed that in *mjl-1* mutants, SUN-1 did not colocalize with PC proteins or form NE patches in transition zone nuclei (Figure 2C). However, PC proteins still appeared to associate with the NE, suggesting that PC proteins may interact directly with the membrane or another NE protein (Figure 4). I crossed *mjl-1(ie142)* mutants to a strain expressing GFP-tagged HIM-8 (Wynne et al., 2012) to analyze chromosome movement. The average speed of HIM-8 foci in early meiotic nuclei was greatly reduced in the absence of MJL-1, from 59.8 nm/s in wild-type oocytes to 22.7 nm/s in *mjl-1(ie142)*, similar to my measurements for *sun-1(jf18)* (18.7 nm/s) (Figure 2D, 2E). Previous analysis has shown that *sun-1(jf18),* which results in a missense mutation (G311V) near the SUN domain, abrogates active chromosome movement (Baudrimont et al., 2010; A. M. Penkner et al., 2009). The residual movement in *mjl-1(ie142)* and *sun-1(jf18)* mutants is likely due to diffusion rather than active motility (Baudrimont et al., 2010; Woglar et al., 2013; Wynne et al., 2012). Thus, I conclude that interaction between PCs and LINC complexes is disrupted in *mjl-1* mutants.

MJL-1 is required to regulate synapsis

Loss of individual PC proteins delays synapsis of the corresponding chromosomes (Phillips et al., 2005; Phillips & Dernburg, 2006). However, in *mjl-1* mutants, I observed extensive synaptonemal complex (SC) assembly during early meiotic prophase, despite very low levels of homolog pairing. Labeling of specific chromosome loci confirmed that this synapsis occurs between nonhomologous chromosomes (Figure 5A, 5B). Similar promiscuous synapsis was observed in *sun-1(jf18)* mutants and following auxin-induced degradation of ZYG-12 (Figure 5A, 5B), consistent with other evidence that the interaction between PCs and LINC complexes regulates synapsis so that it occurs only between homologous chromosomes (A. Penkner et al., 2007; Sato et al., 2009). How these interactions prevent nonhomologous synapsis remains an open question (Sato et al., 2009).

MJL-1 depends on SUN-1 for its NE localization

Unexpectedly, I did not detect MJL-1 by immunofluorescence in *sun-1(ok1282)* null mutants or following auxin-induced degradation of SUN-1 (Figure 6A). The abundance of MJL-1 detected on western blots was also strongly reduced following auxin-induced degradation of SUN-1 (Figure 7). These findings indicate that SUN-1 is required for subcellular localization and/or stabilization of MJL-1. In contrast, neither the *sun-1(jf18)* missense mutation nor auxin-induced degradation of the KASH domain protein ZYG-12 disrupted the NE localization of MJL-1 (Figure 6A), indicating that neither chromosome movement nor ZYG-12 are required for association between MJL-1 and SUN-1. Co-immunoprecipitation of SUN-1 with MJL-1 further supports the idea that these proteins directly interact with each other (Figure 6B).

My genetic screen also identified a separation-of-function mutation in *sun-1* that resulted in meiotic phenotypes similar to *sun-1(jf18)* without disrupting the mitotic functions of SUN-1. This missense mutation, *sun-1(ie143)*, changes tyrosine 128 within the predicted transmembrane domain of SUN-1, very close to the perinuclear domain, to phenylalanine (Y128F). This conserved tyrosine residue lies near the C terminus of the predicted transmembrane domain in SUN-1 and may contribute to anchoring the transmembrane domain through interactions with phospholipid head groups (Chamberlain et al., 2004). In contrast to *sun-1(jf18)*, *sun-1(ie143)*

resulted in loss of MJL-1 protein from the NE (Figure 6C, 8). This suggests that SUN-1 and MJL-1 may interact through their transmembrane domains and/or adjacent regions in the perinuclear lumen (Figure 6D). These regions are relatively highly conserved among *Caenorhabditis* MJL-1 homologs (Figure 9).

MJL-1 was also detected in apoptotic nuclei in the loop region of the germline. These nuclei retain SUN-1 at their NE but not ZYG-12 (Figure 10), which may reflect disruption of the outer nuclear membrane during apoptosis, although this has not been directly demonstrated. The persistence of MJL-1 in these nuclei, together with my evidence that the protein requires SUN-1 for its localization to the NE (above) and connects PCs to SUN-1 (below), indicates that MJL-1 probably resides within the inner nuclear membrane with its N-terminal domain in the nucleoplasm, similar to mouse MAJIN (Shibuya et al., 2015).

MJL-1 associates with PC proteins

Sequence alignment of *Caenorhabditis* MJL-1 homologs revealed a short region of relatively high conservation enriched for acidic residues (Figure 11A). Using two crRNAs flanking this region, I generated an in-frame deletion of amino acids 34-49. The resulting MJL-$1^{\Delta acidic}$ protein was expressed and localized to the NE but did not colocalize with PCs (Figure 11A, 12). Animals homozygous for this deletion allele showed extensive nonhomologous synapsis, similar to *mjl-1* null mutants (Figure 13). Together with evidence that SUN-1 is essential for localization and stability of MJL-1 (above), this suggests that the mutant protein retains the ability to interact with SUN-1 but does not link PC proteins to SUN-1. In contrast, an in-frame deletion of MJL-1 amino acids 9-26, which are also fairly well conserved within MJL-1 homologs, led to no apparent defects (Figure 14). I tested whether the nucleoplasmic domain of MJL-1 interacts with PC proteins using a yeast two-hybrid assay and obtained negative results. However, this could be because PC proteins undergo post-translational modifications during meiosis that may be important for interactions with MJL-1.

The Polo-like kinase PLK-2 is recruited to PCs through Polo-box binding motifs in the PC proteins and is required for colocalization of PCs and the LINC complexes (Harper et al., 2011; Labella et al., 2011). In a kinase-dead *plk-2*(K65M) mutant (Brandt et al., 2020; Link et al., 2018), MJL-1 localized throughout the NE and did not associate with PC proteins (Figure 11B). This indicates that PLK-2 activity is required for association between PC proteins and MJL-1/SUN-1, but presumably not for interaction between MJL-1 and SUN-1. Recruitment of PLK-2 to PCs requires phosphorylation of PC proteins by CHK-2 (Y. Kim et al., 2015). Consistent with this, I found that auxin-induced degradation of CHK-2 also abrogated the colocalization of MJL-1 and PCs (Figure 11C).

I examined the localization of MJL-1 in worm strains expressing two mutant versions of HIM-8, the PC protein specific for the *X* chromosome: HIM-8^{T64A}, which does not recruit PLK-2 due to a point mutation in its Polo-box binding motif (Harper et al., 2011), and HIM-8^{S85F} (encoded by the *him-8(me4)* allele), which fails to recruit both CHK-2 and PLK-2 (Y. Kim et al., 2015), did not colocalize with patches of MJL-1 (Figure 11C). Taken together, I conclude that recruitment of PLK-2 to HIM-8 is required for association of the *X* chromosome PC with MJL-1/SUN-1. This is likely to be true for the autosomal PCs as well, since expression of $PLK2^{K65M}$ abrogates the formation of NE patches, but is more difficult to test since each of the ZIM proteins contains two Polo-box-interacting motifs.

MJL-1 directly promotes homolog pairing

Mutations in SC proteins prevent assembly of the SC, and thus prevent nonhomologous synapsis. Such mutations partially restore *X* chromosome pairing in *sun-1(jf18)* mutants (Sato et al., 2009). To assess the role of MJL-1 in pairing, I compared the extent of *X* chromosome pairing in *aid::zyg-12* following auxin treatment, *sun-1(jf18),* and *mjl-1(ie142),* all in the absence of synapsis. Loss of MJL-1 resulted in more severe pairing defects than depletion of ZYG-12 or the *sun-1(jf18)* mutation, indicating that connection of chromosomes to MJL-1 and LINC complexes promotes limited pairing even in the absence of rapid chromosome movements (Figure 15A, 15B). I also observed a reduction in nonhomologous associations between HIM-8 and other PCs in the absence of MJL-1 compared to *sun-1(jf18)* mutants, suggesting that MJL-1 promotes clustering of PCs (Figure 15C, 15D), which may be required for efficient pairing of homologous PCs (Figure 15E).

PLK-2 plays dual roles in homolog pairing

Interestingly, hermaphrodites expressing kinase-dead PLK-2^{K65M} or HIM-8^{T64A} displayed virtually no *X* chromosome pairing in the absence of synapsis, in contrast to *mjl-1* mutants (Figure 15A, 15B). This indicates that PLK-2 contributes to pairing beyond tethering PCs to MJL-1 during homolog pairing.

Phosphorylation of the nuclear lamina by PLK-2 promotes chromosome mobility along the NE during meiosis, likely by reducing homotypic interactions between LMN-1 proteins (Link et al., 2018). I tested whether mobilization of the lamina by PLK-2 accounts for its essential role in pairing by depleting LMN-1 using RNAi. This did not rescue *X* chromosome pairing in *syp-3(ok758)*; *him-8(T64A)* mutant, indicating that PLK-2 activity at PCs contributes to pairing through a lamin-independent mechanism (Figure 16).

In SC-deficient mutants, homologous PCs dissociate during late prophase (MacQueen et al., 2002, 2005). I found that this occurs concomitant with the disappearance of PLK-2 from PCs, indicating that PLK-2 activity is important to stabilize interactions between homologous PCs (Figure 17).

Discussion

Similarities and differences between MJL-1 and MAJIN

To date, homologs of MJL-1 are only detected within the genus *Caenorhabditis*. PC proteins have been detected in a few related nematode genera (Rillo-Bohn et al., 2021), but show rapid divergence, particularly in their N-terminal domains, which act as scaffolds to recruit kinases and may also directly interact with NE proteins. If PC proteins interact with MJL-1, as suggested by my findings, rapid coevolution of these proteins may account for my inability to detect MJL-1 homologs in other nematode species.

My evidence suggests that MJL-1 connects PC proteins to LINC complexes in *C. elegans*, although direct evidence for protein-protein interactions that mediate these attachments is currently lacking. Similarly, in mice, MAJIN connects shelterin-binding proteins TERB1 and TERB2 to LINC complexes (Shibuya et al., 2015; Y. Wang et al., 2019). MAJIN interacts with SUN1 through its nucleoplasmic domain (G. Wang et al., 2020), while MJL-1 and SUN-1 may interact through their transmembrane domains and/or perinuclear regions. In fission yeast, a direct interaction between NE proteins Bqt3 and -4 and LINC complexes has not been detected (Chikashige et al., 2009). Whereas MJL-1 requires PLK-2 activity to interact with PC proteins,

CDK2 activity is required for interaction between MAJIN and SUN1 in mice (Figure 18) (Tu et al., 2017; G. Wang et al., 2020).

Both mouse MAJIN and fission yeast Bqt4 contain N-terminal DNA-binding motifs that are required for recruitment of telomeres to the NE (Hu et al., 2019; Shibuya et al., 2015). The DNA binding motif of MAJIN has been implicated in "telomere cap exchange," whereby telomeres release shelterin and directly interact with TERB1, -2 and MAJIN (Shibuya et al., 2015). In contrast, MJL-1 lacks an apparent DNA-binding motif, and PCs in *C. elegans* appear to associate with the NE even in the absence of MJL-1 or SUN-1. Thus, while MJL-1 shares similarity with MAJIN and Bqt4, the way it connects to chromosomes is likely distinct from vertebrate MAJIN proteins. Together with the lack of apparent sequence homology, this makes it unclear whether MJL-1 is evolutionarily related to other meiotic NE proteins.

Roles of MJL-1 and LINC complexes in regulation of pairing and synapsis

Connection of PCs to LINC complexes inhibits inappropriate synapsis in *C. elegans* (A. Penkner et al., 2007; Sato et al., 2009). This is consistent with observations that this association and resulting chromosome movements persist after pairing of homologs, which occurs soon after entry into meiosis. Loss of telomere-LINC complex connections and/or chromosome movements in mice also leads to some nonhomologous synapsis, albeit not as extensive as in *C. elegans* (X. Ding et al., 2007; Horn et al., 2013; Shibuya et al., 2015; Y. Wang et al., 2019). Nevertheless, loss of CDK2, which is associated with LINC complexes during early prophase, results in extensive nonhomologous synapsis in mouse spermatocytes (Chen et al., 2021; Mikolcevic et al., 2016; Tu et al., 2017; Viera et al., 2009), suggesting that regulation of synapsis may be a general role of chromosome-LINC complex attachments, despite some differences in the details of this regulation between organisms.

Intriguingly, telomeric attachments in mammals and PC attachments in *C. elegans* each require a kinase (CDK2 and PLK-2, respectively) that is also involved in crossover regulation, suggesting that coordination between chromosome attachments sites and CO intermediates may be a conserved feature of meiosis (Ashley et al., 2001, p. 2; Palmer et al., 2020; Woglar & Villeneuve, 2018)

Materials and Methods

C. elegans strains

N2 Bristol was used as the wild-type *C. elegans* strain; all mutations described here were generated in this background. The Hawaiian isolate CB4856 was used for genetic mapping. All strains were maintained at 20°C under standard laboratory conditions. The following mutations and balancers were used: *mjl-1(ie142) (I:9419844; C to T)*, *mjl-1(tm1651)*, *mjl-1(Δacidic), sun-1(jf18), sun-1(ok1282), sun-1(ie143) (V:13193099; T to A), syp-2(ok307), syp-3(ok758), him-8(me4), him-8(T64A)* (Harper et al., 2011), *plk-2(K65M)::3xflag* (Brandt et al., 2020), *nT1[qIs51] (IV;V)*, *hT2 [bli-4(e937) let-?(q782) qIs48] (I;III)*. The following constructs were used for auxin-inducible degradation: *aid::ha::zyg-12* and *aid::v5::sun-1*, *ha::aid::chk-2* where "aid" designates a 44-amino acid degron sequence (Zhang et al., 2015).

To generate *ha::mjl-1* strains, single-stranded (ss) DNA templates were designed to insert one or two copies of the HA tag at the N-terminus of MJL-1, separated by a flexible linker (GGGGS). These were co-injected with Cas9-NLS prebound to duplexed gRNAs, as well as a

gRNA and ssDNA template for co-CRISPR of *dpy-10* (Arribere et al., 2014). (Final concentrations: *dpy-10* crRNA, 20 μM; *mjl-1* crRNA, 50 μM; trRNA, 40 μM; Cas9-NLS protein, 20 μM; *dpy-10* repair template, 1 μM, *mjl-1* repair template, 1 μM). To label MJL-1 using the split-GFP system and V5 tag, a template to insert GFP11 and V5 was co-injected with the Cas9-gRNA RNP complex into DUP223 *glh-1(sam129[glh-1::T2A::sGFP2(1-10)*]) (Goudeau et al., 2021). Essentially the same procedure was used to generate in-frame deletions in *mjl-1*, except that two gRNAs were used.

Auxin-induced degradation

A stock solution containing 250 mM indole acetic acid (IAA, auxin) in EtOH was diluted to 1 mM in NGM agar just before pouring plates. After drying overnight, plates were seeded with *E. coli*. OP50 freshly cultured overnight to saturation in 50mL of LB was pelleted by centrifugation at 3,000xg for 5 min and resuspended in 500 μl of M9 buffer containing 1 mM auxin. This concentrated bacteria + auxin was spread on the plates and allowed to grow at room temperature for 1-2 days. To deplete degron-tagged proteins, young adult animals aged 24-48 h from L4 were picked onto these plates and analyzed 4-24 h later.

RNA interference

Carbenicillin and IPTG were added to cooled NGM agar to 200 μg/mL and 1 mM final, respectively, just before pouring plates. Clones from the Ahringer laboratory (Fraser et al., 2000) were freshly cultured overnight to saturation in 10mL of LB containing 200 μg/mL carbenicillin. Then the culture was pelleted by centrifugation at 3,000xg for 5 min and resuspended in 50 μl of M9 buffer. Concentrated *E. coli* was spread on the plates and allowed to grow at 37°C for 1 day. For feeding, young adult animals aged 24-48 h from L4 were picked onto these plates and analyzed 24-48 h later. LMN-1 depletion was confirmed by shrunken nuclei in late pachytene-diplotene.

Cytological Methods

Immunofluorescence and *in situ* hybridization were performed essentially as described previously (Dernburg et al., 1998). In brief: young adult worms were cut with a scalpel blade in egg buffer containing 0.05% tetramisole to release their gonads on slides, fixed in 1% formaldehyde in egg buffer for 2 min, transferred to tubes, and incubated with methanol pre-chilled to -30°C for 5 min. The tissue was then washed 3x in PBS containing 0.1% Tween 20 (PBST) at room temperature. Tissues were blocked using 1x Roche Blocking Reagent in PBST for 20 min. Primary antibodies were diluted into the same blocking solution and incubated with the tissues overnight at 4°C. Secondary antibodies were prepared in the blocking solution (1:200), mixed with samples, and incubated 1-2 h at room temperature. Samples were mounted in Prolong Diamond mounting medium containing DAPI (Invitrogen).

For fluorescence in situ hybridization, dissected gonads were fixed in 2% formaldehyde in egg buffer for 5 min, incubated with methanol pre-chilled to -30°C for 5 min, and washed 3x in 2x SSC containing 0.1% Tween 20 (2x SSCT) at room temperature. The tissue was then incubated in 50% formamide in 2x SSCT overnight at 37°C. 0.5-1 μl of 100μM fluorophore-conjugated oligonucleotide probes (IDT) “IV-2” (Adilardi & Dernburg, 2022) were added to 100 μl of hybridization buffer (50% formamide and 10% dextran sulfate in 2x SSCT) and tissues were moved into this mix, incubated 2-3 min at 91°C and then overnight at 37°C. The tissues

were washed 3x in 2x SSCT at room temperature and mounted as for immunofluorescence (above).

Images were acquired using a DeltaVision Elite wide-field microscope system (GE) with a 100X 1.40 or 1.45 NA oil-immersion objective, or CSU-W1 SoRa confocal microscope system equipped with a 100X, 1.49 NA oil-immersion objective (Intelligent Imaging Innovations, Inc. [3i]). Deconvolution, projection, and analysis were performed using the softWoRx package or Slidebook 6 (3i).

Antibodies

All antibodies used in this study were obtained from commercial sources or have been previously described. They include the following antibodies and dilutions: mouse monoclonal anti-HA (Invitrogen 2-2.2.14) (1:250), mouse monoclonal anti-V5 (Invitrogen 46-0705) (1:250), and rabbit polyclonal anti-V5 (Sigma V8137) (1:250). Custom polyclonal antibodies included rabbit anti-SUN-1 (1:250) (Sato et al., 2009), rat anti-HIM-8 (1:500) (Phillips et al., 2005), rabbit anti-SYP-2 (1:500) (Colaiácovo et al., 2003), rabbit anti-phospho-HIM-8/ZIMs (1:1000) (Y. Kim et al., 2015) guinea pig anti-ZIM-2 (1:2000, affinity purified). Fluorophore-conjugated secondary antibodies were purchased from Jackson ImmunoResearch and used at 1:200 dilution.

Quantification of homolog pairing

3D distances between HIM-8 or FISH signals were measured using the "Measure Distance" tool in softWoRx. Foci closer than 0.6 μm were considered to be paired. I defined this threshold based on the maximum width of PC protein patches associated with paired chromosomes in wild-type oocytes. For analysis of pairing of FISH signals, I included only nuclei displaying two clear foci.

***In vivo* imaging and quantification of chromosome movement**

3D confocal image acquisition was performed essentially as described (Wynne et al., 2012) using a Marianas spinning-disc confocal microscope system equipped with a 100X, 1.46 NA oil-immersion objective (Intelligent Imaging Innovations, Inc. [3i]). Exposure time was set to 100-150 ms, depending on the brightness of foci. Stacks of 10–20 optical sections at 0.5 μm *z*-spacing were acquired every 5 s for a total of 5-10 min. 3D time-lapse images were analyzed using Imaris 9.2.0 (Bitplane). Background drift was corrected using the "Reference Frame" tool. Foci were detected using the "Spots" tool with an estimated XY diameter of 1.33 μm and filtered with "Quality" and "Intensity Sum" (Imaris). Tracks were obtained with max distance of 1.75 μm and max gap of 3. Tracks from the background noise were manually removed. *p*-values were calculated using the pairwise *t*-test with *post-hoc* Bonferroni correction.

Western blots

200 young adult animals aged 48 h from the L4 stage were picked into TBST buffer, washed three times, and then incubated in 1x SDS sample buffer at 50°C for 10 min. Samples were vortexed for 2–3 min until no visible solid material remained. Proteins were separated using SDS-PAGE gradient gels (Invitrogen NuPAGE™ 4-12%, Bis-Tris, 1.0 mm, 10-well, MES SDS running buffer) and transferred to Amersham Hybond P 0.45 PVDF Membranes. The membrane was cut into slices and probed with mouse anti-HA (Invitrogen 2-2.2.14) (1:1000), mouse anti-V5 (Invitrogen) (1:1000), or mouse anti-α-tubulin (Sigma DM1A) (1:5000) antibodies overnight at 4°C. HRP-conjugated donkey anti-mouse secondary antibody (Jackson

ImmunoResearch) (1:10,000) was incubated with membranes 1 h at room temperature. SuperSignal West Femto Maximum Sensitivity Substrate (Thermo) was used as HRP substrates for detection. ImageJ Mean Gray Value was used for Quantification.

Immunoprecipitation

Approximately 200,000 young adult animals grown in liquid culture, aged 48 h from the L4 stage, were collected by centrifugation and homogenized with a Douncer in 1x Egg buffer with 250 mM sucrose until 90% of adults were broken. Debris was precipitated by centrifugation at 50xg for 2 min. The supernatant was filtered using 40-micron filters followed by 20-micron filters to remove additional debris. Nuclei were pelleted by centrifugation at 2000xg for 10 min and resuspended in 800 µl of lysis buffer (130 mM NaCl, 2.5mM $MgCl_2$, 25 mM HEPES pH 7.4, 2 mM EGTA, 1% Triton X-100, with Roche cOmplete Mini EDTA-free protease inhibitor cocktail). Nuclei were sonicated in a Bioruptor Twin sonication bath (Diagenode, Denville, NJ) at 4°C for 30-min periods of alternating 30 s on high power and 30 s off. The resulting lysate was centrifuged at 10,000xg for 2 min, and supernatant was incubated with antibody-coated Dynabeads™ Protein A (Invitrogen) at 4°C for 2 hr and eluted in urea solution (6M urea, 6% SDS, and 5% 2-Mercaptoethanol).

References

Adilardi, R. S., & Dernburg, A. F. (2022). Robust, versatile DNA FISH probes for chromosome-specific repeats in Caenorhabditis elegans and Pristionchus pacificus. *G3 (Bethesda, Md.)*. https://doi.org/10.1093/g3journal/jkac121

Arribere, J. A., Bell, R. T., Fu, B. X. H., Artiles, K. L., Hartman, P. S., & Fire, A. Z. (2014). Efficient Marker-Free Recovery of Custom Genetic Modifications with CRISPR/Cas9 in Caenorhabditis elegans. *Genetics*, *198*(3), 837–846. https://doi.org/10.1534/genetics.114.169730

Ashley, T., Walpita, D., & Rooij, D. G. de. (2001). Localization of two mammalian cyclin dependent kinases during mammalian meiosis. *Journal of Cell Science*, *114*(Pt 4), 685–693. https://doi.org/10.1242/jcs.114.4.685

Baudrimont, A., Penkner, A., Woglar, A., Machacek, T., Wegrostek, C., Gloggnitzer, J., Fridkin, A., Klein, F., Gruenbaum, Y., Pasierbek, P., & Jantsch, V. (2010). Leptotene/zygotene chromosome movement via the SUN/KASH protein bridge in Caenorhabditis elegans. *PLoS Genetics*, *6*(11), e1001219. https://doi.org/10.1371/journal.pgen.1001219

Blat, Y., Protacio, R. U., Hunter, N., & Kleckner, N. (2002). Physical and functional interactions among basic chromosome organizational features govern early steps of meiotic chiasma formation. *Cell*, *111*(6), 791–802. https://doi.org/10.1016/s0092-8674(02)01167-4

Brandt, J. N., Hussey, K. A., & Kim, Y. (2020). Spatial and temporal control of targeting Polo-like kinase during meiotic prophase. *The Journal of Cell Biology*, *219*(11), Article 11. https://doi.org/10.1083/jcb.202006094

Cahoon, C. K., & Hawley, R. S. (2016). Regulating the construction and demolition of the synaptonemal complex. *Nature Structural & Molecular Biology*, *23*(5), Article 5. https://doi.org/10.1038/nsmb.3208

Chamberlain, A. K., Lee, Y., Kim, S., & Bowie, J. U. (2004). Snorkeling Preferences Foster an Amino Acid Composition Bias in Transmembrane Helices. *Journal of Molecular Biology*, *339*(2), 471–479. https://doi.org/10.1016/j.jmb.2004.03.072

Chen, Y., Wang, Y., Chen, J., Zuo, W., Fan, Y., Huang, S., Liu, Y., Chen, G., Li, Q., Li, J., Wu, J., Bian, Q., Huang, C., & Lei, M. (2021). The SUN1-SPDYA interaction plays an essential role in meiosis prophase I. *Nature Communications*, *12*(1), Article 1. https://doi.org/10.1038/s41467-021-23550-w

Chikashige, Y., Ding, D. Q., Funabiki, H., Haraguchi, T., Mashiko, S., Yanagida, M., & Hiraoka, Y. (1994). Telomere-led premeiotic chromosome movement in fission yeast. *Science (New York, N.Y.)*, *264*(5156), Article 5156. https://doi.org/10.1126/science.8146661

Chikashige, Y., Tsutsumi, C., Yamane, M., Okamasa, K., Haraguchi, T., & Hiraoka, Y. (2006). Meiotic proteins bqt1 and bqt2 tether telomeres to form the bouquet arrangement of chromosomes. *Cell*, *125*(1), Article 1. https://doi.org/10.1016/j.cell.2006.01.048

Chikashige, Y., Yamane, M., Okamasa, K., Tsutsumi, C., Kojidani, T., Sato, M., Haraguchi, T., & Hiraoka, Y. (2009). Membrane proteins Bqt3 and -4 anchor telomeres to the nuclear envelope to ensure chromosomal bouquet formation. *The Journal of Cell Biology*, *187*(3), Article 3. https://doi.org/10.1083/jcb.200902122

Chua, P. R., & Roeder, G. S. (1997). Tam1, a telomere-associated meiotic protein, functions in chromosome synapsis and crossover interference. *Genes & Development*, *11*(14), Article 14. https://doi.org/10.1101/gad.11.14.1786

Colaiácovo, M. P., MacQueen, A. J., Martinez-Perez, E., McDonald, K., Adamo, A., Volpe, A. L., & Villeneuve, A. M. (2003). Synaptonemal complex assembly in C. elegans is dispensable for loading strand-exchange proteins but critical for proper completion of recombination. *Developmental Cell*, *5*(3), 463–474. https://doi.org/10.1016/s1534-5807(03)00232-6

Conrad, M. N., Dominguez, A. M., & Dresser, M. E. (1997). Ndj1p, a Meiotic Telomere Protein Required for Normal Chromosome Synapsis and Segregation in Yeast. *Science*. https://doi.org/10.1126/science.276.5316.1252

Conrad, M. N., Lee, C.-Y., Chao, G., Shinohara, M., Kosaka, H., Shinohara, A., Conchello, J.-A., & Dresser, M. E. (2008). Rapid Telomere Movement in Meiotic Prophase Is Promoted By NDJ1, MPS3, and CSM4 and Is Modulated by Recombination. *Cell*, *133*(7), Article 7. https://doi.org/10.1016/j.cell.2008.04.047

Cooper, J. P., Watanabe, Y., & Nurse, P. (1998). Fission yeast Taz1 protein is required for meiotic telomere clustering and recombination. *Nature*, *392*(6678), Article 6678. https://doi.org/10.1038/33947

Cruz, I. da, Brochier-Armanet, C., & Benavente, R. (2020). The TERB1-TERB2-MAJIN complex of mouse meiotic telomeres dates back to the common ancestor of metazoans. *BMC Evolutionary Biology*, *20*(1), Article 1. https://doi.org/10.1186/s12862-020-01612-9

Dernburg, A. F., McDonald, K., Moulder, G., Barstead, R., Dresser, M., & Villeneuve, A. M. (1998). Meiotic recombination in C. elegans initiates by a conserved mechanism and is dispensable for homologous chromosome synapsis. *Cell*, *94*(3), 387–398. https://doi.org/10.1016/s0092-8674(00)81481-6

Ding, D.-Q., Yamamoto, A., Haraguchi, T., & Hiraoka, Y. (2004). Dynamics of Homologous Chromosome Pairing during Meiotic Prophase in Fission Yeast. *Developmental Cell*, *6*(3), Article 3. https://doi.org/10.1016/S1534-5807(04)00059-0

Ding, X., Xu, R., Yu, J., Xu, T., Zhuang, Y., & Han, M. (2007). SUN1 is required for telomere attachment to nuclear envelope and gametogenesis in mice. *Developmental Cell*, *12*(6), Article 6. https://doi.org/10.1016/j.devcel.2007.03.018

Doitsidou, M., Poole, R. J., Sarin, S., Bigelow, H., & Hobert, O. (2010). C. elegans Mutant Identification with a One-Step Whole-Genome-Sequencing and SNP Mapping Strategy. *PLoS ONE*, *5*(11), e15435. https://doi.org/10.1371/journal.pone.0015435

Fraser, A. G., Kamath, R. S., Zipperlen, P., Martinez-Campos, M., Sohrmann, M., & Ahringer, J. (2000). Functional genomic analysis of C. elegans chromosome I by systematic RNA interference. *Nature*, *408*(6810), 325–330. https://doi.org/10.1038/35042517

Goudeau, J., Sharp, C. S., Paw, J., Savy, L., Leonetti, M. D., York, A. G., Updike, D. L., Kenyon, C., & Ingaramo, M. (2021). Split-wrmScarlet and split-sfGFP: tools for faster, easier fluorescent labeling of endogenous proteins in Caenorhabditis elegans. *Genetics*, *217*(4), iyab014. https://doi.org/10.1093/genetics/iyab014

Grün, D., Kirchner, M., Thierfelder, N., Stoeckius, M., Selbach, M., & Rajewsky, N. (2014). Conservation of mRNA and Protein Expression during Development of C. elegans. *Cell Reports*, *6*(3), 565–577. https://doi.org/10.1016/j.celrep.2014.01.001

Han, S., Schroeder, E. A., Silva-García, C. G., Hebestreit, K., Mair, W. B., & Brunet, A. (2017). Mono-unsaturated fatty acids link H3K4me3 modifiers to C. elegans lifespan. *Nature*, *544*(7649), 185–190. https://doi.org/10.1038/nature21686

Harper, N. C., Rillo, R., Jover-Gil, S., Assaf, Z. J., Bhalla, N., & Dernburg, A. F. (2011). Pairing centers recruit a Polo-like kinase to orchestrate meiotic chromosome dynamics in C.

elegans. *Developmental Cell*, *21*(5), Article 5. https://doi.org/10.1016/j.devcel.2011.09.001

Hiraoka, Y. (1998). Meiotic telomeres: A matchmaker for homologous chromosomes. *Genes to Cells: Devoted to Molecular & Cellular Mechanisms*, *3*(7), Article 7. https://doi.org/10.1046/j.1365-2443.1998.00205.x

Hiraoka, Y., & Dernburg, A. F. (2009). The SUN rises on meiotic chromosome dynamics. *Developmental Cell*, *17*(5), Article 5. https://doi.org/10.1016/j.devcel.2009.10.014

Hodgkin, J., Horvitz, H. R., & Brenner, S. (1979). Nondisjunction Mutants of the Nematode CAENORHABDITIS ELEGANS. *Genetics*, *91*(1), 67–94. https://doi.org/10.1093/genetics/91.1.67

Horn, H. F., Kim, D. I., Wright, G. D., Wong, E. S. M., Stewart, C. L., Burke, B., & Roux, K. J. (2013). A mammalian KASH domain protein coupling meiotic chromosomes to the cytoskeleton. *The Journal of Cell Biology*, *202*(7), Article 7. https://doi.org/10.1083/jcb.201304004

Hu, C., Inoue, H., Sun, W., Takeshita, Y., Huang, Y., Xu, Y., Kanoh, J., & Chen, Y. (2019). The Inner Nuclear Membrane Protein Bqt4 in Fission Yeast Contains a DNA-Binding Domain Essential for Telomere Association with the Nuclear Envelope. *Structure (London, England: 1993)*, *27*(2), 335-343.e3. https://doi.org/10.1016/j.str.2018.10.010

Kelly, K. O., Dernburg, A. F., Stanfield, G. M., & Villeneuve, A. M. (2000). Caenorhabditis elegans msh-5 is required for both normal and radiation-induced meiotic crossing over but not for completion of meiosis. *Genetics*, *156*(2), 617–630. https://doi.org/10.1093/genetics/156.2.617

Kim, H. J., Liu, C., Zhang, L., & Dernburg, A. F. (2023). MJL-1 is a nuclear envelope protein required for homologous chromosome pairing and regulation of synapsis during meiosis in *C. elegans*. *Science Advances*, *9*(6), eadd1453. https://doi.org/10.1126/sciadv.add1453

Kim, Y., Kostow, N., & Dernburg, A. F. (2015). The Chromosome Axis Mediates Feedback Control of CHK-2 to Ensure Crossover Formation in C. elegans. *Developmental Cell*, *35*(2), Article 2. https://doi.org/10.1016/j.devcel.2015.09.021

Kleckner, N. (2006). Chiasma formation: Chromatin/axis interplay and the role(s) of the synaptonemal complex. *Chromosoma*, *115*(3), 175–194. https://doi.org/10.1007/s00412-006-0055-7

Labella, S., Woglar, A., Jantsch, V., & Zetka, M. (2011). Polo kinases establish links between meiotic chromosomes and cytoskeletal forces essential for homolog pairing. *Developmental Cell*, *21*(5), Article 5. https://doi.org/10.1016/j.devcel.2011.07.011

Link, J., & Jantsch, V. (2019). Meiotic chromosomes in motion: A perspective from Mus musculus and Caenorhabditis elegans. *Chromosoma*, *128*(3), Article 3. https://doi.org/10.1007/s00412-019-00698-5

Link, J., Paouneskou, D., Velkova, M., Daryabeigi, A., Laos, T., Labella, S., Barroso, C., Piñol, S. P., Montoya, A., Kramer, H., Woglar, A., Baudrimont, A., Markert, S. M., Stigloher, C., Martinez-Perez, E., Dammermann, A., Alsheimer, M., Zetka, M., & Jantsch, V. (2018). Transient and Partial Nuclear Lamina Disruption Promotes Chromosome Movement in Early Meiotic Prophase. *Developmental Cell*, *45*(2), Article 2. https://doi.org/10.1016/j.devcel.2018.03.018

MacQueen, A. J., Colaiácovo, M. P., McDonald, K., & Villeneuve, A. M. (2002). Synapsis-dependent and -independent mechanisms stabilize homolog pairing during meiotic

prophase in *C. elegans*. *Genes & Development*, *16*(18), 2428–2442. https://doi.org/10.1101/gad.1011602

MacQueen, A. J., Phillips, C. M., Bhalla, N., Weiser, P., Villeneuve, A. M., & Dernburg, A. F. (2005). Chromosome sites play dual roles to establish homologous synapsis during meiosis in C. elegans. *Cell*, *123*(6), Article 6. https://doi.org/10.1016/j.cell.2005.09.034

McKim, K. S., Howell, A. M., & Rose, A. M. (1988). The effects of translocations on recombination frequency in Caenorhabditis elegans. *Genetics*, *120*(4), 987–1001. https://doi.org/10.1093/genetics/120.4.987

Mikolcevic, P., Isoda, M., Shibuya, H., Barrantes, I. del B., Igea, A., Suja, J. A., Shackleton, S., Watanabe, Y., & Nebreda, A. R. (2016). Essential role of the Cdk2 activator RingoA in meiotic telomere tethering to the nuclear envelope. *Nature Communications*, *7*(1), Article 1. https://doi.org/10.1038/ncomms11084

Page, S. L., & Hawley, R. S. (2004). The genetics and molecular biology of the synaptonemal complex. *Annual Review of Cell and Developmental Biology*, *20*, 525–558. https://doi.org/10.1146/annurev.cellbio.19.111301.155141

Palmer, N., Talib, S. Z. A., Singh, P., Goh, C. M. F., Liu, K., Schimenti, J. C., & Kaldis, P. (2020). A novel function for CDK2 activity at meiotic crossover sites. *PLoS Biology*, *18*(10), Article 10. https://doi.org/10.1371/journal.pbio.3000903

Penkner, A. M., Fridkin, A., Gloggnitzer, J., Baudrimont, A., Machacek, T., Woglar, A., Csaszar, E., Pasierbek, P., Ammerer, G., Gruenbaum, Y., & Jantsch, V. (2009). Meiotic Chromosome Homology Search Involves Modifications of the Nuclear Envelope Protein Matefin/SUN-1. *Cell*, *139*(5), Article 5. https://doi.org/10.1016/j.cell.2009.10.045

Penkner, A., Tang, L., Novatchkova, M., Ladurner, M., Fridkin, A., Gruenbaum, Y., Schweizer, D., Loidl, J., & Jantsch, V. (2007). The Nuclear Envelope Protein Matefin/SUN-1 Is Required for Homologous Pairing in C. elegans Meiosis. *Developmental Cell*, *12*(6), Article 6. https://doi.org/10.1016/j.devcel.2007.05.004

Phillips, C. M., & Dernburg, A. F. (2006). A family of zinc-finger proteins is required for chromosome-specific pairing and synapsis during meiosis in C. elegans. *Developmental Cell*, *11*(6), Article 6. https://doi.org/10.1016/j.devcel.2006.09.020

Phillips, C. M., Meng, X., Zhang, L., Chretien, J. H., Urnov, F. D., & Dernburg, A. F. (2009). Identification of chromosome sequence motifs that mediate meiotic pairing and synapsis in C. elegans. *Nature Cell Biology*, *11*(8), 934–942. https://doi.org/10.1038/ncb1904

Phillips, C. M., Wong, C., Bhalla, N., Carlton, P. M., Weiser, P., Meneely, P. M., & Dernburg, A. F. (2005). HIM-8 Binds to the X Chromosome Pairing Center and Mediates Chromosome-Specific Meiotic Synapsis. *Cell*, *123*(6), Article 6. https://doi.org/10.1016/j.cell.2005.09.035

Rillo-Bohn, R., Adilardi, R., Mitros, T., Avşaroğlu, B., Stevens, L., Köhler, S., Bayes, J., Wang, C., Lin, S., Baskevitch, K. A., Rokhsar, D. S., & Dernburg, A. F. (2021). Analysis of meiosis in Pristionchus pacificus reveals plasticity in homolog pairing and synapsis in the nematode lineage. *ELife*, *10*. https://doi.org/10.7554/eLife.70990

Rog, O., & Dernburg, A. F. (2013). Chromosome pairing and synapsis during Caenorhabditis elegans meiosis. *Current Opinion in Cell Biology*, *25*(3), Article 3. https://doi.org/10.1016/j.ceb.2013.03.003

Rosenbluth, R. E., & Baillie, D. L. (1981). The genetic analysis of a reciprocal translocation, eT1(III; V), in Caenorhabditis elegans. *Genetics*, *99*(3–4), 415–428. https://doi.org/10.1093/genetics/99.3-4.415

Sato, A., Isaac, B., Phillips, C. M., Rillo, R., Carlton, P. M., Wynne, D. J., Kasad, R. A., & Dernburg, A. F. (2009). Cytoskeletal forces span the nuclear envelope to coordinate meiotic chromosome pairing and synapsis. *Cell*, *139*(5), Article 5. https://doi.org/10.1016/j.cell.2009.10.039

Scherthan, H. (2001). A bouquet makes ends meet. *Nature Reviews. Molecular Cell Biology*, *2*(8), Article 8. https://doi.org/10.1038/35085086

Scherthan, H., Weich, S., Schwegler, H., Heyting, C., Härle, M., & Cremer, T. (1996). Centromere and telomere movements during early meiotic prophase of mouse and man are associated with the onset of chromosome pairing. *The Journal of Cell Biology*, *134*(5), 1109–1125. https://doi.org/10.1083/jcb.134.5.1109

Shibuya, H., Hernández-Hernández, A., Morimoto, A., Negishi, L., Höög, C., & Watanabe, Y. (2015). MAJIN Links Telomeric DNA to the Nuclear Membrane by Exchanging Telomere Cap. *Cell*, *163*(5), Article 5. https://doi.org/10.1016/j.cell.2015.10.030

Shibuya, H., Ishiguro, K., & Watanabe, Y. (2014). The TRF1-binding protein TERB1 promotes chromosome movement and telomere rigidity in meiosis. *Nature Cell Biology*, *16*(2), Article 2. https://doi.org/10.1038/ncb2896

Spencer, W. C., Zeller, G., Watson, J. D., Henz, S. R., Watkins, K. L., McWhirter, R. D., Petersen, S., Sreedharan, V. T., Widmer, C., Jo, J., Reinke, V., Petrella, L., Strome, S., Stetina, S. E. V., Katz, M., Shaham, S., Rätsch, G., & Miller, D. M. (2011). A spatial and temporal map of C. elegans gene expression. *Genome Research*, *21*(2), 325–341. https://doi.org/10.1101/gr.114595.110

Swan, K. A., Curtis, D. E., McKusick, K. B., Voinov, A. V., Mapa, F. A., & Cancilla, M. R. (2002). High-throughput gene mapping in Caenorhabditis elegans. *Genome Research*, *12*(7), 1100–1105. https://doi.org/10.1101/gr.208902

Tu, Z., Bayazit, M. B., Liu, H., Zhang, J., Busayavalasa, K., Risal, S., Shao, J., Satyanarayana, A., Coppola, V., Tessarollo, L., Singh, M., Zheng, C., Han, C., Chen, Z., Kaldis, P., Gustafsson, J.-Å., & Liu, K. (2017). Speedy A-Cdk2 binding mediates initial telomere-nuclear envelope attachment during meiotic prophase I independent of Cdk2 activation. *Proceedings of the National Academy of Sciences of the United States of America*, *114*(3), Article 3. https://doi.org/10.1073/pnas.1618465114

Viera, A., Rufas, J. S., Martínez, I., Barbero, J. L., Ortega, S., & Suja, J. A. (2009). CDK2 is required for proper homologous pairing, recombination and sex-body formation during male mouse meiosis. *Journal of Cell Science*, *122*(12), Article 12. https://doi.org/10.1242/jcs.046706

Villeneuve, A. M. (1994). A cis-acting locus that promotes crossing over between X chromosomes in Caenorhabditis elegans. *Genetics*, *136*(3), 887–902. https://doi.org/10.1093/genetics/136.3.887

Wang, G., Wu, X., Zhou, L., Gao, S., Yun, D., Liang, A., & Sun, F. (2020). Tethering of Telomeres to the Nuclear Envelope Is Mediated by SUN1-MAJIN and Possibly Promoted by SPDYA-CDK2 During Meiosis. *Frontiers in Cell and Developmental Biology*, *8*. https://doi.org/10.3389/fcell.2020.00845

Wang, Y., Chen, Y., Chen, J., Wang, L., Nie, L., Long, J., Chang, H., Wu, J., Huang, C., & Lei, M. (2019). The meiotic TERB1-TERB2-MAJIN complex tethers telomeres to the nuclear envelope. *Nature Communications*, *10*(1), Article 1. https://doi.org/10.1038/s41467-019-08437-1

Wicks, S. R., Yeh, R. T., Gish, W. R., Waterston, R. H., & Plasterk, R. H. (2001). Rapid gene mapping in Caenorhabditis elegans using a high density polymorphism map. *Nature Genetics*, *28*(2), 160–164. https://doi.org/10.1038/88878

Woglar, A., Daryabeigi, A., Adamo, A., Habacher, C., Machacek, T., Volpe, A. L., & Jantsch, V. (2013). Matefin/SUN-1 phosphorylation is part of a surveillance mechanism to coordinate chromosome synapsis and recombination with meiotic progression and chromosome movement. *PLoS Genetics*, *9*(3), e1003335. https://doi.org/10.1371/journal.pgen.1003335

Woglar, A., & Villeneuve, A. M. (2018). Dynamic Architecture of DNA Repair Complexes and the Synaptonemal Complex at Sites of Meiotic Recombination. *Cell*, *173*(7), 1678-1691.e16. https://doi.org/10.1016/j.cell.2018.03.066

Wynne, D. J., Rog, O., Carlton, P. M., & Dernburg, A. F. (2012). Dynein-dependent processive chromosome motions promote homologous pairing in C. elegans meiosis. *The Journal of Cell Biology*, *196*(1), Article 1. https://doi.org/10.1083/jcb.201106022

Zhang, L., Ward, J. D., Cheng, Z., & Dernburg, A. F. (2015). The auxin-inducible degradation (AID) system enables versatile conditional protein depletion in C. elegans. *Development (Cambridge, England)*, *142*(24), Article 24. https://doi.org/10.1242/dev.129635

Zickler, D., & Kleckner, N. (1998). The leptotene-zygotene transition of meiosis. *Annual Review of Genetics*, *32*, 619–697. https://doi.org/10.1146/annurev.genet.32.1.619

Zickler, D., & Kleckner, N. (1999). Meiotic chromosomes: Integrating structure and function. *Annual Review of Genetics*, *33*, 603–754. https://doi.org/10.1146/annurev.genet.33.1.603

Zickler, D., & Kleckner, N. (2015). Recombination, Pairing, and Synapsis of Homologs during Meiosis. *Cold Spring Harbor Perspectives in Biology*, *7*(6), Article 6. https://doi.org/10.1101/cshperspect.a016626

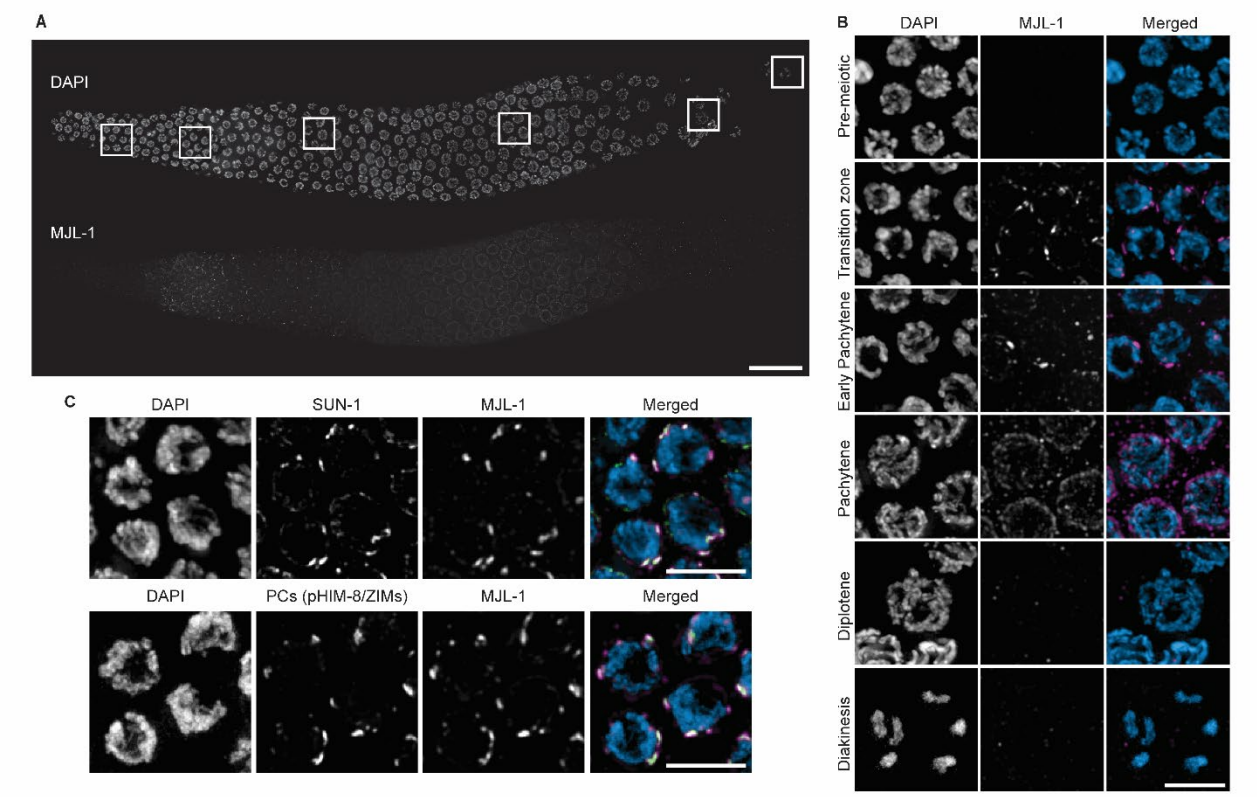

Figure 1. MJL-1 is a meiosis-specific NE protein that associates with PCs and LINC complexes. (A), Composite maximum-intensity projection images of whole gonads from *ha::mjl-1* hermaphrodites, stained with DAPI (top) and anti-HA antibodies (bottom). Scale bar, 20 µm. **(B)**, Examples of nuclei at different stages of meiotic prophase. Scale bar, 5 µm. **(C)**, MJL-1 colocalizes with SUN-1 (top) and phosphorylated PC proteins HIM-8 and ZIM-1, -2, and -3 (bottom) in *ha::mjl-1* hermaphrodites. PC proteins were detected using a phospho-specific antibody that recognizes these proteins when phosphorylated by CHK-2. Scale bars, 5 µm.

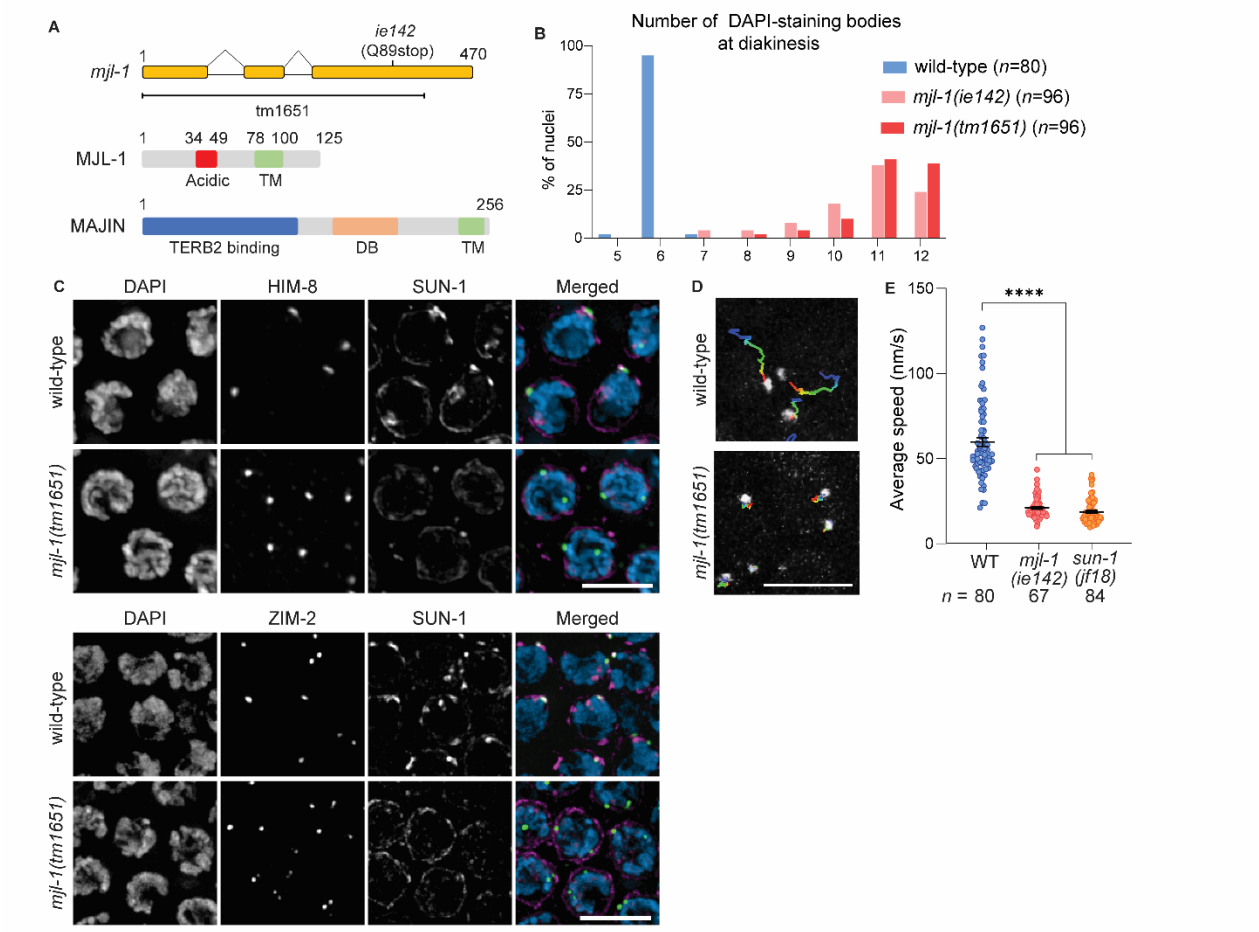

Figure 2. Loss of MJL-1 disrupts PC function. (A), Diagram of the *mjl-1* gene, indicating the mutations described in this work (top). Primary structure of MJL-1 in *C. elegans* and MAJIN in *M. musculus* (bottom) (TM: Transmembrane; DB: DNA binding domain). **(B)**, Number of DAPI-staining bodies in oocyte nuclei at diakinesis in wild-type and *mjl-1* mutant hermaphrodites. **(C)**, Loss of MJL-1 disrupts the connection between PC proteins and LINC complex. Transition zone nuclei were stained with antibodies against HIM-8 (top) or ZIM-2 (bottom) (green), which marks *X* chromosome or chromosome *V* PCs, respectively, and SUN-1 (magenta). Scale bars, 5 µm. **(D)**, Projection of 75 s time course displacement track of GFP::HIM-8 in transition zone nuclei in wild-type and *mjl-1(ie142)*. Scale bar, 5 µm. **(E)**, Average speed of GFP::HIM-8 foci in transition zone nuclei in wild-type, *mjl-1*(ie142) ($p < 0.0001$), and *sun-1(jf18)* ($p < 0.0001$) hermaphrodites. Each point represents a single nucleus. *p*-values were computed using Student's *t*-test was used with Bonferroni *post-hoc* correction.

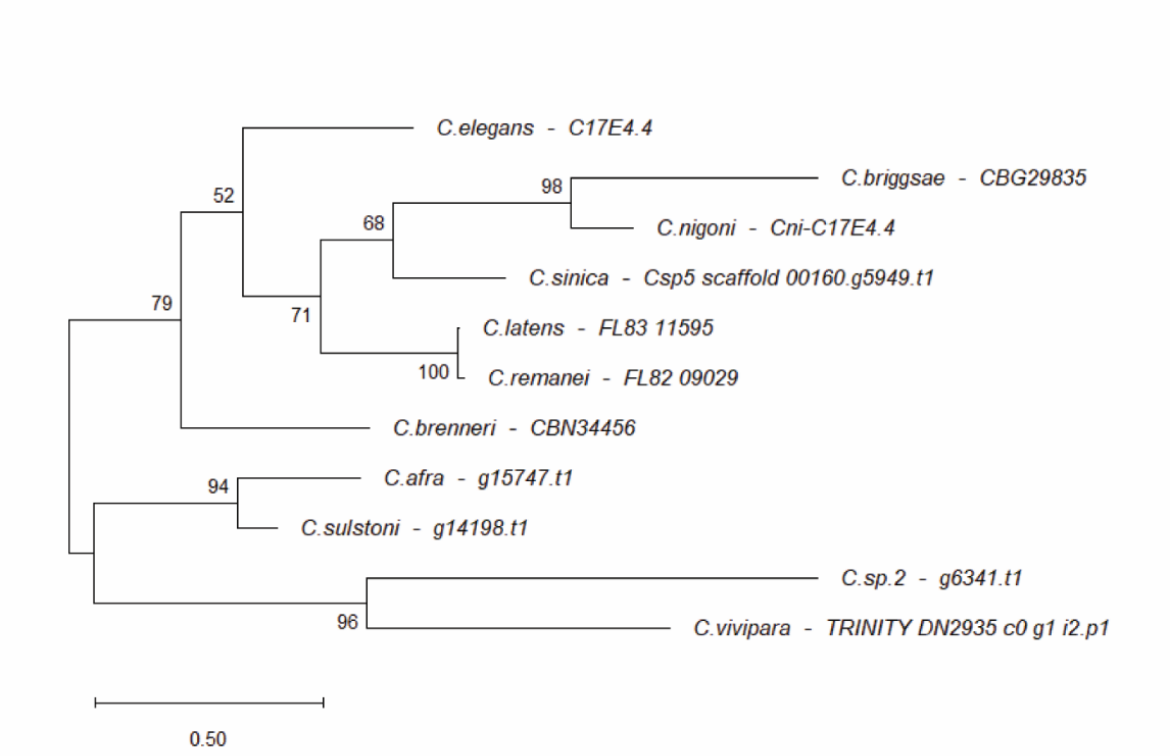

Figure 3. Phylogenetic tree of MJL-1 homologs in *Caenorhabditis.* A phylogenetic tree of MJL-1 homologs from representative *Caenorhabditis* species, based on maximum-likelihood estimates. Numbers on each node are Bootstrap values. Scale bar, 0.5 substitutions per site.

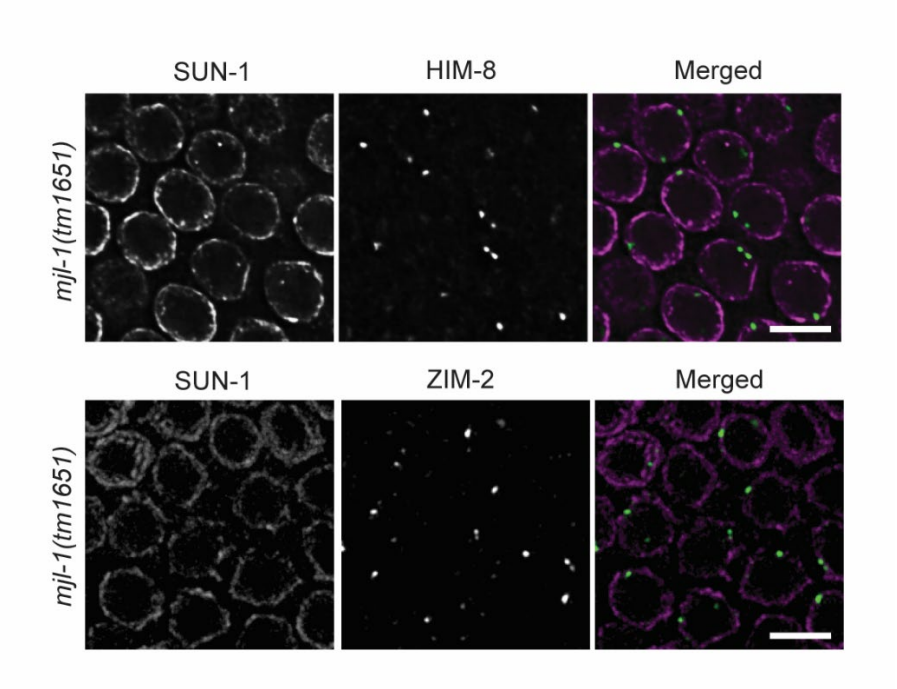

Figure 4. PCs localize at the NE in the absence of MJL-1. Cross-section images of transition zone nuclei. SUN-1 (left) marks the NE in meiotic cells; HIM-8 and ZIM-2 (center) mark *X* chromosome and chromosome *V* PCs, respectively. Although pairing is severely reduced in *mjl-1(tm1615)*, PCs are still associated with the NE. Scale bars, 5 μm.

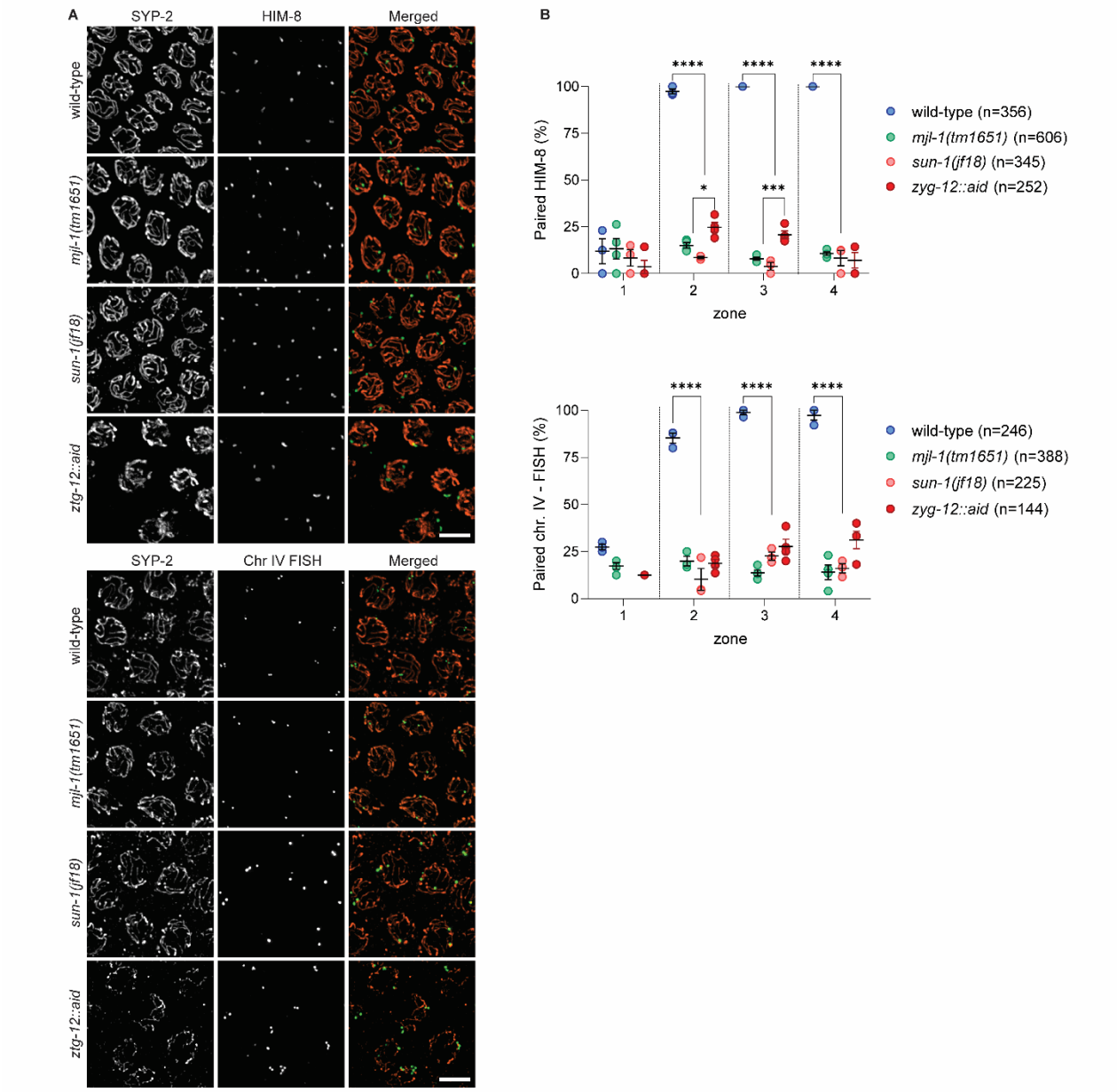

Figure 5. Deletion of *mjl-1* results in promiscuous nonhomologous synapsis. (A), Nonhomologous synapsis in *mjl-1(tm1651)* and *sun-1(jf18)* mutants and following depletion of ZYG-12::AID by treatment with auxin for 12 h. Mid-pachytene nuclei are stained with antibodies against HIM-8 (green) and SYP-2 (orange). Scale bars, 5µm. **(B)**, Quantification of chromosome pairing in wild-type and mutant hermaphrodites using immunofluorescence (HIM-8) and FISH (Chr IV) (* $p < 0.5$; *** $p < 0.001$; **** $p < 0.0001$). Gonads were divided into four zones (zone 1: pre-meiotic cells; zones 2-4: region spanning early prophase through pachytene, divided into three zones of equal length). *p*-values were calculated by one-way ANOVA with pairwise Bonferroni *post-hoc* correction.

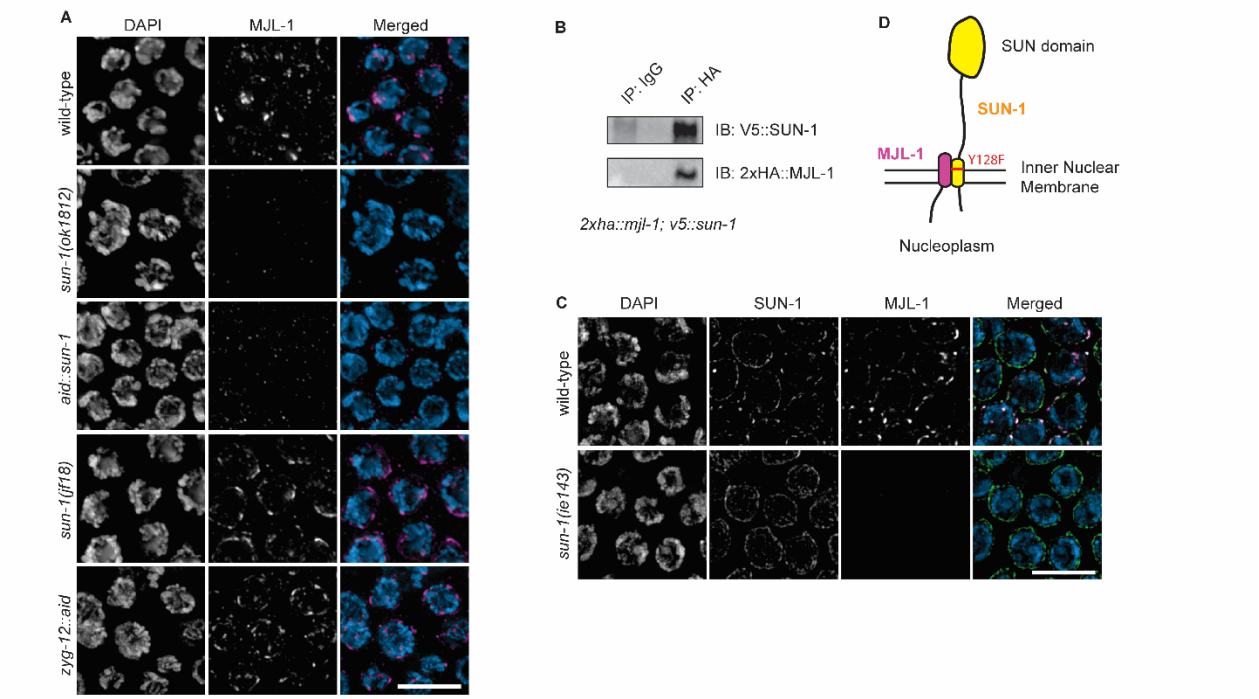

Figure 6. SUN-1 is required for NE localization of MJL-1. (A), Transition zone nuclei in wild-type and mutant hermaphrodites expressing HA::MJL-1, stained with anti-HA antibodies (magenta in merged images). Scale bar, 5 µm. **(B)**, Co-immunoprecipitation of SUN-1 and MJL-1. HA::MJL-1 was immunoprecipitated using an anti-HA antibody in *ha::mjl-1; v5::sun-1* hermaphrodite lysate. Immunoprecipitated and co-precipitated proteins were resolved by SDS-polyacrylamide gel electrophoresis and detected using anti-HA and anti-V5 antibodies. **(C)**, The Y128F mutation in *sun-1(ie143)* disrupts interaction between MJL-1 and SUN-1. Transition zone nuclei were stained with antibodies against SUN-1 (green in merged images) and HA (magenta) from wild-type and mutant hermaphrodites expressing HA::MJL-1. Scale bar, 5 µm. **(D)**, Illustration of the inferred interaction between MJL-1 and SUN-1.

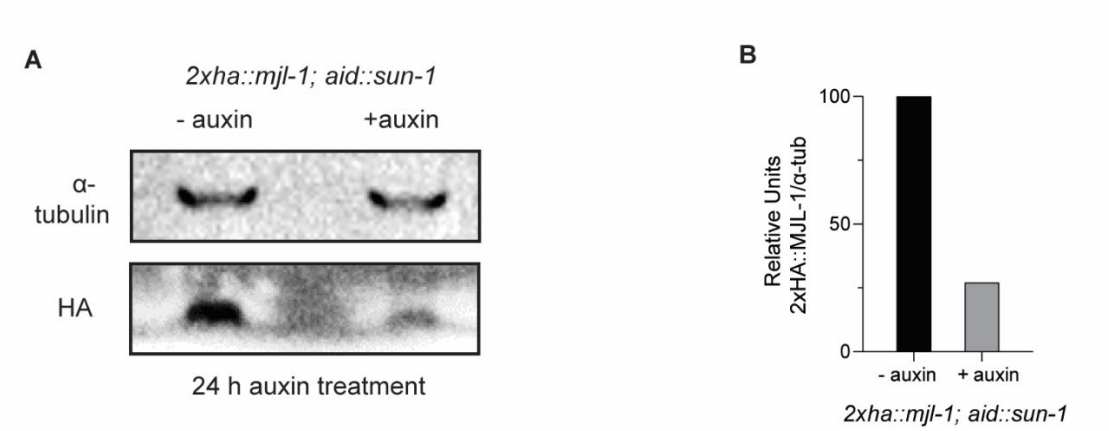

Figure 7. MJL-1 abundance is greatly reduced in the absence of SUN-1. (A) Western blot of proteins in strains expressing 2xHA::MJL-1 and (degron-tagged) AID::SUN-1. The abundance of MJL-1 is detected with anti-HA antibodies, either in the absence of auxin treatment or following depletion with auxin for 24 hours. α-tubulin is used as a control. (B) Quantification of (A).

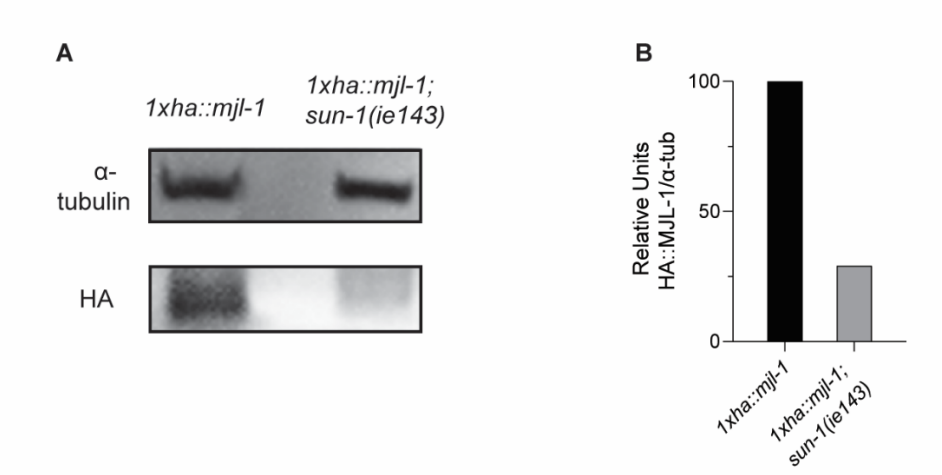

Figure 8. MJL-1 abundance is greatly reduced in *sun-1(ie143)*. (A) Western blot of proteins in strains expressing either 1xHA::MJL-1 or 1xHA::MJL-1 and SUN-1(ie143). The abundance of MJL-1 is detected with anti-HA antibodies. α-tubulin is used as a control. (B) Quantification of (A).

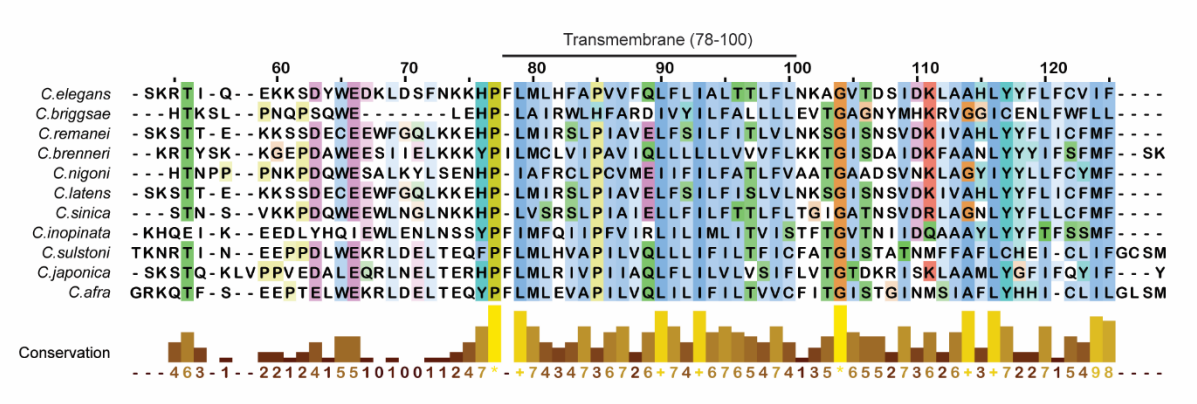

Figure 9. Sequence alignment of transmembrane and perinuclear regions in C*aenorhabditis* MJL-1 homologs. Alignment was generated using MAFFT.

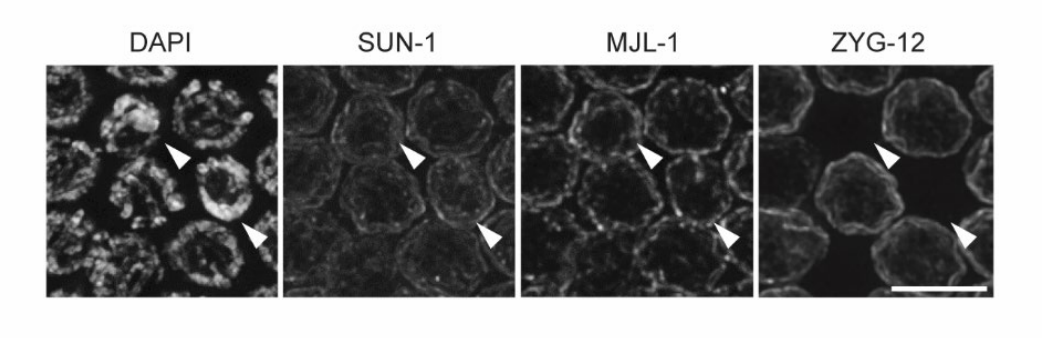

Figure 10. MJL-1 and SUN-1 are detected at the NE of oocyte nuclei undergoing apoptosis, while ZYG-12 is absent. Maximum-intensity projection images showing late pachytene nuclei. Arrowheads indicate apoptotic nuclei. Scale bar, 5 μm.

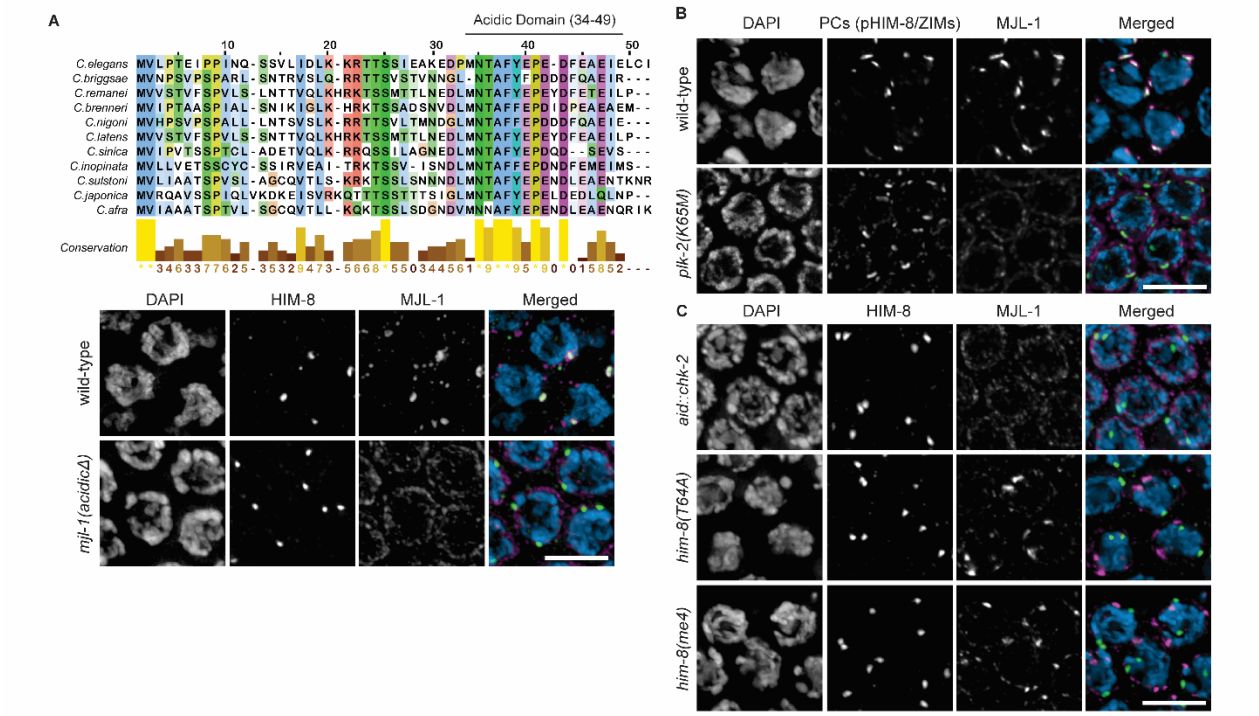

Figure 11. MJL-1 requires a small domain enriched in acidic amino acids to interact with PC proteins. (A), Sequence alignment of the N-terminal region of MJL-1 homologs within *Caenorhabditis,* generated using MAFFT. **(B)**, Maximum intensity projection images showing transition zone nuclei stained with antibodies against HIM-8 (green in merged images) and HA (magenta) from hermaphrodites expressing HA::MJL-1 (top) or HA::MJL-1$^{acidic\Delta}$ (bottom). Scale bar, 5 µm. **(C)**, PLK-2 activity is required for interaction between MJL-1 (magenta) and PC proteins (green). Scale bar, 5 µm. **(D)**, Recruitment of PLK-2 by HIM-8 (green) is required for the association of HIM-8 with the MJL-1 (magenta). Scale bar, 5 µm.

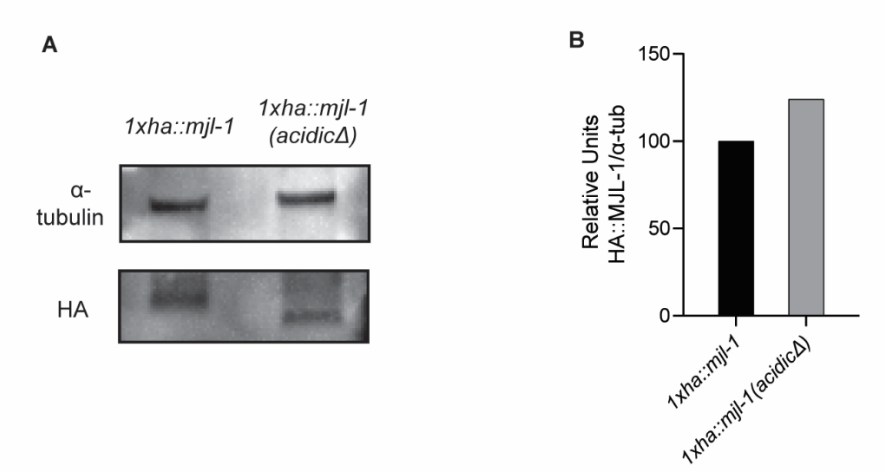

Figure 12. Deletion of acidic residues does not affect stability of MJL-1. (A) Western blot of proteins in strains expressing either 1xHA::MJL-1 or 1xHA::MJL-1$^{acidic\Delta}$. The abundance of MJL-1 is detected with anti-HA antibodies. α-tubulin is used as a control. **(B)** Quantification of (A).

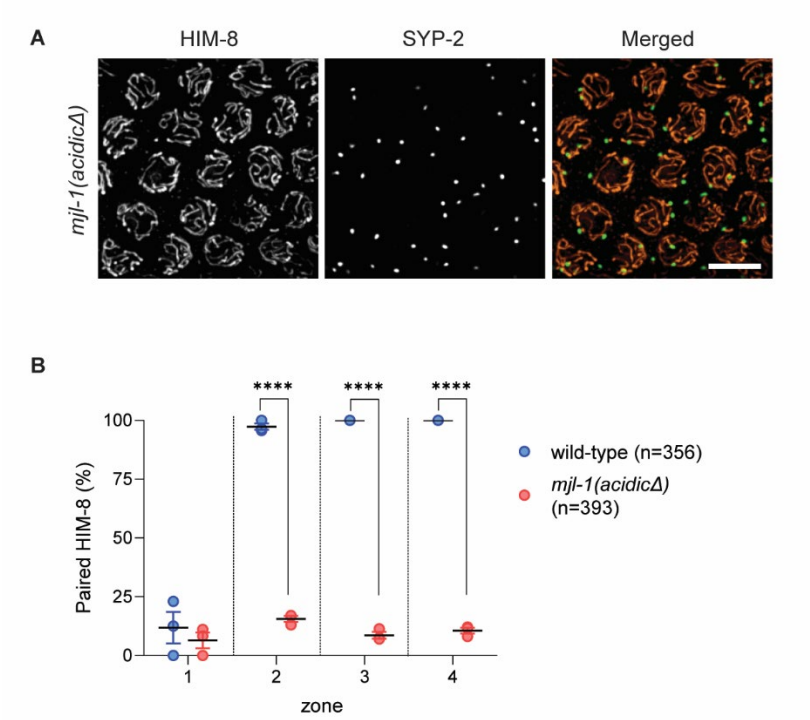

Figure 13. Deletion of a small acidic region in MJL-1 results in nonhomologous synapsis. (A) Maximum-intensity projection images of pachytene nuclei stained with antibodies against HIM-8 (green) and SYP-2 (orange). Scale Bar, 5 µm. (B) Quantification of *X* chromosome pairing in wild-type and *mjl-1(acidicΔ)* hermaphrodites ($p<0.0001$). Each point represents a single gonad. *p*-values were computed using Student's *t*-test with Bonferroni *post-hoc* correction.

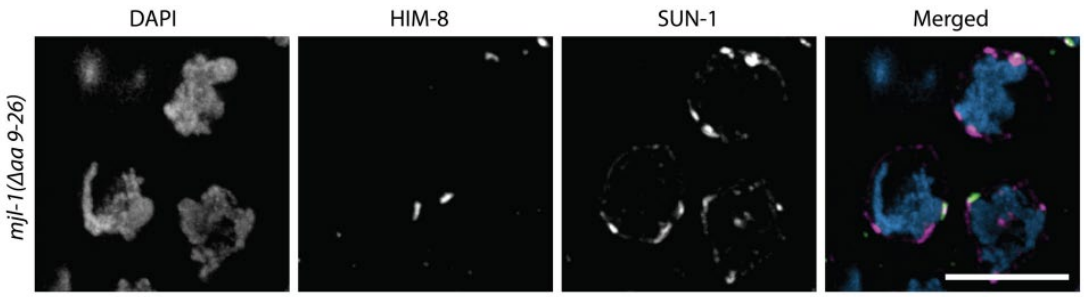

Figure 14. Deletion of amino acids 9-26 in MJL-1 dose not disrupt the colocalization of HIM-8 and LINC complex. (A), Maximum-intensity projection images of transition zone nuclei stained with antibodies against HIM-8 (green) and SUN-1 (magenta). Scale Bar, 5 μm.

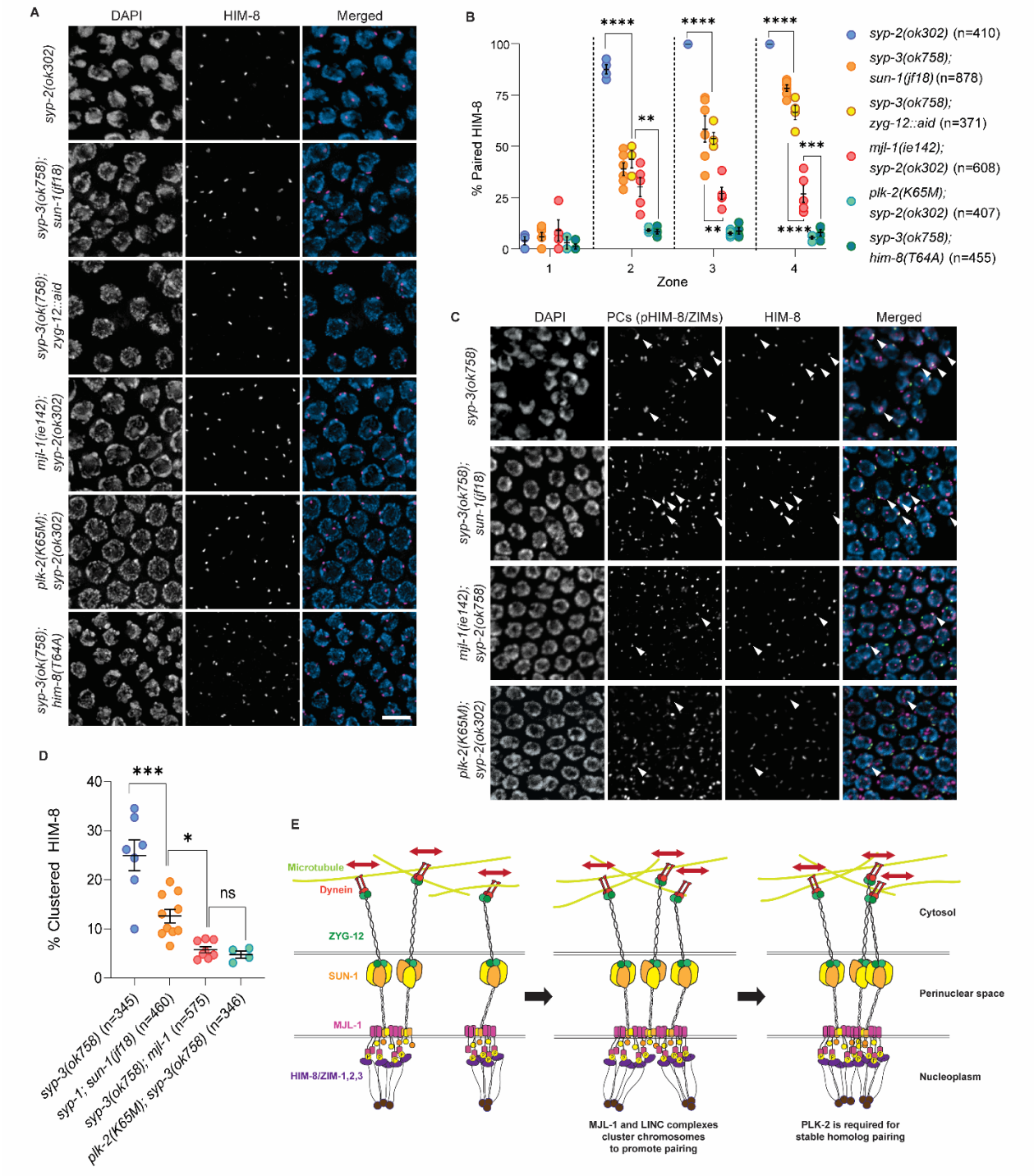

Figure 15. MJL-1 promotes pairing even in the absence of chromosome movements. (A), Blocking synapsis does not restore pairing of HIM-8 in *mjl-1(ie142)* mutants, in contrast to *sun-1(jf18)* or depletion of ZYG-12::AID. AID::SYP-3 was depleted by treatment with auxin for 24 h. Nuclei display polarized morphology due to lack of synapsis. Scale bar, 5 µm. **(B)**,

Quantification of *X* chromosome pairing. The extended transition zone was divided into three equal regions (zones 2-4) by length (zone 1: pre-meiotic). Each point represents a single gonad. *p*-values were calculated by one-way ANOVA with pairwise *post-hoc* Bonferroni correction (** $p < 0.01$; *** $p < 0.001$; **** $p < 0.0001$). **(C)**, In the absence of synapsis, clustering of HIM-8 with other PC proteins is lower in *mjl-1(ie142)* than in *sun-1(jf18)*. Scale bar, 5 μm. **(D)**, Quantification of clustering between HIM-8 and other PC proteins in various mutants. Only nuclei in zone 2 were analyzed, since pHIM-8/ZIM staining decreases in zone 3-4. *p*-values were calculated by one-way ANOVA with *post-hoc* pairwise Bonferroni correction (* $p < 0.05$; *** $p < 0.001$). **(E)**, Overview of homolog pairing. Upon meiotic entry, PCs recruit PC proteins (purple) and are connected to MJL-1 (magenta) and SUN-1 (yellow/orange). CHK-2 and PLK-2 are required for this association. MJL-1 interacts with SUN-1 through transmembrane/perinuclear regions. SUN-1 trimers interact with ZYG-12 dimers (green) that are connected to dynein (red) to generate processive chromosome movements (red arrows). These movements promote homolog searching (left). MJL-1 and SUN-1 cluster to promote homolog pairing (middle). PLK-2 phosphorylates unknown substrates to stabilize homolog pairing (right).

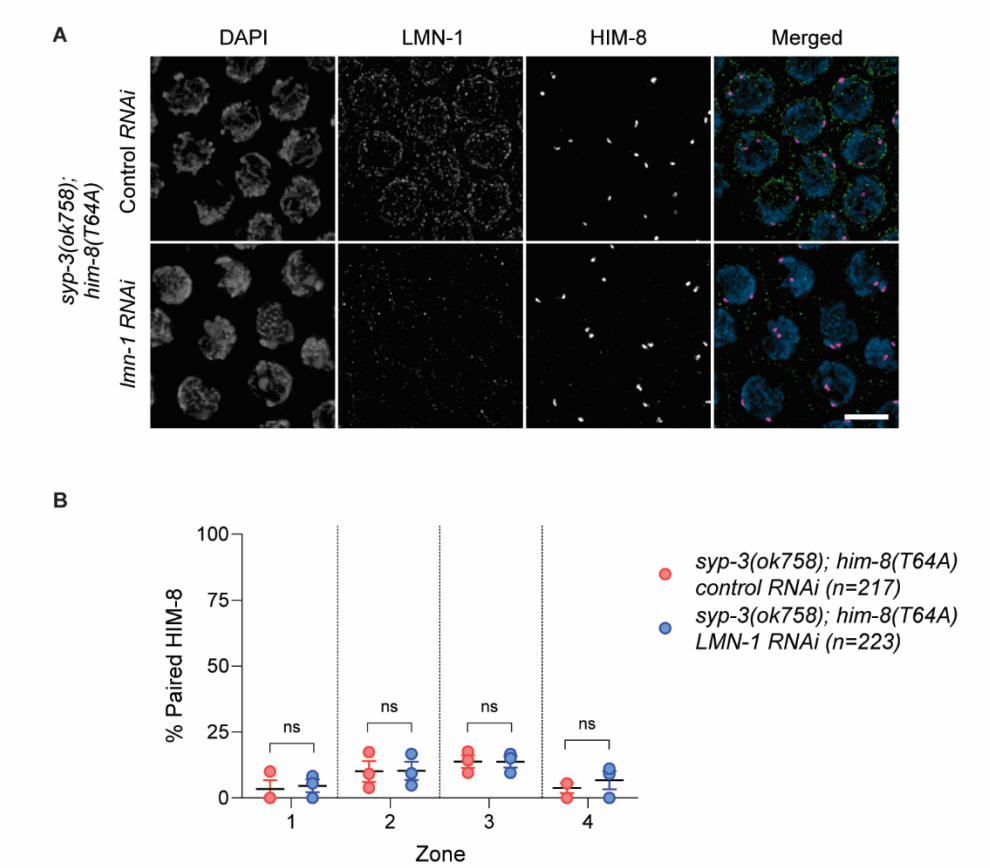

Figure 16. Depletion of LMN-1 by RNAi fails to rescue pairing in HIM-8^{T64A}. (A) Maximum-intensity projection images of transition zone-pachytene nuclei in *syp-3(ok758); him-8(T64A)* hermaphrodites, either following 48 hr depletion of LMN-1 by RNAi or control RNAi. Nuclei are stained with antibodies against LMN-1 (green) and HIM-8 (magenta). Scale Bar, 5 µm. (B) Quantification of *X* chromosome pairing. The extended transition zone was divided into zones 2-4, with zone 1 corresponding to the pre-meiotic region. Each point represents a single gonad. *p*-values were computed using Student's *t*-test with Bonferroni *post-hoc* correction.

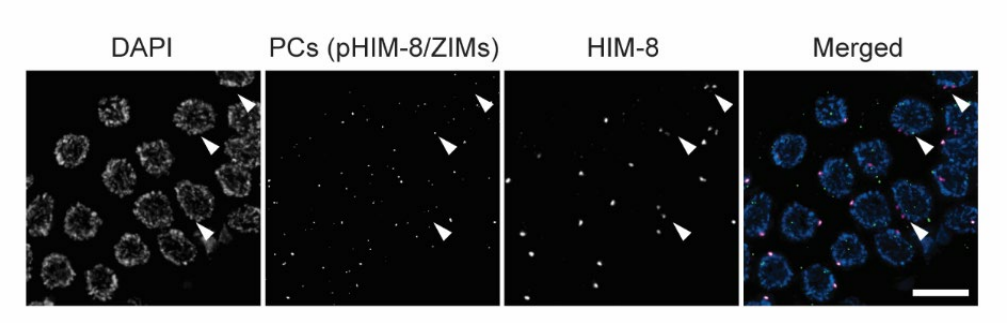

Figure 17. Loss of PLK-2 correlates with dissociation of synapsis-independent pairing. Images show maximum-intensity projections of the proximal region of the gonad, corresponding to the end of the extended transition zone, in *syp-2(ok307)* hermaphrodites. Gonads were stained with antibodies against phosphorylated PC proteins (green) and HIM-8 (magenta). Separation of HIM-8 foci correlates with a loss phosphorylation of HIM-8, indicative of loss of PLK-2 from the X chromosome PC.

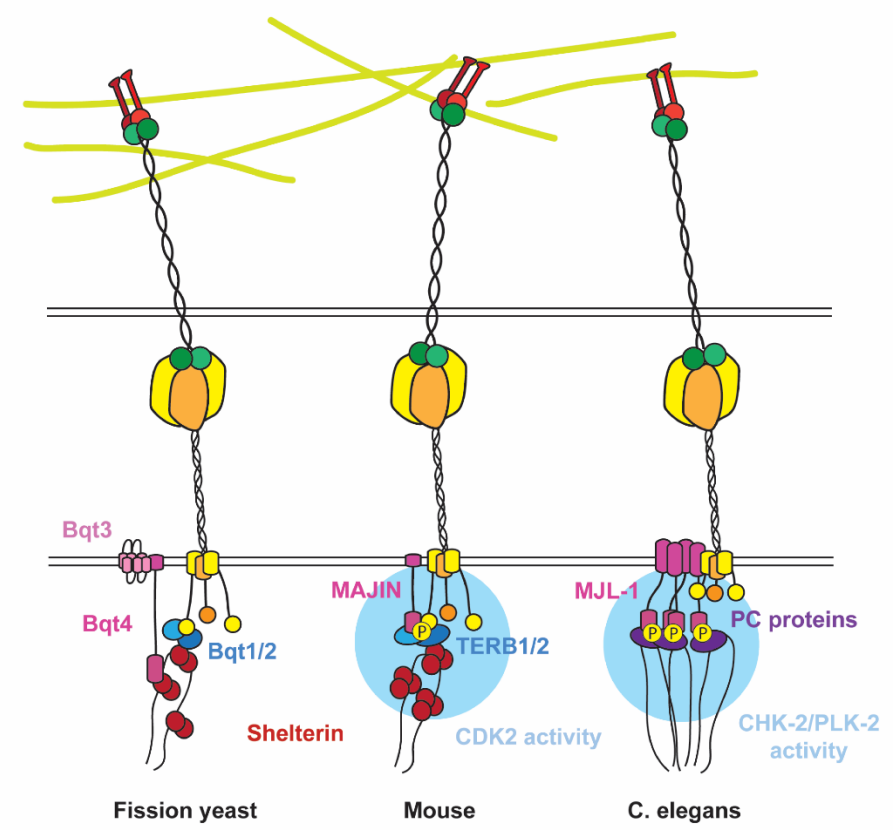

Figure 18. Similarities in molecular architecture of chromosome end-LINC complex attachments in fission yeast, mouse, and *C. elegans.* In fission yeasts, Bqt4 (magenta) connects shelterin (red) to NE during vegetative cycle. Bqt4 interacts with multi-pass NE protein Bqt3 (pink). Meiosis-specific shelterin binding proteins Bqt1 and Bqt2 (blue) connect NE-recruited telomeres to LINC complexes (yellow/orange) (left). In mice, TERB2 (blue) interacts with MAJIN (magenta), and TERB1 (blue) interacts with SUN1. MAJIN also associates with SUN1 (yellow/orange). This requires CDK2 (middle). In *C. elegans*, MJL-1 (magenta) connects PC proteins (purple) to SUN-1 (yellow/orange). This requires CHK-2 and PLK-2. MJL-1 and SUN-1 cluster to promote homolog pairing (right).

Appendix 1. Efficient pipeline for Green eggs and Him screen and sequencing based mutation mapping

This protocol was modified from the original Green Eggs and Him screen protocol (Kelly et al., 2000) and adapted as a multiplexed screen for higher throughput.

1. Approximately 1000 synchronized L4 to young adult *xol-1p::gfp* worms are treated with mutagen in 4 mL of M9 buffer (50 mM EMS or 1mM ENU) for 4 hrs. The worms are then washed with M9 buffer 10 times and transferred to plates with a limited amount of food. This causes them to lay eggs and become starved soon after, leading to the arrest of their F1 progeny (which may contain induced mutations) at the L1 stage.

2. Collect the L1 progeny by washing plates with M9 buffer and transferring them into S. Basal liquid culture with a density of ~30 worms per 10 µl. A 1 L overnight culture of OP50 bacteria was pelleted and resuspended in M9 buffer and used as food. Grow them until gravid and bleach to obtain synchronized F2 progeny.

3. Grow the F2 worms in liquid culture. Once the worms reach the young adult stage (0-4 eggs), collect the adult progeny and remove bacteria from them by flotation in a 30% sucrose solution (w/v). The harvested worms were then resuspended in S. Basal buffer and left to starve for 24 hours.

4. Starved worms are harvested by centrifugation at 100 g for 2 minutes. The worms are then rinsed three times in M9 buffer. Adult worms with green eggs are picked up under a fluorescence microscope.

5. Each young worm is placed on a plate for rescue and crossed with 2-3 Hawaiian males, allowing them to lay eggs for 3 days. After 3 days, the parental worms are dissected for phenotypic analysis via immunofluorescence.

6. During dissection, each worm is marked differently (e.g., 1 - cut head, 2 - cut tail, 3 - cut in the middle, 4 - cut head and tail) and then combined for immunofluorescence analysis. Up to 9 worms are imaged together on the same slide, and the phenotype of interest can be revisited based on their marking.

7. F1 progeny from the parents with the phenotype of interest are singled, and their F2 progeny are singled again to validate reduced fertility and/or elevated male frequency before being crossed with Hawaiian males.

8. Step 6 is repeated once more.

9. Progeny are singled, and around 20 worms showing reduced fertility and/or elevated male frequency are collected (supposed to be homozygotes) in 20 ul of M9 buffer. Genomic DNA is then extracted and sequenced.

10. The sequenced FASTQ files were mapped to the WS235 reference genome using Bowtie2 (paired end, -X 2000), and SNPs were called by LoFreq package Call variants (SNVs and indels, Strictly no filtering). The VCF file is then analyzed as below.

Appendix 2. Python Code for identifying the chromosome region where the affected mutation resides

This Python script compares Single Nucleotide Polymorphism (SNP) data obtained from two distinct sources: Mutant SNP data and Hawaiian SNP data. Mutant SNP data (Mutant.vcf) is generated from my mutant strains (hybrid with Hawaiian) prepared as Appendix 1. Hawaiian SNP data (Hawaiian.vcf) is directly generated by sequencing genome of Hawaiian strains used for crossing in Appendix 1.

The primary objective is to identify chromosome regions where causal mutation resides, which is potentially within the mutant SNP dataset that lack Hawaiian SNP representation. The SNP data for each sample is obtained from sequencing experiments and is processed to identify variations compared to the reference genome of *C. elegans* using the LoFreq package.

```
########################################
# input file names
Hawaiian_SNP_file = "Hawaiian.vcf"  # File containing Hawaiian SNP data
mutant_SNP_file = "Mutant.vcf"      # File containing mutant SNP data

# parameters for Hawaiian SNP plotting (AF= Allele Frequency)
Hawaiian_AF_cut = 0.7       # Allele Frequency cutoff for Hawaiian SNPs
Hawaiian_score_cut = 20     # Score cutoff for Hawaiian SNPs
Mutant_AF_cut = 0.5         # Allele Frequency cutoff for mutant SNPs
Mutant_score_cut = 20       # Score cutoff for mutant SNPs

########################################
import pandas as pd

# Reading data from the Hawaiian SNP file
f1 = open(Hawaiian_SNP_file, "r")
data = f1.readlines()

array_Hawaiian = []    # Hawaiian SNP data table
for count in range(len(data)):
   if count > 17:  # Skipping header lines
      temp = data[count].split("\t")      # Formatting for data table
      AF_index = temp[-1].split(";")   # Extracting Allele Frequency
      if int(temp[5]) > Hawaiian_score_cut:  # Filtering based on score cutoff
         if float(AF_index[1][3:]) > Hawaiian_AF_cut:  # Filtering based on allele frequency
cutoff
            array_Hawaiian.append(temp)
```

```
f1.close()

# Reading data from the mutant SNP file
f2 = open(mutant_SNP_file, "r")
data_Mutant = f2.readlines()

array_Mutant = []       # Mutant SNP data table
for count in range(len(data_Mutant)):
   if count > 17:  # Skipping header lines
      temp = data_Mutant[count].split("\t")    # Formatting for data table
      AF_index = temp[-1].split(";")   # Extracting Allele Frequency
      if int(temp[5]) > Mutant_score_cut:  # Filtering based on score cutoff
         if float(AF_index[1][3:]) > Mutant_AF_cut:  # Filtering based on allele frequency cutoff
            array_Mutant.append(temp)
f2.close()

#####################################################
# Creating dictionaries for easy lookup
Dic_Hawaiian = {i[1]: i for i in array_Hawaiian}
Dic_array_Mutant = {i[1]: i for i in array_Mutant}

result = []
result_AF80 = []

# Mapping mutant SNPs to Hawaiian SNPs
for i in array_Mutant:
   if i[1] in Dic_Hawaiian:  # Checking if the SNP exists in the Hawaiian dataset
      recall = Dic_Hawaiian[i[1]]  # Retrieving the corresponding SNP from the Hawaiian dataset
      if i[0] == recall[0] and i[3] == recall[3] and i[4] == recall[4]:  # Comparing SNP attributes
         temp = []
         temp.append("mutant")
         temp.append(i[0])
         temp.append(i[1])
         temp.append(i[3])
         temp.append(i[4])
         temp.append(i[5])
         n = i[-1].split(";")
         temp.append(float(n[1][3:]))  # Extracting allele frequency
         temp.append("Hawaiian")
         j = Dic_Hawaiian[i[1]]
         temp.append(j[0])
         temp.append(j[1])
         temp.append(j[3])
         temp.append(j[4])
         temp.append(j[5])
         n = j[-1].split(";")
```

```
        temp.append(float(n[1][3:]))  # Extracting allele frequency
        result.append(temp)

# Converting results to DataFrame and saving to CSV
df1 = pd.DataFrame(result, columns=["mutant", "chr", 'pos', 'Ref', 'SNP_mutant', 'SCORE',
'AF_mutant', 'Hawaiian', 'chr', 'pos', 'Ref', 'SNP_Hawaiian', 'SCORE', 'AF_Hawaiian'])
df1.to_csv(mutant_SNP_file[:-7] + 'mapping_result.csv')  # Saving the mapped results to a CSV
file
print("plotting done")
print('\a')  # Producing a system beep to indicate completion
#########################################################
```

The resulting .csv file can be opened using Excel (below).

	mutant	chr	pos	Ref	SNP_mutant	SCORE	AF_mutant	Hawaiian	chr	pos	Ref	SNP_Hawaiian	SCORE	AF_Hawaiian
0	mutant	I	921	G	A	157	0.482456	Hawaiian	I	921	G	A	1670	0.764493
1	mutant	I	962	G	T	778	0.669065	Hawaiian	I	962	G	T	2839	0.838806
2	mutant	I	1048	G	A	570	0.6	Hawaiian	I	1048	G	A	636	0.572973
3	mutant	I	1062	G	T	377	0.492754	Hawaiian	I	1062	G	T	158	0.403101
4	mutant	I	1066	G	T	441	0.523077	Hawaiian	I	1066	G	T	210	0.448819
5	mutant	I	1076	T	A	263	0.474576	Hawaiian	I	1076	T	A	293	0.436893
6	mutant	I	1083	G	A	357	0.492308	Hawaiian	I	1083	G	A	303	0.446602
7	mutant	I	1097	A	T	395	0.527273	Hawaiian	I	1097	A	T	298	0.4375
8	mutant	I	1120	G	A	575	0.557692	Hawaiian	I	1120	G	A	487	0.529412
9	mutant	I	1187	A	T	721	0.539683	Hawaiian	I	1187	A	T	931	0.5
10	mutant	I	1216	A	T	943	0.628571	Hawaiian	I	1216	A	T	1274	0.564516
11	mutant	I	1222	A	C	1164	0.671053	Hawaiian	I	1222	A	C	3409	0.992754
12	mutant	I	1290	T	A	981	0.561644	Hawaiian	I	1290	T	A	943	0.428571
13	mutant	I	1309	A	T	123	0.119403	Hawaiian	I	1309	A	T	1536	0.613139
14	mutant	I	1412	T	C	396	0.527778	Hawaiian	I	1412	T	C	197	0.322581
15	mutant	I	1414	G	A	376	0.514286	Hawaiian	I	1414	G	A	195	0.3125
16	mutant	I	1421	G	A	381	0.472222	Hawaiian	I	1421	G	A	177	0.3125
17	mutant	I	1471	T	C	269	0.288889	Hawaiian	I	1471	T	C	130	0.214286
18	mutant	I	1542	C	T	164	0.25	Hawaiian	I	1542	C	T	235	0.3
19	mutant	I	1713	T	G	155	0.191489	Hawaiian	I	1713	T	G	1216	1
20	mutant	I	2622	T	A	108	0.363636	Hawaiian	I	2622	T	A	371	1
21	mutant	I	2651	T	A	106	0.375	Hawaiian	I	2651	T	A	288	0.944444
22	mutant	I	3611	T	A	116	0.333333	Hawaiian	I	3611	T	A	1408	0.938776
23	mutant	I	3659	C	T	136	0.333333	Hawaiian	I	3659	C	T	1538	1
24	mutant	I	4101	A	G	168	0.363636	Hawaiian	I	4101	A	G	1366	0.957447
25	mutant	I	4776	T	A	110	0.166667	Hawaiian	I	4776	T	A	965	1
26	mutant	I	6581	T	C	107	0.190476	Hawaiian	I	6581	T	C	1181	1
27	mutant	I	7235	C	T	197	0.272727	Hawaiian	I	7235	C	T	1028	0.971429
28	mutant	I	7640	G	A	160	0.214286	Hawaiian	I	7640	G	A	1078	1
29	mutant	I	7824	T	A	182	0.291667	Hawaiian	I	7824	T	A	1281	1
30	mutant	I	8174	C	T	174	0.25	Hawaiian	I	8174	C	T	1058	1
31	mutant	I	8241	A	G	147	0.206897	Hawaiian	I	8241	A	G	1709	1
32	mutant	I	9007	A	T	103	0.3	Hawaiian	I	9007	A	T	458	1
33	mutant	I	10291	C	G	121	0.135135	Hawaiian	I	10291	C	G	1182	1
34	mutant	I	12837	T	C	121	0.222222	Hawaiian	I	12837	T	C	2014	1
35	mutant	I	15024	A	G	145	0.2	Hawaiian	I	15024	A	G	1615	0.98
36	mutant	I	15955	G	A	131	0.416667	Hawaiian	I	15955	G	A	683	1
37	mutant	I	15957	A	C	145	0.416667	Hawaiian	I	15957	A	C	705	1
38	mutant	I	17160	G	A	154	0.212121	Hawaiian	I	17160	G	A	1168	1

"Ref" refers to the base in the reference genome; SNPs in the mutant and Hawaiian samples that match each other but differ from the reference genome are recorded in the file. "SCORE" is the score calculated by the LoFreq package, with higher scores indicating greater fidelity for the SNP based on allele frequency, sequencing quality, and other factors.

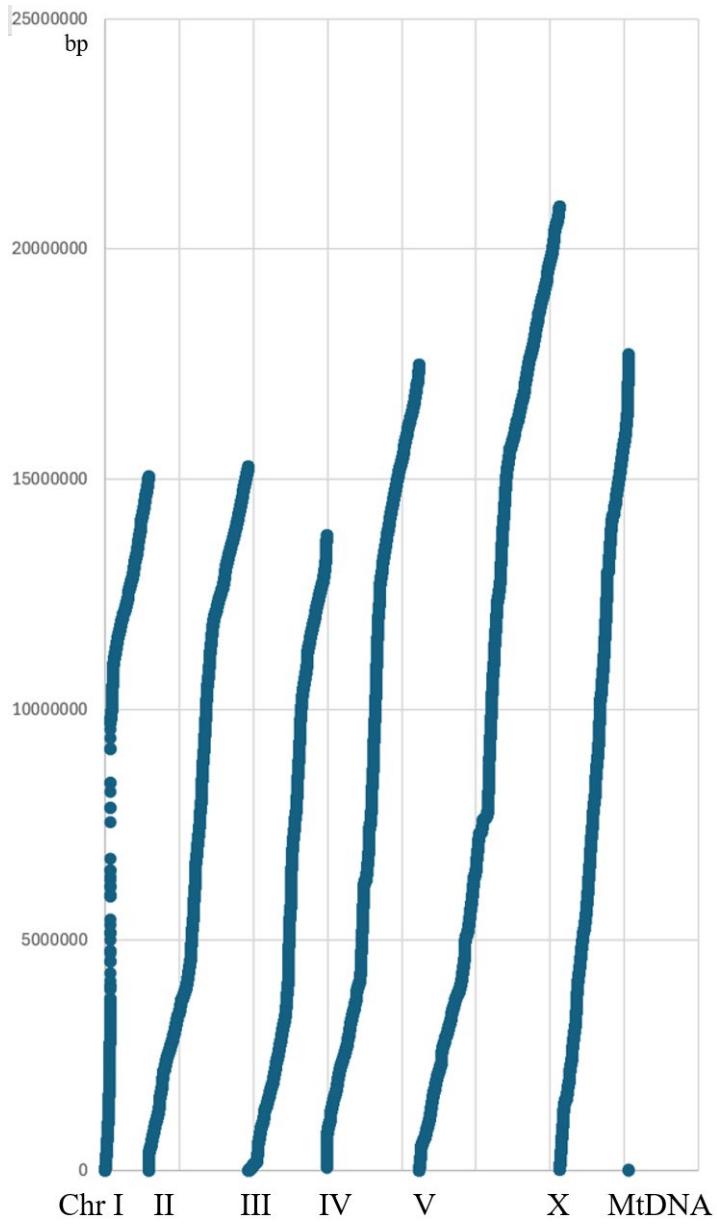

The plot can be created using the "chr" (chromosome) and "pos" (position) columns from the .csv files (above). Each data point represents a Hawaiian SNP with an allele frequency higher than a designated cutoff. The chromosome region with the fewest "hits" is most likely where the causative mutation is located (in this case, within the Chr I: 5-10 Mbp range).

Appendix 3. Python Code for mutation mapping on chromosome found using Appendix 2

This Python script identifies single nucleotide polymorphisms (SNPs) unique to mutant strains (hybrids) that are absent in both Hawaiian and unmutagenized *xol-1p::gfp* strains. Then it checks whether each SNP is located within known *C. elegans* genes, using the *C. elegans* reference gene annotation file WBcel235.gtf. The analysis can be confined to a designated

chromosome region as identified in Appendix 2. The unique SNPs that are found within known genes are then written to a new table for further analysis.

```
########################################
# Input file names
Hawaiian_SNP_file = "Hawaiian.vcf"        # File containing Hawaiian SNP data
background_SNP_file = "XolGFP.vcf"        # File containing background SNP data
mutant_SNP_file = "Mutant.vcf"            # File containing mutant SNP data

# Parameters for mutant-specific SNP calling
chr_for_SNP_calling = 'I'                 # Chromosome for SNP calling
pos_start = 0                             # Start position for SNP calling
pos_end = 100000000                       # End position for SNP calling
background_score_cut = 20                 # Score cutoff for background SNPs
background_AF_cut = 0.2                   # Allele Frequency cutoff for background SNPs
mutant_score_cut = 10                     # Score cutoff for mutant SNPs
mutant_AF_cut = 0.6                       # Allele Frequency cutoff for mutant SNPs
annotation_of_interest = 'exon'           # Annotation of interest for SNP mapping

########################################
import pandas as pd

# Loading background SNP data
f = open(background_SNP_file, "r")
data = f.readlines()
del data[0:18]  # Remove header
f.close()

array_background = []           # Generating SNP data table for untreated negative control
for count in range(len(data)):
   temp = data[count].split("\t")         # Formatting for data table
   if temp[0] == chr_for_SNP_calling:          # Selecting for specific chromosome
      AF_index = temp[-1].split(";")           # Extracting Allele Frequency
      if float(AF_index[1][3:]) > background_AF_cut:          # Filtering based on Allele
Frequency cutoff
         if int(temp[5]) > background_score_cut or AF_index[-2] == "INDEL": # Filtering based
on score cutoff or base insertion/deletion
            array_background.append(temp)

Dic_background = {}
for i in array_background:
   Dic_background[(i[0], i[1])] = i
print("Background SNP loaded")

# Loading Hawaiian SNP data
f = open(Hawaiian_SNP_file, "r")
```

```
data = f.readlines()
f.close()
del data[0:18]

array_Hawaiian = []    # Generating SNP data table for Hawaiian varient
for count in range(len(data)):
    temp = data[count].split("\t")
    if temp[0] == chr_for_SNP_calling:
        array_Hawaiian.append(temp)

Dic_Hawaiian = {}
for i in array_Hawaiian:
    Dic_Hawaiian[(i[0], i[1])] = i
print("Hawaiian SNP loaded")

# Loading mutant SNP data
f = open(mutant_SNP_file, "r")
data = f.readlines()
f.close()
del data[0:18]

array_mutant = []        # Generating SNP data table for my mutant
for count in range(len(data)):
    temp = data[count].split("\t")
    if temp[0] == chr_for_SNP_calling:
        AF_index = temp[-1].split(";")
        if float(AF_index[1][3:]) > mutant_AF_cut:
            if int(temp[5]) > mutant_score_cut or AF_index[-2] == "INDEL":
                array_mutant.append(temp)
print("Mutant SNP loaded")

# SNP calling and processing
result_SNP = []
for i in array_mutant:
    n = i[7].split(";")
    if (i[0], i[1]) in Dic_background:
        recall = Dic_background[(i[0], i[1])]
        if i[3] == recall[3] and i[4] == recall[4]:  # If SNP is in Hawaiian, remove
            a = 1  # NO INSERT.. SKIP..
        else:
            n = i[7].split(";")
            temp = []
            temp.append("mutant")
            temp.append(i[0])
            temp.append(i[1])
            temp.append(i[3])
```

```
            temp.append(i[4])
            if n[-2] == "INDEL":
                temp.append("INDEL")
            else:
                temp.append(i[5])  # SCORE
            temp.append(n[0])  # DP read depth
            temp.append(float(n[1][3:]))  # AF
            temp.append("null")
            temp.append("null")
            result_SNP.append(temp)

        elif (i[0], i[1]) in Dic_Hawaiian:
            recall = Dic_Hawaiian[(i[0], i[1])]
            if i[3] == recall[3] and i[4] == recall[4]:  # If SNP is in background (untreated XolGFP),
remove
                a = 1  # NO INSERT.. SKIP..
            else:
                n = i[7].split(";")
                temp = []
                temp.append("mutant")
                temp.append(i[0])
                temp.append(i[1])
                temp.append(i[3])
                temp.append(i[4])
                if n[-2] == "INDEL":
                    temp.append("INDEL")
                else:
                    temp.append(i[5])  # SCORE
                temp.append(n[0])  # DP read depth
                temp.append(float(n[1][3:]))  # AF
                temp.append("null")
                temp.append("null")
                result_SNP.append(temp)

        else:  # Position not in background or Hawaiian means mutant specific SNP
            n = i[7].split(";")
            temp = []
            temp.append("mutant")
            temp.append(i[0])
            temp.append(i[1])
            temp.append(i[3])
            temp.append(i[4])
            if n[-2] == "INDEL":
                temp.append("INDEL")
            else:
                temp.append(i[5])  # SCORE
```

```
        temp.append(n[0])  # DP read depth
        temp.append(float(n[1][3:]))  # AF
        temp.append("null")
        temp.append("null")
        result_SNP.append(temp)

# GTF indexing with SNP position data - identifies which gene each SNP is in
f = open("WBcel235.gtf", "r")
data = f.readlines()
array_gtf = []
f.close()

for count in range(len(data)):
    if count > 4:
        temp = data[count].split("\t")
        if temp[0] == chr_for_SNP_calling:
            if temp[2] == annotation_of_interest:
                array_gtf.append(temp)

result_SNP_genename_added = []

for i in result_SNP:     # each SNP in mutant dataset
    index = 0
    for j in array_gtf:
        if int(i[2]) >= int(j[3]) - 3 and int(i[2]) <= int(j[4]) + 3:            # if SNP is within a +/- 3 bp
range of an exon (to include splicing variants)
            char = j[8].split(";")
            del char[-1]  # Remove '\n' at the end
            for k in char:
                if k[0:10] == ' gene_name':
                    name = k[12:-1]
                    index = 1
                    break

    if index == 1:
        final_temp = []
        final_temp.append(i[1])
        final_temp.append(i[2])
        final_temp.append(i[3])
        final_temp.append(i[4])
        final_temp.append(i[5])
        final_temp.append(i[6])
        final_temp.append(i[7])
        final_temp.append(name)
        result_SNP_genename_added.append(final_temp)
        print(i[2])
```

```
# Convert results to DataFrame and save to CSV
df = pd.DataFrame(result_SNP_genename_added, columns=["chr", 'pos', 'Ref', 'SNP_mutant',
'SCORE', 'Read_Count', 'AF_mutant', 'gene'])
df.to_csv(mutant_SNP_file[:-7] + chr_for_SNP_calling + '_SNP_position.csv')
################################################################
```

The resulting .csv file can be opened using Excel (below).

chr	pos	Ref	SNP_muta	SCORE	Read_Count	AF_mutant	gene
I	1091635	G	A	2042	DP=69	0.84058	"R06A10.4"
I	1848234	C	T	1679	DP=58	0.862069	"tag-96"
I	2786712	C	T	1902	DP=68	0.823529	"W03D8.10"
I	3035401	G	T	811	DP=27	0.925926	"mod-5"
I	3984896	C	T	1462	DP=40	1	"aars-2"
I	4184311	C	T	2435	DP=71	1	"kel-20"
I	4597931	C	A	1849	DP=53	0.962264	"nrd-1"
I	5301419	C	T	2353	DP=73	0.958904	"let-526"
I	5564892	C	T	2044	DP=56	1	"fubl-4"
I	5596926	C	T	2113	DP=61	1	"tns-1"
I	5749054	G	A	2451	DP=71	1	"che-14"
I	5823427	C	T	2311	DP=61	1	"C32F10.8"
I	5902563	C	T	2002	DP=53	1	"stam-1"
I	6058887	C	T	1996	DP=61	1	"ari-1.1"
I	6410368	C	T	1839	DP=51	1	"ZC328.3"
I	6943362	C	T	2063	DP=57	1	"T10B11.6"
I	7202408	C	T	1423	DP=38	1	"col-61"
I	7349328	G	A	2440	DP=71	0.985915	"kbrl-1"
I	7643062	C	T	2091	DP=56	1	"ncbp-2"
I	7956704	C	T	2698	DP=70	1	"T22C1.8"
I	8445896	T	C	2263	DP=61	0.983607	"F10D11.6"
I	8512189	C	T	2620	DP=70	1	"K02B12.2"
I	8695066	C	T	2076	DP=59	0.983051	"K07A12.5"
I	8909902	T	A	2780	DP=77	1	"T08G11.1"
I	9010962	T	G	2540	DP=71	1	"rbpl-1"
I	9330892	T	A	3230	DP=86	1	"cbl-1"
I	9419844	C	T	2551	DP=66	1	"C17E4.4"
I	9519899	C	T	3052	DP=86	0.988372	"set-32"
I	10267613	G	T	24	DP=2	1	"ZC247.1"
I	10267619	C	A	7	DP=1	1	"ZC247.1"
I	10267620	T	C	21	DP=1	1	"ZC247.1"
I	10276425	C	G	508	DP=14	1	"ZC247.1"
I	10606512	T	C	2093	DP=56	1	"pash-1"
I	10905928	C	T	2130	DP=57	1	"srt-61"
I	10945289	C	A	1590	DP=45	1	"Y95D11A.1"
I	10945869	C	G	9939	DP=272	0.992647	"Y95D11A.4"
I	11179921	C	T	1198	DP=32	1	"rsr-1"
I	11241613	C	T	2	DP=5	1	"F46A8.4"

Chapter 2: Development of germline-specific chromatin profiling techniques in *C. elegans*

Summary

Chromosome organization plays a crucial role in various meiotic processes. However, in *C. elegans*, obtaining high-quality, germline-specific profiling data for key meiotic chromosome-interacting proteins, including cohesins and meiotic axis proteins, has been challenging due to limitations in genome-wide mapping techniques, such as ChIP-seq. To address this, I collaborated with Rui Jiang from our lab and Peter Meister from the University of Bern to adapt the highly sensitive chromatin profiling technique CUT&RUN to manually dissected *C. elegans* germline. This adaptation enabled us to generate germline-specific profiling data for histone modifications and various meiotic chromosome-interacting proteins. Through this approach, we uncovered correlations among active chromatin marks, cohesins, meiotic chromosome axis protein HTP-3, and one of the meiotic double-strand break (DSB) induction factor DSB-2 during meiosis in *C. elegans*.

Introduction

Until now, only a limited set of genome-wide profiling data for chromosome-interacting proteins involved in meiosis—such as cohesins, chromosome axis proteins, and those required for double-strand break (DSB) induction—has been produced in *C. elegans*. This has limited our understanding of the functions of these proteins during meiosis. The modENCODE project sought to map various proteins using Chromatin Immunoprecipitation and sequencing (ChIP-seq), but because they used whole worms, they were unable to generate germline-specific protein profiles, resulting in data for only a few germline-specific proteins in *C. elegans* (Gerstein et al., 2010; T. Liu et al., 2011). Other groups attempted to exploit ChIP-seq on isolated germline nuclei (Han et al., 2019). However, this method requires millions of worms as starting material due to inefficiencies in the isolation step, which creates a challenge in studying mutations that affect fertility. In addition, ChIP-seq involves crosslinking proteins and DNA, fragmenting whole genomic DNA, and immunoprecipitation, which often results in a low signal-to-background ratio, variable data quality, and extensive optimization requirements for fixation and sonication conditions.

For these reasons, I collaborated with Rui Jiang from our lab and Peter Meister from the University of Bern to adapt the low-input, high-sensitivity chromatin profiling method known as CUT&RUN (Cleavage Under Targets and Release Using Nuclease) to dissected *C. elegans* gonads, overcoming the limitations encountered in ChIP-seq (Skene & Henikoff, 2017). The preliminary protocol was initially developed by Gina Caldas and Fan Wu in our lab. CUT&RUN uses micrococcal nuclease (MNase) fused to protein A and/or protein G to recruit the enzyme to the protein of interest via interaction with antibody. This enables MNase to cut the nearby DNA after it is directed to the targeted protein. The digestion takes place in permeabilized nuclei or cells without the need for genomic DNA fragmentation outside the region of interest, resulting in a high signal-to-noise ratio, which in turn requires less starting material and sequencing depth (Skene & Henikoff, 2017). Additionally, CUT&RUN does not require fixation, making it compatible with a wider range of proteins that are sensitive to fixation.

We permeabilized dissected *C. elegans* gonads and allowed only the digested DNA fragments to diffuse out of the tissue, achieving a very high signal-to-background ratio. We found that the entire process provides great reproducibility with as few as 40 dissected *C. elegans* gonads, with a combined total of up to 20,000 nuclei. Here, we successfully mapped histone modifications, meiotic cohesins COH-3 and REC-8, the meiotic HORMA domain protein HTP-3, and the double-strand break (DSB) promoting factor DSB-2 in the *C. elegans* germline.

Results

Profiling of histone modifications using CUT&RUN

To validate our method, we profiled two abundant histone modifications in chromatin: H3K4me3, which marks promoters and enhancers, and H3K27me3, which marks chromatin regions silenced by the Polycomb Repressive Complex 2 (PRC2). The peaks mapped in replicate experiments showed high consistency, and no apparent peaks were observed in negative controls in which rabbit anti-mouse IgG was used. As anticipated, H3K4me3 and H3K27me3 peaks displayed a strong anti-correlation (Figure 1A, 1B).

We compared our data with ChIP-seq datasets generated by the modENCODE project (Gerstein et al., 2010; T. Liu et al., 2011). Although the modENCODE data were generated using extracts made from whole young adults, we found strong correlations for the same histone modifications between our data and modENCODE data, confirming the validity of our mapping results. This high correlation might be due to the abundance of meiotic nuclei in the worms, similarities in the distribution of histone marks between somatic and germline nuclei, or a combination of these factors. We calculated the correlation between each dataset and clustered them based on these values. We found that replicate experiments clustered together, and that both our data and the modENCODE data which map the same histone modifications also clustered together, while datasets representing different histone modifications formed distinct clusters (Figure 1A, 1B).

During transcription initiation, Serine 5 in the C-terminal repeat domain (CTD) of RNA polymerase II is phosphorylated by CDK7. Subsequently, during promoter-proximal pausing, Serine 2 of CTD is phosphorylated by CTDK-1, leading to double phosphorylation of Ser5 (pSer5) and Ser2 (pSer2). As transcription proceeds, the level of pSer5 decreases, while pSer2 persists (reviewed in Bartkowiak & Greenleaf, 2011). Using antibodies specific to pSer5 and pSer2, we profiled both markers as indicators of active gene transcription. Notably, peaks of pSer5 and pSer2 colocalized with each other and with H3K4me3 (Figure 1C). The correlation analysis showed that both pSer5 and pSer2 were strongly correlated with H3K4me3, but not with H3K27me3, as expected (Figure 1D).

Analysis of chromatin feature enrichment at transcription start and end sites (TSS and TES, respectively) revealed that H3K27me3 was depleted from both regions, whereas H3K4me3 showed greater enrichment at the TSS, as is typical promoter and enhancer marks. Unexpectedly, both pSer5 and pSer2 exhibited a similar pattern with greater enrichment at the TES than the TSS, contradicting the known pattern in which pSer5 is typically enriched at the TSS (Figure 1E). It remains unclear whether this inconsistency is due to the unique characteristics of *C. elegans*.

We also note that H3K4me3 peaks were depleted from X chromosomes. This is consistent with microscopy data showing a paucity of H3K4me3 on the inactive X chromosome in the *C. elegans* germline (Kelly et al., 2002; Rappaport et al., 2021). We also note that H3K4me3 was enriched at motifs recognized by the X chromosome PC protein HIM-8 (data not shown).

Mapping cohesins and meiotic axis protein HTP-3 using CUT&RUN

Using CUT&RUN on dissected gonads, we profiled the genome-wide binding of cohesins on chromosomes during meiosis in *C. elegans*. Cohesins, together with meiotic HORMA domain proteins (HORMA: Hop1/Rev7/Mad2), form the meiotic chromosome axis,

which organizes chromatin loops and supports the assembly of synaptonemal complexes (SCs) during meiosis (Kim et al., 2014; Rog & Dernburg, 2013; Severson et al., 2009; Severson & Meyer, 2014).

We profiled meiotic cohesin complexes containing meiosis-specific kleisin subunits COH-3 and REC-8. Both kleisins were tagged with HA using CRISPR. No meiotic defects were detected in either strain (<0.5% male self-progeny). Using CUT&RUN we successfully profiled each meiotic cohesin, while negative controls using the same anti-HA antibody in wild-type gonads did not show any apparent peaks. COH-3 and REC-8 peaks showed significant overlap, which was unexpected given their distinct functions and independent mechanisms for recruitment/localization (Figure 2A) (Severson & Meyer, 2014).

Next, we profiled HTP-3, the core HORMA domain protein in *C. elegans* that recruits other HORMA domain proteins, HIM-3 and HTP-1/2, through closure motifs (Kim et al., 2014). Recruitment of HTP-3 to the chromosome axis depends on both REC-8 and COH-3/4 cohesins (Severson et al., 2009; Severson & Meyer, 2014). Conversely, REC-8 cohesin also relies on HTP-3 for its localization to the axis, suggesting their potential co-localization (Severson et al., 2009). HTP-3 tagged with HA was used for CUT&RUN mapping.

We detected significant overlap between peaks of HTP-3 and those of COH-3 and REC-8, as expected (Figure 2A). We also observed strong correlations between replicate experiments, as well as between COH-3, REC-8, and HTP-3. However, HTP-3 ChIP-seq data generated by modENCODE showed weaker correlation with our CUT&RUN data (Figure 2B). Although the modENCODE HTP-3 data were consistent across replicates, both replicates exhibited unusually sharp peaks that did not follow Gaussian distributions, indicating potential data quality issues such as insufficient read depth.

The analysis, using COH-3 data as a representative, showed stronger correlations between COH-3 and active chromatin marks such as H3K4me3 and phosphorylated RNA polymerase II, than with the repressive mark H3K27me3 (Figure 2C, 2D). Enrichment of each chromatin feature centered on COH-3 peaks revealed enrichment of H3K4me3, active RNA polymerase II phosphorylation, REC-8, and HTP-3 at the COH-3 peaks (Figure 2E). At gene start and end sites (TSS and TES, respectively), COH-3, REC-8, and HTP-3 showed enrichment at TES, possibly due to displacement of cohesin along the gene body as transcription progresses, which aligns with previous studies (Busslinger et al., 2017; Glynn et al., 2004; Kogut et al., 2009; Lengronne et al., 2004) (Figure 2F).

DSB-2 is co-enriched with cohesin and active chromatin marks.

In *C. elegans*, loss of HTP-3 or meiotic cohesin complexes results in a complete loss of meiotic DSBs (Goodyer et al., 2008; Severson & Meyer, 2014). However, how chromosome axis promotes DSBs remains elusive.

In *C. elegans* there are two Rec114 homologs, known as DSB-1 and DSB-2, which promote DSB formation by SPO-11 (Rosu et al., 2013; Stamper et al., 2013). Loss of DSB-1 results in a complete loss of DSBs, while a few DSBs are detected in the absence of DSB-2. It is unclear whether these proteins work together; they both localize to meiotic chromatin but do not show extensive overlap in their cytological distribution.

We profiled the genome-wide distribution of DSB-2 during meiosis in *C. elegans* using FLAG-tagged DSB-2 and compared its localization with active and repressive chromatin marks and chromosome axis proteins. DSB-2 peaks showed significant correlation with cohesin COH-3 and phosphorylated RNA polymerase marks at active chromatin (Figure 3A, 3B). Enrichment of

each marks centered on DSB-2 peaks also revealed this enrichment of active chromatin marks and COH-3, suggesting that DSB-2 is recruited to active chromatin and co-localizes with COH-3 to induce DSBs.

Discussion

The high correlation between COH-3 and REC-8 are interesting given that these proteins do not show cytological overlap (Woglar et al., 2020), and they play distinct roles in meiosis. However, our genome-wide mapping experiments detect the average localization of each protein in a population of nuclei; thus, the localization of COH-3 and REC-8 in individual nuclei may vary.

The association between cohesins and active chromatin marks is consistent with previous studies indicating that cohesins are often found at active gene conversion sites during interphase (Glynn et al., 2004; Kogut et al., 2009; Lengronne et al., 2004). Our finding in meiotic chromosomes of *C. elegans* suggests that this pattern continues to persist during meiosis. This observation also aligns with the co-localization of H3K4me3, induced by the histone methyltransferase PRDM9, and cohesins at DSB hot spots in mice (Bhattacharyya et al., 2019)

The enrichment of cohesin and DSB-promoting factor DSB-2 at active chromatin agrees with the general enrichment of cohesins and DSB hotspots in active chromatins during meiosis observed in other organisms (Bhattacharyya et al., 2019; Tock & Henderson, 2018). However, it remains unclear why DSB-2 exhibits a concentrated pattern at the center of chromosomes, similar to active chromatin marks and cohesins/HTP-3, while extensive genetic mapping in *C. elegans* has revealed that the central regions have fewer crossovers than the arms. This may suggest that DSB-2 is merely not well correlated with DSBs, although it promotes DSB formation. A more direct method for mapping DSBs, such as END-seq (Canela et al., 2016), or germline-specific mapping of RAD-51 during meiosis would be necessary for accurate mapping of DSBs.

Although we have tried to map other DSB-associated factors, including RAD-51, by CUT&RUN, these experiments have not been successful. We suspect that our failure to map RAD-51 might be due to the single-stranded DNA (ssDNA) structure or other unknown structural characteristics of RAD-51-coated ssDNAs that prevent the MNase from fragmenting DNA in a way that is compatible with its incorporation into sequencing libraries.

Materials and Methods

CUT&RUN

C. elegans gonads were manually dissected and collected in CUT&RUN Wash-150 buffer (Skene & Henikoff, 2017) containing 0.05% digitonin and 2mM EDTA to inhibit metal-dependent enzymes. Then the permeabilized gonads were incubated with Concanavalin A (ConA) coated magnetic bead for easy precipitation during wash. Other processes were followed as described in the original description of CUT&RUN (Skene & Henikoff, 2017). Fragments were captured using the Zymo Research ChIP DNA Clean and Concentrator kit (D5201) and proceeded with library construction based on the protocol for low amount DNA fragments (N. Liu, 2019) (dx.doi.org/10.17504/protocols.io.wvgfe3w)

For optimization, we compared different MNases fused with protein A or A/G from various sources. We assessed their enzymatic activity by digesting lambda DNA. We found that the MNase synthesized at UC Berkeley Macrolab demonstrated much greater efficiency than commercially available enzymes when used in equivalent amounts (specifically, those from Epicypher and Cell Signaling Technology). Additionally, we tested various permeabilization conditions, including different concentrations of digitonin and combinations of various detergents, and found that 0.05%-0.25% digitonin alone was sufficient without the need for other detergents. We confirmed that fixation is not necessary for the experiment.

C. elegans strains

N2 Bristol was used as the wild-type *C. elegans* strain. The following strains were used: *coh-3::ha* (CA1495), *dsb-2(ie57[dsb-2::AID::3xFLAG]), meIs8[GFP-cosa-1] II; ieSi38[sun-1p::TIR1::mRuby::sun-1 3'UTR, Cbr-unc-119(+)] IV* (CA1419), *ha::aid::htp-3; ieSi64[gld-1p::TIR1::mRuby::gld-1 3'UTR, Cbr-unc-119(+)] II; ieSi38[sun-1p::TIR1::mRuby::sun-1 3'UTR, Cbr-unc-119(+)] IV* (CA1670), and *rec-8::2xha* (generated in this research), where "aid" designates a 44-amino acid degron sequence for auxin induced degradation (AID) (Zhang et al., 2015). Auxin depletion was not used in the mapping experiments. All strains have been characterized and found to have no meiotic defects in the absence of depletion.

To generate *ha::rec-8* strains, single-stranded (ss) DNA templates were designed to insert two copies of the HA tag, separated by a flexible linker (GGGS), at the C-terminus of REC-8. These were co-injected with Cas9-NLS prebound to duplexed gRNAs, as well as a duplexed gRNA and ssDNA template for co-CRISPR of dpy-10 (66). (Final concentrations in the injection mix: *dpy-10* crRNA, 20 μM; *rec-8* crRNA, 50 μM; trRNA, 40 μM; Cas9-NLS protein, 20 μM; *dpy-10* repair template, 1 μM, *rec-8* repair template, 1 μM).

Antibodies

All antibodies used for CUT&RUN were obtained from commercial sources. They include the following antibodies and dilutions: rabbit polyclonal anti-H3K4me3 (Active Motif, 39160) (1:100), rabbit polyclonal anti-H3K27me3 (Active Motif, 39055) (1:100), rabbit polyclonal anti-RNA Pol II phospho-Ser 2 (Active Motif, 39564) (1:100), rabbit polyclonal anti-RNA Pol II phospho-Ser 5 (Active Motif, 39234) (1:100), rabbit polyclonal anti-HA (Abcam, ab9110) (1:100), mouse monoclonal anti-FLAG (M2) (Sigma Aldrich, F1804) (1:100), rabbit monoclonal anti-mouse (Abcam, 46540) (1:100)

Data analysis

Sequencing was done using Novaseq 6000 system. 2-3 Gb of data were generated per sample and reads were analyzed using Nextflow pipeline (https://zenodo.org/records/10606804). Most parameters were default. For peak colocalization analysis, IGV was used. For correlation analysis, deepTools multiBigwigSummary (Bin size: 100 bp, Blacklisted: ce10-blacklist.bed (v1) (Amemiya et al., 2019)) and plotCorrelation were used. For heat map analysis, deepTools computeMatrix (Regions to plot: ce10.refGene.gtf or CUT&RUN called peaks using MACS2 bdgpeakcall-default setting, scale-regions for genes, reference-point (center of region) for COH-3 or DSB-2; --regionBodyLength 3000, --before/afterRegionStartLength 3000, --binSize 50, --sortRegions descending order, --missingDataAsZero yes, --skipZeros yes, --blackListFileName ce10-blacklist.bed) and plotHeatmap were used.

References

Bartkowiak, B., & Greenleaf, A. L. (2011). Phosphorylation of RNAPII: To P-TEFb or not to P-TEFb? *Transcription*, *2*(3), 115–119. https://doi.org/10.4161/trns.2.3.15004

Bhattacharyya, T., Walker, M., Powers, N. R., Brunton, C., Fine, A. D., Petkov, P. M., & Handel, M. A. (2019). Prdm9 and Meiotic Cohesin Proteins Cooperatively Promote DNA Double-Strand Break Formation in Mammalian Spermatocytes. *Current Biology*, *29*(6), 1002-1018.e7. https://doi.org/10.1016/j.cub.2019.02.007

Busslinger, G. A., Stocsits, R. R., van der Lelij, P., Axelsson, E., Tedeschi, A., Galjart, N., & Peters, J.-M. (2017). Cohesin is positioned in mammalian genomes by transcription, CTCF and Wapl. *Nature*, *544*(7651), 503–507. https://doi.org/10.1038/nature22063

Canela, A., Sridharan, S., Sciascia, N., Tubbs, A., Meltzer, P., Sleckman, B. P., & Nussenzweig, A. (2016). DNA Breaks and End Resection Measured Genome-wide by End Sequencing. *Molecular Cell*, *63*(5), 898–911. https://doi.org/10.1016/j.molcel.2016.06.034

Gerstein, M. B., Lu, Z. J., Van Nostrand, E. L., Cheng, C., Arshinoff, B. I., Liu, T., Yip, K. Y., Robilotto, R., Rechtsteiner, A., Ikegami, K., Alves, P., Chateigner, A., Perry, M., Morris, M., Auerbach, R. K., Feng, X., Leng, J., Vielle, A., Niu, W., … Waterston, R. H. (2010). Integrative Analysis of the *Caenorhabditis elegans* Genome by the modENCODE Project. *Science*, *330*(6012), 1775–1787. https://doi.org/10.1126/science.1196914

Glynn, E. F., Megee, P. C., Yu, H.-G., Mistrot, C., Unal, E., Koshland, D. E., DeRisi, J. L., & Gerton, J. L. (2004). Genome-Wide Mapping of the Cohesin Complex in the Yeast Saccharomyces cerevisiae. *PLoS Biology*, *2*(9), e259. https://doi.org/10.1371/journal.pbio.0020259

Goodyer, W., Kaitna, S., Couteau, F., Ward, J. D., Boulton, S. J., & Zetka, M. (2008). HTP-3 Links DSB Formation with Homolog Pairing and Crossing Over during C. elegans Meiosis. *Developmental Cell*, *14*(2), 263–274. https://doi.org/10.1016/j.devcel.2007.11.016

Han, M., Wei, G., McManus, C. E., Hillier, L. W., & Reinke, V. (2019). Isolated C. elegans germ nuclei exhibit distinct genomic profiles of histone modification and gene expression. *BMC Genomics*, *20*(1), 500. https://doi.org/10.1186/s12864-019-5893-9

Kelly, W. G., Schaner, C. E., Dernburg, A. F., Lee, M.-H., Kim, S. K., Villeneuve, A. M., & Reinke, V. (2002). X-chromosome silencing in the germline of *C. elegans*. *Development*, *129*(2), 479–492. https://doi.org/10.1242/dev.129.2.479

Kim, Y., Rosenberg, S. C., Kugel, C. L., Kostow, N., Rog, O., Davydov, V., Su, T. Y., Dernburg, A. F., & Corbett, K. D. (2014). The Chromosome Axis Controls Meiotic Events through a Hierarchical Assembly of HORMA Domain Proteins. *Developmental Cell*, *31*(4), 487–502. https://doi.org/10.1016/j.devcel.2014.09.013

Kogut, I., Wang, J., Guacci, V., Mistry, R. K., & Megee, P. C. (2009). The Scc2/Scc4 cohesin loader determines the distribution of cohesin on budding yeast chromosomes. *Genes & Development*, *23*(19), 2345–2357. https://doi.org/10.1101/gad.1819409

Lengronne, A., Katou, Y., Mori, S., Yokobayashi, S., Kelly, G. P., Itoh, T., Watanabe, Y., Shirahige, K., & Uhlmann, F. (2004). Cohesin relocation from sites of chromosomal loading to places of convergent transcription. *Nature*, *430*(6999), 573–578. https://doi.org/10.1038/nature02742

Liu, N. (2019). *Library Prep for CUT&RUN with NEBNext® Ultra™ II DNA Library Prep Kit for Illumina® (E7645) v1*. https://doi.org/10.17504/protocols.io.wvgfe3w

Liu, T., Rechtsteiner, A., Egelhofer, T. A., Vielle, A., Latorre, I., Cheung, M.-S., Ercan, S., Ikegami, K., Jensen, M., Kolasinska-Zwierz, P., Rosenbaum, H., Shin, H., Taing, S., Takasaki, T., Iniguez, A. L., Desai, A., Dernburg, A. F., Kimura, H., Lieb, J. D., … Liu, X. S. (2011). Broad chromosomal domains of histone modification patterns in *C. elegans*. *Genome Research*, *21*(2), 227–236. https://doi.org/10.1101/gr.115519.110

Rappaport, Y., Achache, H., Falk, R., Murik, O., Ram, O., & Tzur, Y. B. (2021). Bisection of the X chromosome disrupts the initiation of chromosome silencing during meiosis in Caenorhabditis elegans. *Nature Communications*, *12*(1), 4802. https://doi.org/10.1038/s41467-021-24815-0

Rog, O., & Dernburg, A. F. (2013). Chromosome pairing and synapsis during Caenorhabditis elegans meiosis. *Current Opinion in Cell Biology*, *25*(3), Article 3. https://doi.org/10.1016/j.ceb.2013.03.003

Rosu, S., Zawadzki, K. A., Stamper, E. L., Libuda, D. E., Reese, A. L., Dernburg, A. F., & Villeneuve, A. M. (2013). The C. elegans DSB-2 Protein Reveals a Regulatory Network that Controls Competence for Meiotic DSB Formation and Promotes Crossover Assurance. *PLoS Genetics*, *9*(8), e1003674. https://doi.org/10.1371/journal.pgen.1003674

Severson, A. F., Ling, L., van Zuylen, V., & Meyer, B. J. (2009). The axial element protein HTP-3 promotes cohesin loading and meiotic axis assembly in *C. elegans* to implement the meiotic program of chromosome segregation. *Genes & Development*, *23*(15), 1763–1778. https://doi.org/10.1101/gad.1808809

Severson, A. F., & Meyer, B. J. (2014). Divergent kleisin subunits of cohesin specify mechanisms to tether and release meiotic chromosomes. *ELife*, *3*, e03467. https://doi.org/10.7554/eLife.03467

Skene, P. J., & Henikoff, S. (2017). An efficient targeted nuclease strategy for high-resolution mapping of DNA binding sites. *ELife*, *6*, e21856. https://doi.org/10.7554/eLife.21856

Stamper, E. L., Rodenbusch, S. E., Rosu, S., Ahringer, J., Villeneuve, A. M., & Dernburg, A. F. (2013). Identification of DSB-1, a Protein Required for Initiation of Meiotic Recombination in Caenorhabditis elegans, Illuminates a Crossover Assurance Checkpoint. *PLoS Genetics*, *9*(8), e1003679. https://doi.org/10.1371/journal.pgen.1003679

Tock, A. J., & Henderson, I. R. (2018). Hotspots for Initiation of Meiotic Recombination. *Frontiers in Genetics*, *9*, 521. https://doi.org/10.3389/fgene.2018.00521

Woglar, A., Yamaya, K., Roelens, B., Boettiger, A., Köhler, S., & Villeneuve, A. M. (2020). Quantitative cytogenetics reveals molecular stoichiometry and longitudinal organization of meiotic chromosome axes and loops. *PLOS Biology*, *18*(8), e3000817. https://doi.org/10.1371/journal.pbio.3000817

Zhang, L., Ward, J. D., Cheng, Z., & Dernburg, A. F. (2015). The auxin-inducible degradation (AID) system enables versatile conditional protein depletion in C. elegans. *Development (Cambridge, England)*, *142*(24), Article 24. https://doi.org/10.1242/dev.129635

Figures

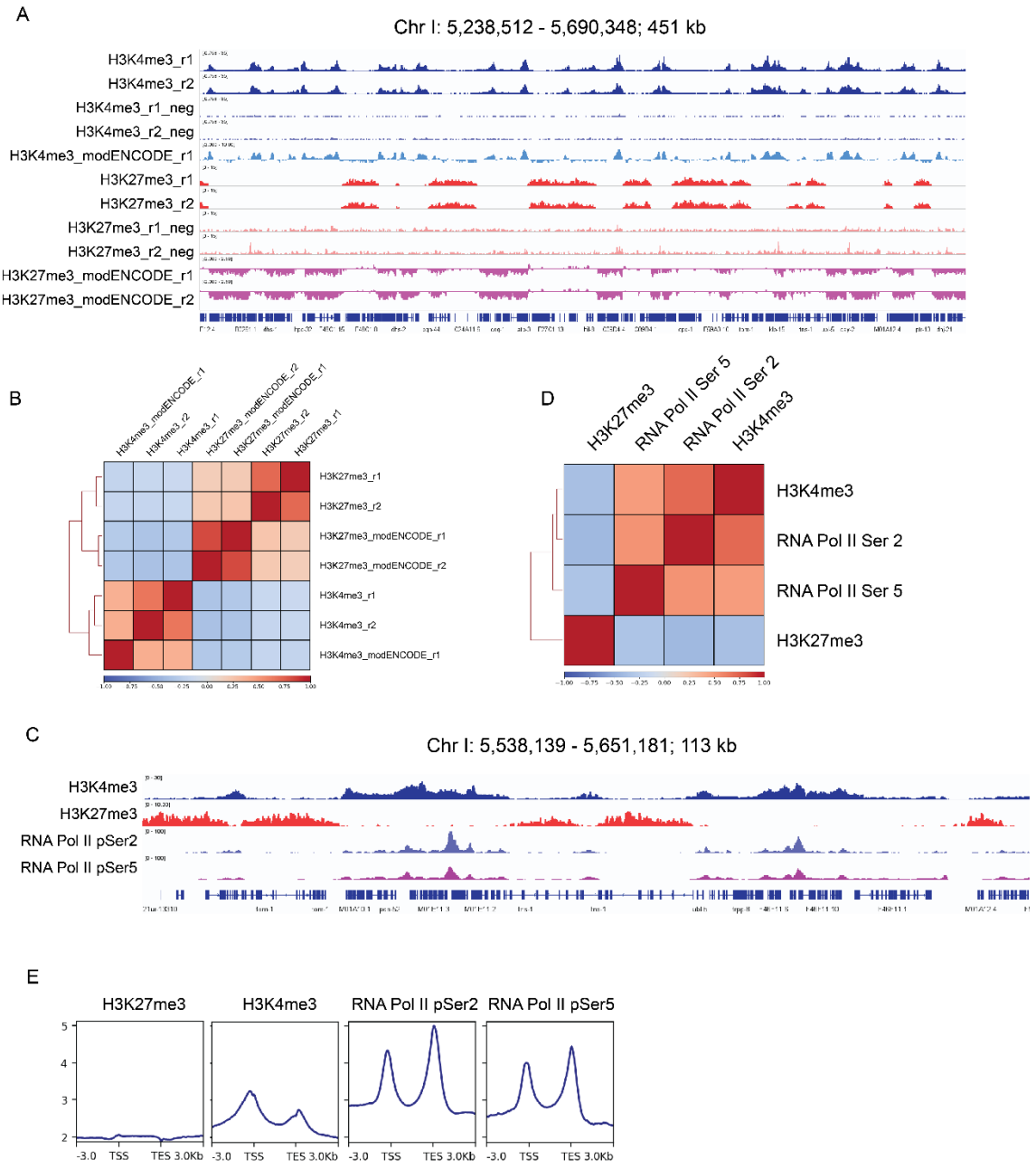

Figure 1. CUT&RUN successfully profiled the active histone modification H3K4me3 and the repressive histone modification H3K27me3, which match with the modENCODE dataset. (A) Genome browser representation of CUT&RUN normalized reads for H3K4me3 (dark blue) and H3K27me3 (red) in *C. elegans* germline. r1 and r2 represent replicates and neg represents the negative control. modENCODE ChIP-seq reads for H3K4me3 (light blue) and H3K27me3 (magenta) were also presented. (B) Pairwise correlation analysis of the datasets in (A) and hierarchical clustering based on correlation scores. (C) Genome browser representation

of CUT&RUN reads for H3K4me3, H3K27me3, and RNA polymerase II phospho-Ser 2 (gray-blue) and 5 (purple). (D) Pairwise correlation analysis and hierarchical clustering of the dataset in (C). (E) Enrichment of each chromatin feature at the transcription start site (TSS) and the transcription end site (TES). The window is -3 kb from the TSS and +3 kb from the TES.

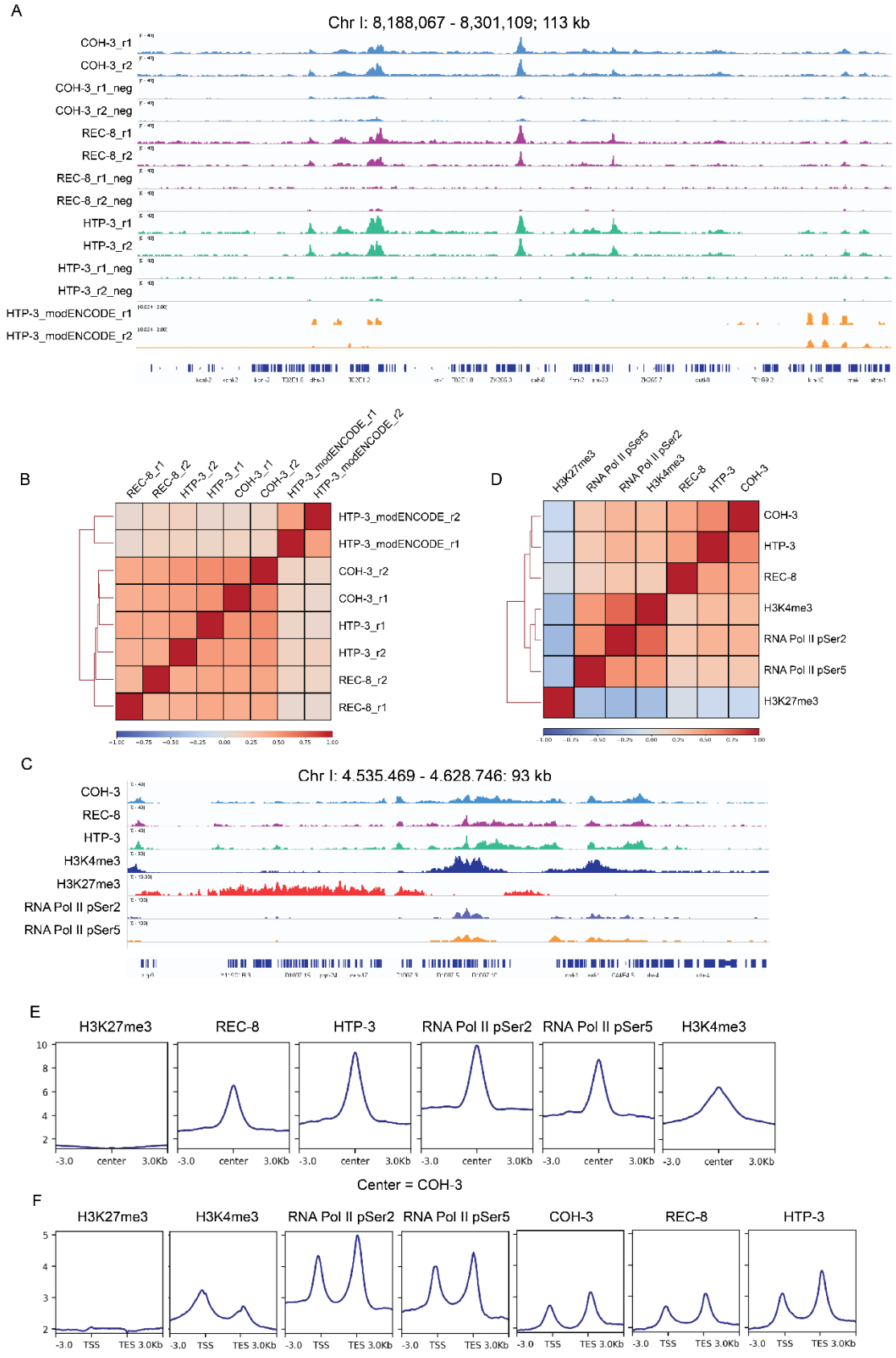
A
Chr I: 8,188,067 - 8,301,109; 113 kb
COH-3_r1
COH-3_r2
COH-3_r1_neg
COH-3_r2_neg
REC-8_r1
REC-8_r2
REC-8_r1_neg
REC-8_r2_neg
HTP-3_r1
HTP-3_r2
HTP-3_r1_neg
HTP-3_r2_neg
HTP-3_modENCODE_r1
HTP-3_modENCODE_r2
B
REC-8_r1
REC-8_r2
HTP-3_r2
HTP-3_r1
COH-3_r1
COH-3_r2
HTP-3_modENCODE_r1
HTP-3_modENCODE_r2
HTP-3_modENCODE_r2
HTP-3_modENCODE_r1
COH-3_r2
COH-3_r1
HTP-3_r1
HTP-3_r2
REC-8_r2
REC-8_r1
D
H3K27me3
RNA Pol II pSer5
RNA Pol II pSer2
H3K4me3
REC-8
HTP-3
COH-3
COH-3
HTP-3
REC-8
H3K4me3
RNA Pol II pSer2
RNA Pol II pSer5
H3K27me3
C
Chr I: 4,535,469 - 4,628,746: 93 kb
COH-3
REC-8
HTP-3
H3K4me3
H3K27me3
RNA Pol II pSer2
RNA Pol II pSer5
E
H3K27me3
REC-8
HTP-3
RNA Pol II pSer2
RNA Pol II pSer5
H3K4me3
10
8
6
4
2
-3.0
center
3.0Kb
Center = COH-3
F
H3K27me3
H3K4me3
RNA Pol II pSer2
RNA Pol II pSer5
COH-3
REC-8
HTP-3
5
4
3
2
-3.0
TSS
TES 3.0Kb

Figure 2. Meiotic cohesin complexes and the chromosome axis protein HTP-3 profiled by CUT&RUN in dissected *C. elegans* germlines. (A) Genome browser representation of CUT&RUN normalized reads for COH-3 (light blue), REC-8 (purple), and HTP-3 (green). modENCODE ChIP-seq reads for HTP-3 (yellow) are also presented. (B) Pairwise correlation analysis and hierarchical clustering of the datasets in (A). (C) Genome browser representation of normalized CUT&RUN reads for COH-3 (light blue), REC-8 (purple), HTP-3 (green), H3K4me3 (dark blue), H3K27me3 (red), and RNA polymerase II pSer2 (gray-blue) and 5 (yellow). (D) Pairwise correlation analysis and hierarchical clustering of the datasets in (C). (E) Enrichment of each chromatin feature at the center of COH-3 peaks. The window is -3 and +3 kb from the center. (F) Enrichment of each chromatin feature at the transcription start site (TSS) and the transcription end site (TES). The window is -3 kb from the TSS and +3 kb from the TES.

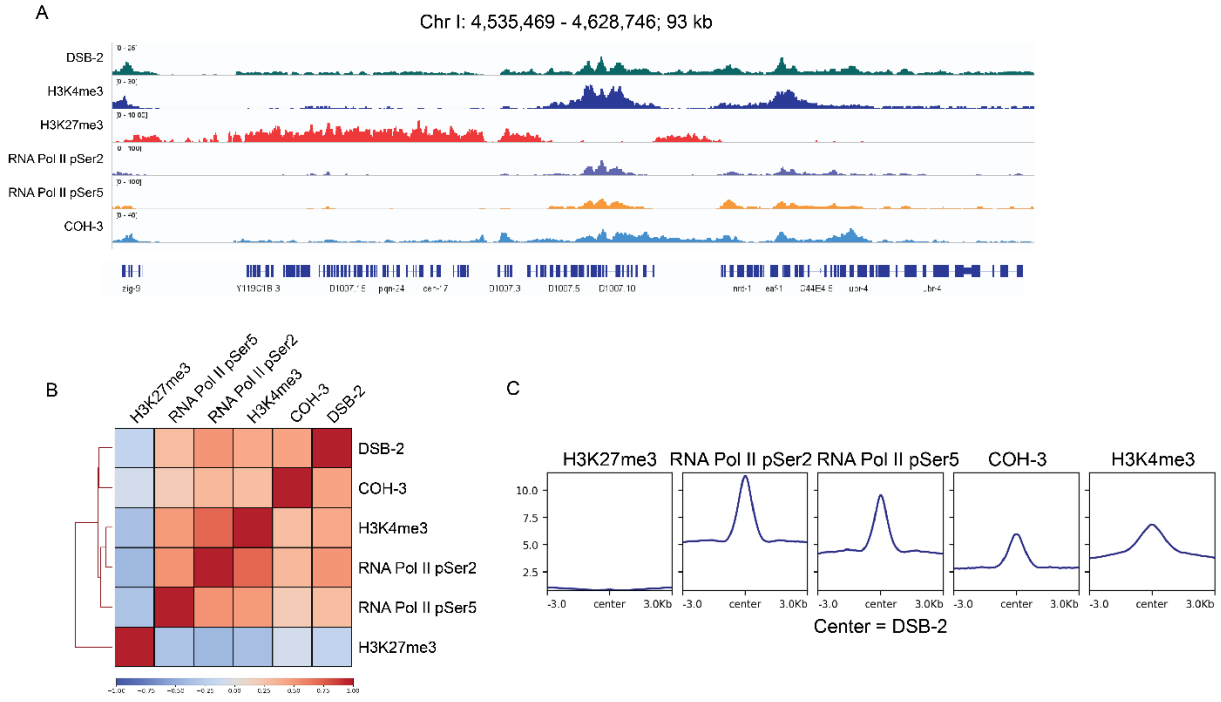

Figure 3. DSB-2 enrichment correlates with cohesin and active chromatin marks. (A) Genome browser representation of CUT&RUN normalized reads for DSB-2 (dark green), H3K4me3 (dark blue), H3K27me3 (red), RNA polymerase II phosphorylated Ser 2 (gray-blue) and 5 (yellow), and COH-3 (light blue). (B) Pairwise correlation analysis and hierarchical clustering of the datasets in (A). (C) Enrichment of each chromatin feature at the center of DSB-2 peaks. The window is -3 and +3 kb from the center.